University of Alberta

Dense and Porous ZnO Thin Films Produced by Pulsed Laser Deposition

by

Yang-Wen Sun 

A thesis submitted to the Faculty of Graduate Studies and Research in partial fulfillment of the

requirements for the degree of *Master of Science*

Department of *Electrical and Computer Engineering*

Edmonton, Alberta
Spring 2005

Abstract

The study of fabrication and characterization of dense and porous Zinc Oxide (ZnO) thin films by Pulsed Laser Deposition is presented here. ZnO thin films were deposited onto p- type Si (100) substrates at room temperature using 15 ns krypton fluoride (248 nm) laser pulses in vacuum or in ~10^{-1} torr oxygen background with or without annealing. In additional to dense ZnO thin films, porous ZnO thin films consisting of isolated straight columns and helical structures with diameters on the order of 100 nm were produced. The structural, compositional, morphological, and photoluminescence properties of these dense and porous ZnO thin films were studied in detail. We have also measured the absolute UV emission in terms of number of photons per steradian for these films. It was found that both O_2 background during deposition and annealing after deposition are essential to give a good crystalline structure and strong UV emission.

Acknowledgement

Fist, I would like to thank my supervisor Dr. Ying Tsui for his mentoring, inspiration, and knowledgeable comments throughout the three years of study. I also want to thank my colleagues for helping me with the experimental setups. They are Blair Harwood, Rick Cornad, Hong Sang, Mike Taschuk, Christ Germain, Cristina Serbanescu, Rahim Janmohamed, Igor Cravetchi, Sean Kirkwood, Mike Argument, Matt Reid, Sanjay Singh, Serife Yalcin, and Roman Holenstein. Trainings given by Dr. Robert Fedosejevs on how to give formal presentations have also been wonderful assets of mine.

I also appreciate George Braybrook, the SEM technician, for spending so much time on finding tiny structures and produce the best-looking pictures out of my samples. Serqi Matveev and Diane Caird, who lend their expertise on Electron Microprobe and XRD analysis to me, have both done excellent jobs. Their results form an invaluable part of my thesis.

Finally, I especially want to thank my parents, my sister, my brother, and Isaac Fan for giving me the greatest support during my study. It's them who gave me the warmest cares during the cold winter in Edmonton.

Table of Contents

List of Tables

List of Figures

Chapter 1 Introduction

1.1 Motivation

The purpose of the research is to fabricate and characterize dense and porous ZnO thin films produced by pulsed laser deposition (PLD) as a candidate material for the fabrication of optoelectronic devices in the UV region. The effects of depositing with and without O_2, and the effects of annealing on these ZnO thin films' various properties will be presented in this thesis in detail.

1.2 ZnO

Zinc Oxide is a wide band gap (3.37eV at room temperature, as shown in Fig 1), II-VI semiconductor material and it is a promising material for ultraviolet (UV) light emitting diodes (LED) [1], UV lasers, thin film transistors (TFT) [2], gas sensors [3], varistor [4], solar cell [5], surface electro-acoustic wave (SAW) devices [6], transparent conductors [7], waveguides [8]etc.

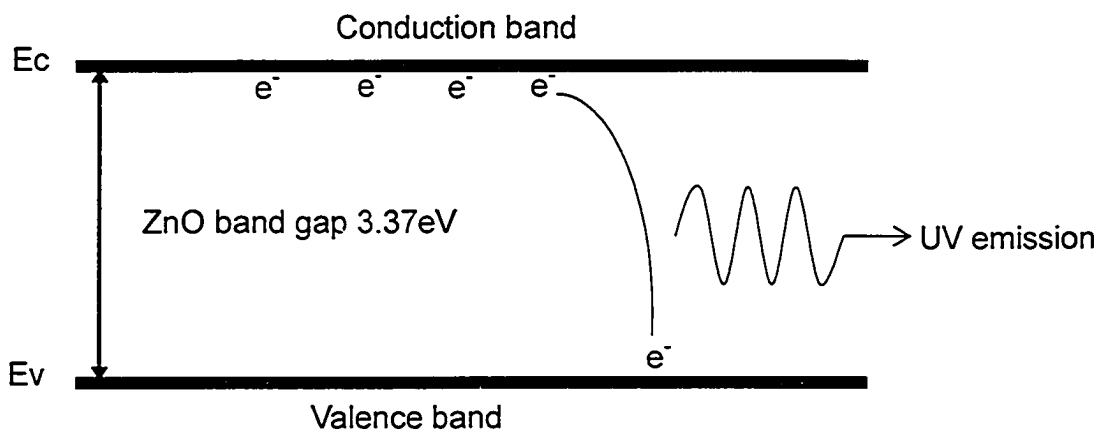

Fig 1 ZnO is a semiconductor material that has a wide direct band gap of 3.37eV at room temperature.

ZnO has a direct band gap with the conduction band minimum and the valence band maximum located at k=0 in the Brillouin zone[9]. Stoichiometric ZnO is an insulator that has a wurtzite (hexagonal) crystal structure, which is its most stable phase under thermal equilibrium as shown in Fig 2. While the ideal wurtzite structure has four-fold coordination with a hexagonal unit cell having two lattice parameters of a=3.25Å, c=5.12Å (c/a=$\sqrt{8}/3$=1.633), the actual lattice of ZnO deviates from the ideal lattices with c/a=1.602 [9]. Each zinc atom is tetrahedrally coordinated to four oxygen atoms as shown in Fig 3. The zinc d-electrons hybridize with the oxygen p-electrons. The chemical bonding in ZnO is predominantly covalent but has a significant contribution from ionic bonding.

ZnO excitons have a binding energy of 60meV, which is significantly larger than the effective thermal energy at room temperature, $K_B T = 26meV$. Thus, excitonic gain mechanisms could be expected to play a significant role in ZnO based devices.

ZnO is an n-type semiconductor in which the donor is associated with oxygen vacancy and interstitial zinc atoms. Hall mobility in ZnO single crystals is on the order of 200 $cm^2v^{-1}s^{-1}$ [10]. The large background n-type carrier (free electrons) concentration in ZnO results from non-stoichiometry such as oxygen vacancies and zinc interstitials [11].

Table 1 is the comparison of several wide band gap semiconductor materials including ZnO, ZnS ZnSe, GaN, and GaAs. ZnO has large band gap, and the high exciton binding energy of 60 meV. Excitonic recombination in semiconductors is a more efficient radiation process than electron hole plasma process (EHP), and can facilitate low-threshold stimulated emission [12]. In order to facilitate room temperature lasing, the exciton binding energy of a material must be greater than the thermal energy at room

temperature, and therefore the large excitonic binding energy for ZnO in principle would allow room temperature lasing. Conversely, the low exciton binding energy of ZnSe (20meV) makes room temperature excitonic lasing difficult.

GaN is the chief competitor to ZnO as a material for making short wavelength laser diodes and LEDs. Although GaN UV/blue laser diode and LEDs have been reported before [13], ZnO has fundamental advantages over GaN, especially a free exciton binding energy (60meV), which is much higher than that of GaN (21meV). In addition ZnO is harder and more resistant to radiation damage than GaN [14].

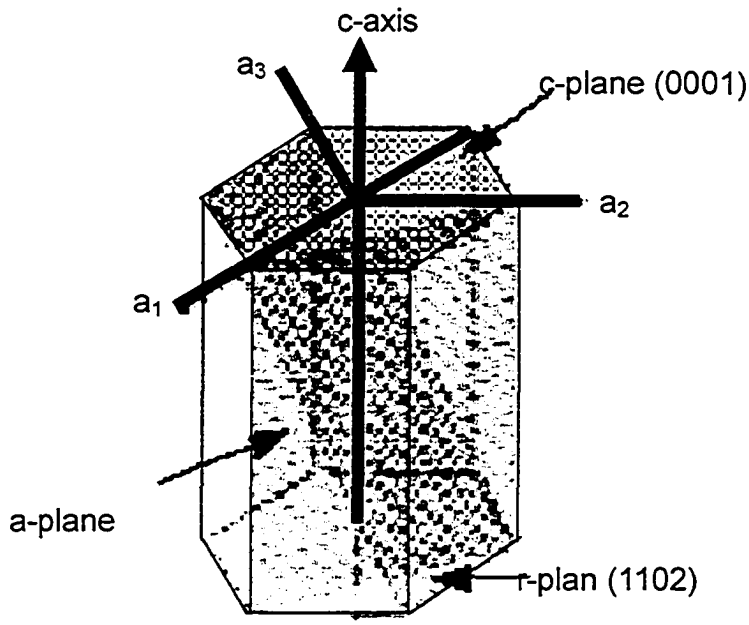

Fig 2 Wurtzite type structure of ZnO

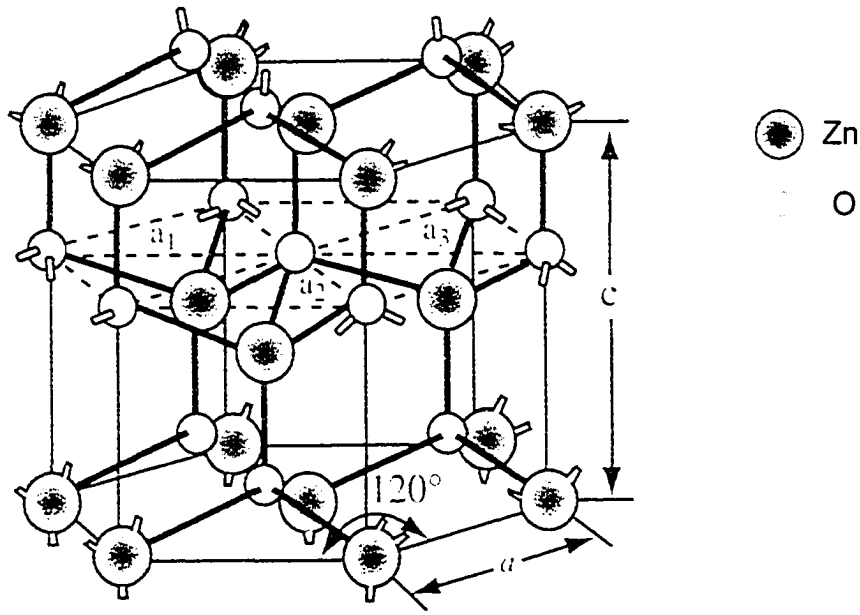

Fig 3 Chemical bonding of ZnO [15]

Table 1 Material properties of wide band gap semiconductors [9]

Material	Crystal Structure	Lattice Const. a (Å)	c (Å)	Cohesive energy	Melting point Tm (K)	Thermal conductivity κ ($Wcm^{-1}K^{-1}$)	Hybrid polarity α_P	Band gap Eg (RT) (eV)	Electron and hole effective mass m_e^*	m_h^*	Dielectric constant ε_0	ε_∞	Exciton binding energy E_b(meV)
ZnO	WZ[1]	3.25	5.21	1.89	2250	0.60	0.60	3.37	0.28	0.59	8.75	3.75	60
ZnS	WZ	3.82	6.26	1.59	2103	0.46	0.56	3.8	0.28	1.4/ 0.49	9.6	5.7	29
ZnSe	ZB[2]	5.67	---	1.29	1793	0.14	0.56	2.7	0.16	0.14/ 1.44	9.1	6.3	20
GaN	WZ	3.19	5.19	2.24	1973	1.3	0.4	3.39	0.19	---	8.9	5.35	21
GaAs	ZB	5.65	---	1.63	1513	0.56	0.32	1.42	0.06	0.51/ 0.08	13.2	10.9	4.9

[1]Wz - wurtzite structure

[2]ZB - cubic zinc blende structure

1.3 Introduction to pulsed laser deposition and review of previous work done in our laboratory

Pulsed laser deposition (PLD) is a thin film deposition technique that has been applied to a wide variety of materials for the production of high quality thin films. There are many advantages of pulsed laser deposition: the technique is easy to use and flexible, produces film stoichiometry close to that of the target, good quality films can be grown at room temperature, films can be grown in vacuum or in background gases, etc. For materials with high melting temperature, it is easier to produce thin films by pulsed laser deposition compared to other conventional physical vapour deposition (PVD) techniques, such as evaporation. PLD technique has been applied successfully to a wide variety of chemically and structurally complex materials such as chalcogenide glasses [16], because of its ability to maintain the stoichiometry of the target material in thin film form during ablation (congruent evaporation). PLD can also be used to produce nanostructure films without the use of catalyst or etching.

However, there are disadvantages in PLD such as difficulty in producing uniform films over a large area, and the presence of micro size debris particles on the film surface.

In order to produce debris-free thin films, a Magnetically Guided Pulsed Laser Deposition (MGPLD) technique [17] has been developed in our laboratory.

Pulsed laser deposition has also been used in our laboratory to produce Er doped chalcogenide glass thin films for integrated optics applications. The biggest challenge of making the chalcogenide thin film is to transfer the stoichiometry from the target to the film with good homogeneity. Thermal vacuum evaporation usually results in non-homogeneous films and in the change of film composition due to different volatility of components. Rare-earth ions have very low vapor pressure compared to components of

the chalcogenide glass. Therefore, the concentration of rare-earth ions in these films is very low. In contrast, PLD has the advantage of the ability to reproduce the same composition of the target, and congruent evaporation. The Er doped chalcogenide films deposited in our laboratory have composition very close to that of the original target. In addition, the film shows very promising luminescence at 1542 nm [18].

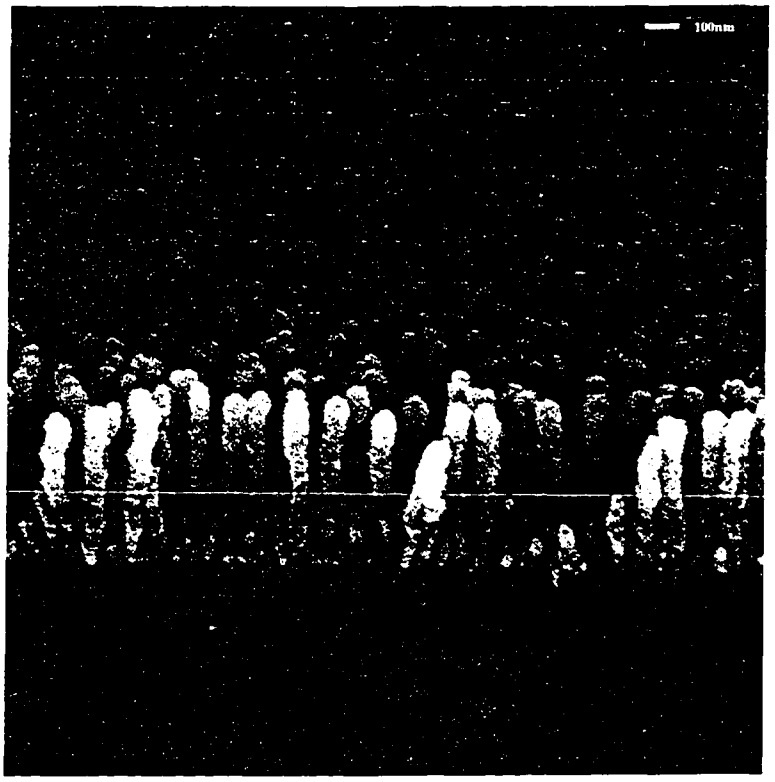

Fig 4 Porous diamond-like-carbon (DLC) film consists of 30 nm wide and 0.3μm high isolated wires produced by PLD.

Both dense and porous diamond-like-carbon (DLC) films by PLD have been deposited in our laboratory. Fig 4 is a porous DLC film which consists of typically 0.3 micron thick and 30nm diameter carbon wires generated by laser ablation of a carbon target in a vacuum chamber at laser fluence of ~ 5J/cm^2. The carbon nanowires were formed due to nuclei self-shadowing effect by orienting the substrate with its surface almost parallel to the axis of the deposition plume [19]. Diamond-like carbon thin films

are excellent protective coatings because of their low friction coefficient, high hardness value, and high wear resistance.

Dense and porous ZnO thin films have been deposited using the same technique as that of DLC thin films with the exception that O_2 background gas was used. The study of these dense and porous ZnO thin films is the focus of this thesis.

1.4 Review on the progress of the development of ZnO UV thin films

Research to fabricate optoelectronic devices in the visible and UV wavelength region is currently very active. ZnO has promising optical properties and it is one of the prime candidates to be used for UV light emitting sources.

There are several groups involved in the research of fabricating UV optoelectronic devices based on ZnO thin films. Bagnall et al. and Segawa et al. were the first two groups to observe the stimulated emission from ZnO thin films at room temperature by molecular beam epitaxy[20] [21]. Huang et al. was the first group that reported lasing in ZnO nanowires thin films produced by vapour transport and condensation process. These nanowires have diameters varying from 20 to 150 nm and have lengths up to 10 μm as shown in Fig 5. Under optical excitation, UV emission at room temperature was observed at 385nm with a linewidth less than 0.3nm from these ZnO nanowires films [12].

High carrier concentration is usually required in order to reach an optical gain that is high enough for lasing in a conventional laser diode operation. If the medium is in a lower dimension material, such as 1D (nanowires) or 0D (nanoparticles), reduction of lasing threshold and hence low power operation would be possible because of the quantum confinement effect. The quantum effect yields a substantial increase of density of states at the band edges and enhance radiative recombination due to carrier

confinement [12]. Segawa et al report the binding energy of ZnO/ZnMgO multi-quantum wells is greatly enhanced by quantum confinement effects [22].

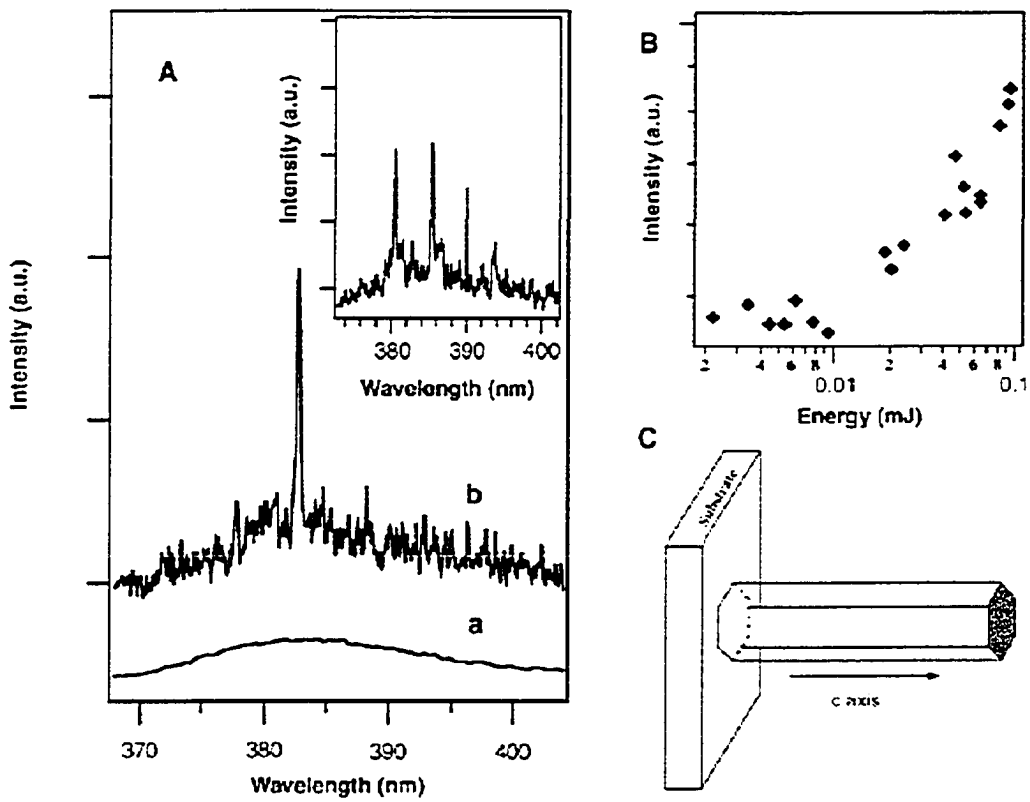

Fig 5 (A) Emission spectra from nanowires arrays below (line a) and above (line b and inset) the lasing threshold. The pump power for these spectra are 20, 100 and 150 KW/cm^2, respectively. (B) Integrated emission intensity from nanowires as a resonance cavity with two naturally faced hexagonal end faces acting as reflecting mirrors. Stimulated emission from the nanowires was collected in the direction along the nanowire's c-axis with a monochromator combined with a Peltier-cooled charge-coupled device. The 266 nm pump beam was focused to the nanowire area at an angle 10° to the c-axis at room temperature [12].

For all these devices, optically stimulated emission has been observed, but there is still no report of emission by electrically pumping. The main obstacle to create a ZnO LED and laser diodes is the difficulty of making good p-type ZnO. Some research groups have tried to produce p-type ZnO by doping acceptors such as N, As [23][24][25], or to enhance the n-type ZnO [26]. Efficient electrically pumped ZnO laser will probably await for the development of good p-type materials [27].

Many deposition techniques have been employed for the growth of ZnO thin film. These include pulsed laser deposition [28][29], magnetron sputtering [30], plasma-assisted Molecule Beam Epitaxy (P-MBE) [31], chemical vapor deposition (CVD) [32], and charged liquid cluster beam etc. Among these techniques, PLD is easy to use, is flexible, and can be used directly to produce nanostructure thin films.

It is known that ZnO exhibits three major luminescence emission bands: a UV near-band-edge (NBE) emission peak at approximately 380nm, a green emission and a red emission [33]. The green and red emissions are believed to be due to defects, which are related to excess zinc interstitials and oxygen vacancies in the film.

Generally speaking, the ZnO thin films, regardless of the growth technique used, contain defects of Zn interstitials and oxygen vacancies [34][35][36], which results in n-type ZnO thin film and reduces the UV emission of the film. During PLD, some amount of oxygen ambient gas is introduced to help reduce the oxygen vacancies in the film and hence improve the film crystallinity [37] [36].

Annealing process also plays an important role in the crystallinity and hence the photoluminescence emission [38]. ZnO thin films produced by pulsed laser deposition (PLD) are typically deposited at $\sim 10^{-1}$ torr O_2 with the substrate heated to temperatures of few 100 ^{0}C [5][34][36][39]. The effects of annealing on ZnO films deposited by PLD

with substrate heating have also been studied. It was found that annealing tends to increase the grain size of the ZnO crystals [38] and degrade the UV photoluminescence emissions while increasing the visible emissions when films were annealed at > 400 ^{0}C in oxygen background [9][40]. The photoluminescence (PL) spectra of ZnO films deposited at substrate temperatures of 400°C and annealed at various temperatures was reported and results are shown in Fig 6 [40]. The ratio of UV to green emissions from the ZnO thin films decreases as the annealing temperature increases [41] as shown in Fig 7. In contrast Liu et al reported that by annealing the zinc-implanted silica at 700°C in oxygen ambient for 2 hours, more intense UV emission was observed [42].

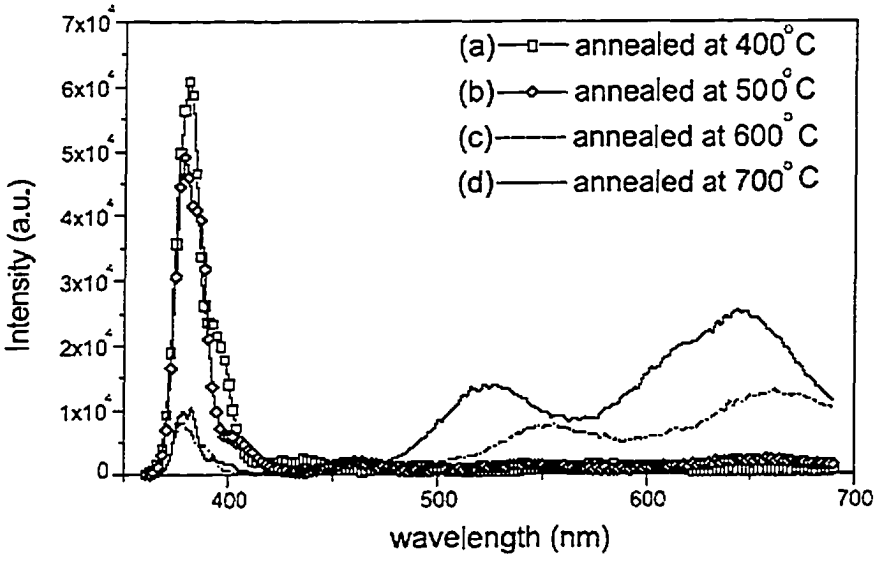

Fig 6 Photoluminescence spectra of ZnO thin films annealed at (a) 400°C, (b) 500°C, (c) 600 °C, (d) 700 °C [40].

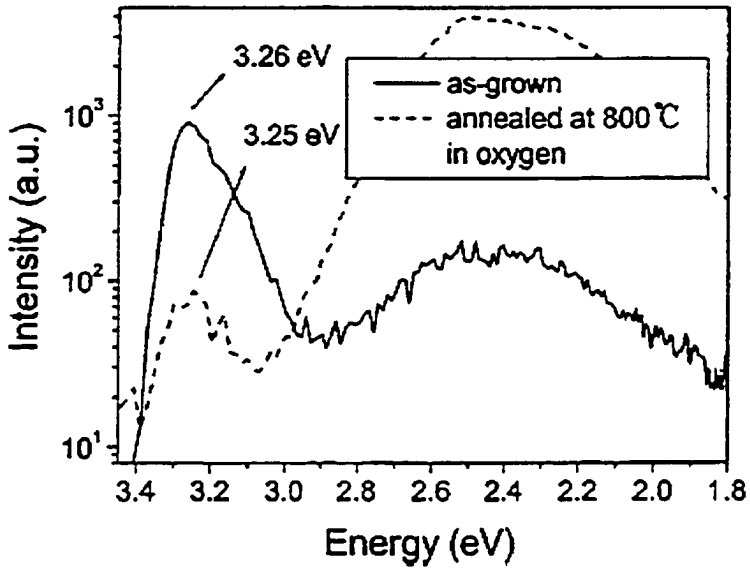

Fig 7 The photoluminescence spectra of as-grown and annealed ZnO films [41].

There are only a few published results on porous ZnO thin films produced by PLD. Yan et al. [43] reported the highly oriented Ga-doped ZnO nanorod arrays fabricated on GaN and sapphire substrates by PLD. Zinc oxide and gallium oxide targets were used to produce 0%-5% Ga doped ZnO films. Their best results were the 1% Ga doped ZnO film which consists of 40-60 nm diameter nanorod array produced in 10^{-2} torr O_2 partial pressure and at 750°C substrate temperature (see Fig 8). Hartanto et al. [44] reported ZnO film consists of 100 nm diameter nanorod grown by PLD with high background gas pressure of 5 torr, and substrate temperature of 600°C (see Fig 9). They suggested that high background gas pressure is essential for the nanoparticles form in the gas phase and high substrate temperature is essential for the nanoparticles to melted and form the nanorod film.

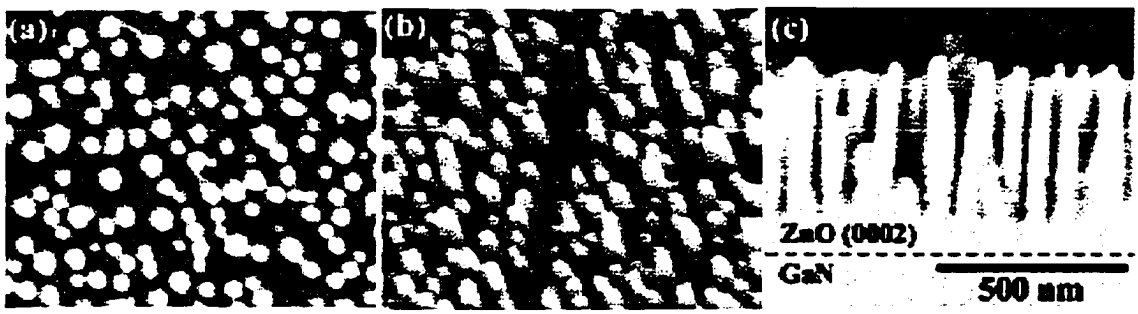

Fig 8 SEM images of 1% ZnO on C-plane GaN: (a) Top view, (b) 60° tilted view, and (c) cross-section view. The scale bar applies to all images [43].

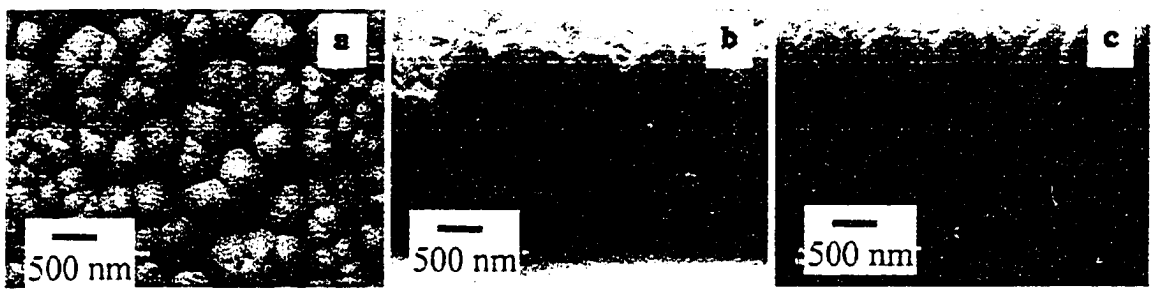

Fig 9 SEM images of ZnO rods. (a) Top view of the film deposited at 600°C for 10 min (Step 1), (b) Cross-section view of the film deposited at 300°C for 1 min after Step 1 (Step 2), nanoparticles stacked on top of the nanorods can be observed, (c) Cross-section view of the film annealed at 700°C for 20 min after Step 2, the nanoparticles disappeared [44].

1.5 Outline of this thesis

This thesis is divided into five chapters. Chapter 1 gives the introduction. Chapter 2 describes the Pulsed Laser Deposition experimental setup. Chapter 3 describes the equipments used for measuring the properties of the films. In Chapter 4, experimental results are presented and discussed. In Chapter 5 conclusions and recommendations for future work are presented.

Chapter 2 Pulsed Laser Deposition System

2.1 Setup for Pulsed Laser Deposition

The pulsed laser deposition (PLD) system basically consists of a pulsed excimer laser, a target and a substrate placed inside a vacuum chamber typically evacuated to ~10^{-5} Torr and then backfilled with O_2 in some cases as shown in Fig 10. Mirror and lens are used to direct and focus the laser beam onto the target surface. The focused laser beam is used to vaporize the target material to produce a vapour plume and thin films are formed when the vapour plume is condensed onto the substrate surface.

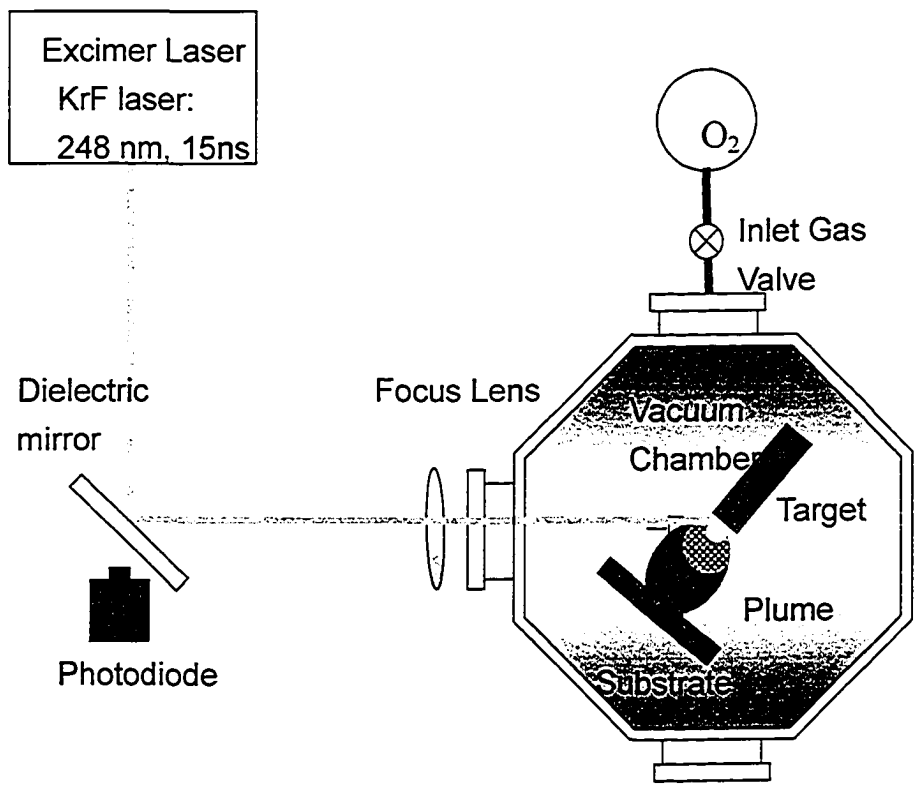

Fig 10 Schematic diagram of the PLD system

Typically, the plume consists of free electrons, ions, neutral atoms, molecules, clusters, and debris particles of various sizes (submicron to micron).

The important parameters in the formation of ZnO thin films are as follows:

I. Laser wavelength and fluence

Typically, laser light in the ultraviolet and near ultraviolet is used for PLD because most materials exhibit strong absorption in this spectral region. Normally, the absorption coefficient increases and the penetration depth decreases as the laser wavelength become shorter. Large absorption coefficient and small penetration depth are preferred since this leads to the lowering of the threshold fluence for material ablation, as well as decreasing the amount of mass ablated per laser pulse, giving a better control of thin films thickness.

For wavelength below 200nm (the vacuum ultraviolet regime), because of the strong absorption of oxygen, vacuum or nitrogen filled beam tubes must be used making experimental setup more complicated and expensive.

In our work, Krypton Fluoride (KrF) laser, emitting at 248nm, was used in the PLD experiments. The KrF laser is one of the most efficient UV laser systems.

Typically low laser fluence (or energy density i.e. energy per unit area) is kept as low as possible to avoid the generation of large amount of debris particles [45].

II. Background Gases

The background gas is also an important parameter that may influence the quality of the thin films deposited. Typically, oxygen is used as a reactive gas during ZnO film deposition.

The ZnO plume can experience photon and electron-impact decomposition during the ablation process producing atomic oxygen which may subsequently form molecular oxygen instead of recombining with Zn to form ZnO during the transfer to the substrate. This would lead to oxygen deficiency in the thin film [46]. The interaction of the plume with a reactive background gas is expected to play an important role in the production of

the precursors required for the oxidation process [47], and thus increase the oxygen content of the film. In addition, the oxygen background gas may also decrease the energy of the plume. The pressure of oxygen can also be used to tune the internal structure of ZnO film by increasing or decreasing the defects in the ZnO films.

Fig 11 is a picture taken during the ZnO film deposited in oxygen (10^{-1} torr). A much larger emission zone was observed for plasma plume in oxygen compared to that in vacuum, Fig 12.

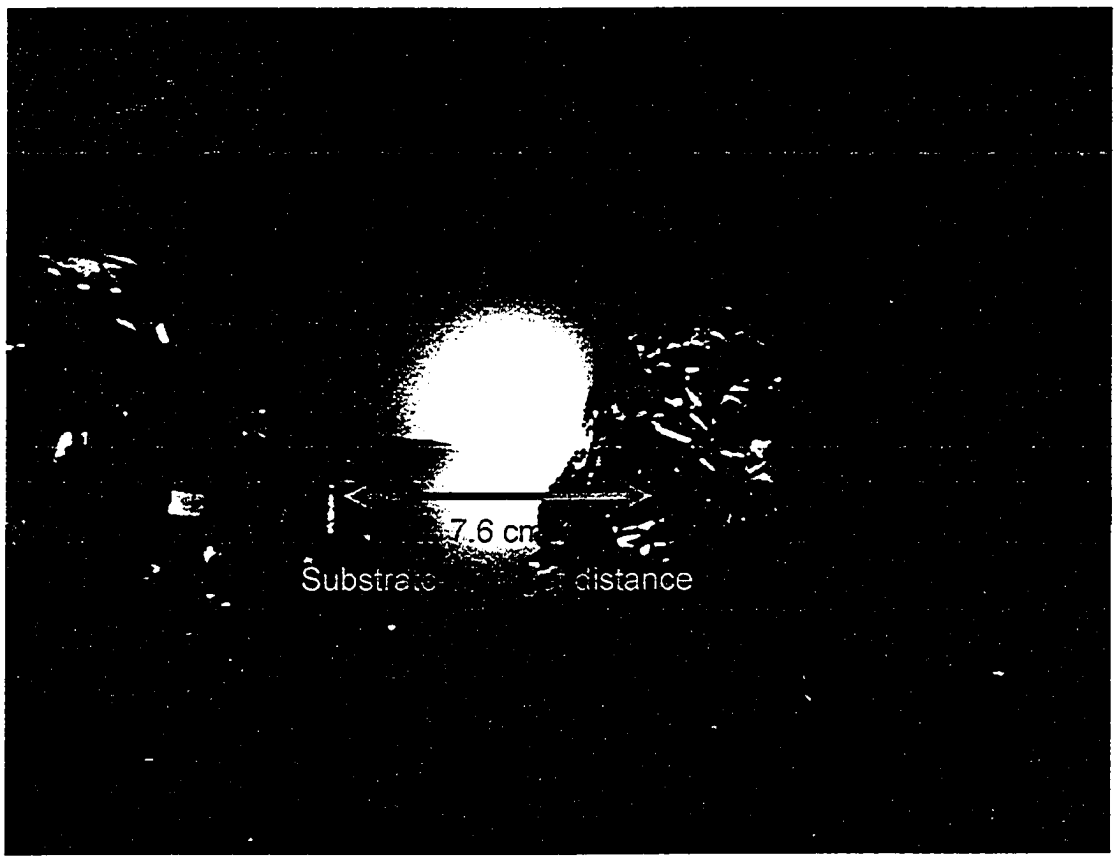

Fig 11 Plasma plume observed in 100m torr O_2 (laser fluence is 2.9 J/cm^2).

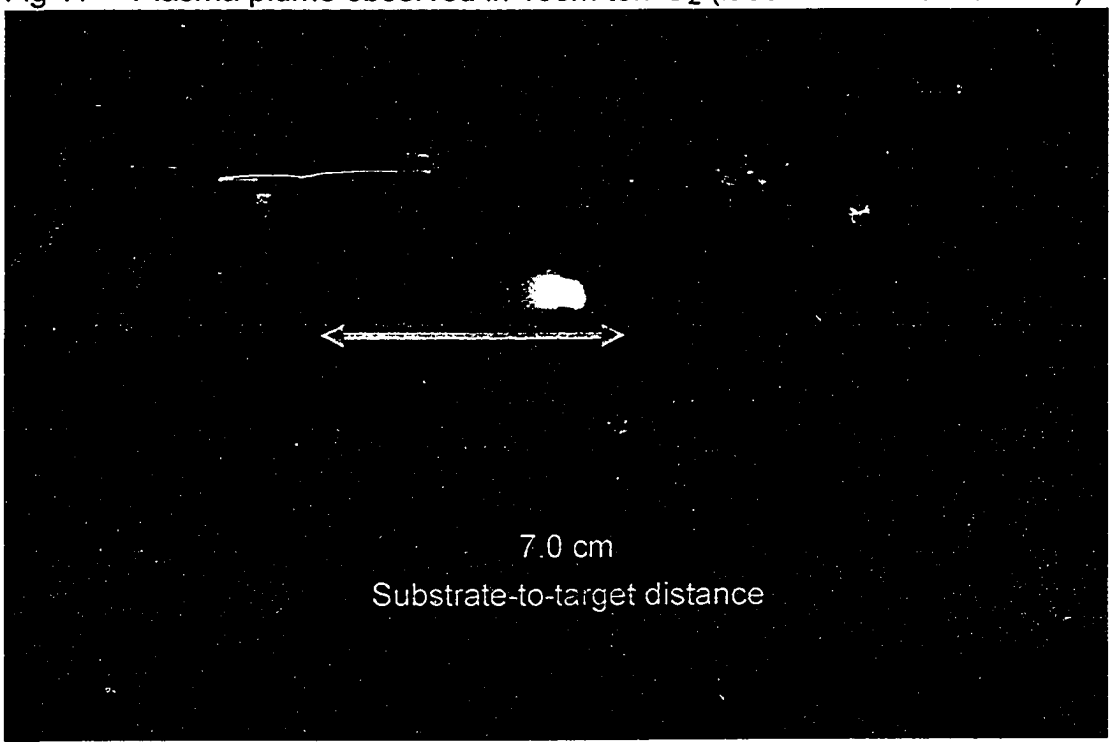

Fig 12 Plasma plume observed in vacuum (laser fluence is 3.0 J/cm^2).

2.2 Technique for the production of porous ZnO thin films

The substrate orientation angle is an important parameter for the generation of nanostructures. When the substrate surface is almost parallel to the axis of the expanding deposition plume, due to the self-shadowing effect, porous thin films can be created.

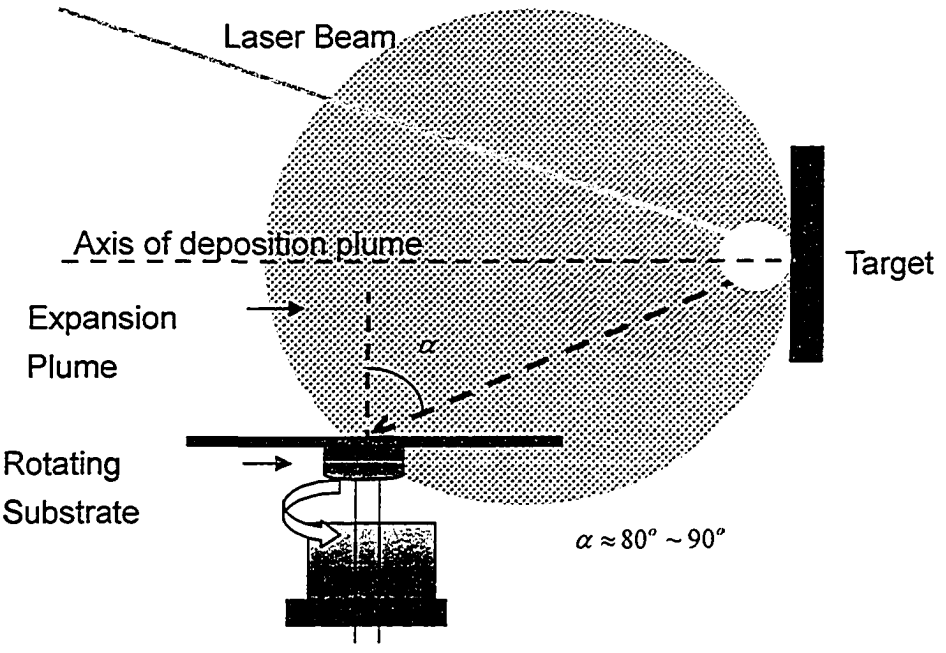

Fig 13 Setup for the production of porous thin films

2.2.1 Setup

The target and substrate are placed in a vacuum chamber as shown in Fig 13. Typically, the substrate is located ~5cm from the target surface. The target surface was oriented almost parallel to the axis of the deposition. Both target and substrate were rotating during the deposition. The target was rotating to avoid the formation of a deep laser ablated crater.

2.2.2 Mechanism-Adatom diffusion and Self-Shadowing effect

During deposition, the plume comes in contact with the substrate surface, and the growth of the thin film begins. There is an initial growth of spherical droplets on the substrate surface and this process is called nucleation as shown in Fig 14, where the nucleus start to form with a radius larger than the critical radius.

Adatom diffusion is the motion of adatoms, across the surface of the films, while in a physical absorbed state. Because of the excess energy of the textured surface, adatoms preferentially 'fill in' voids [48], i.e. the energy barrier to surface bonding from adtom is less at defect sites and step edges. This effect leads to surface roughening. But adatom diffusion tends to smooth film structure. The average distance that an adatom will diffuse on the film surface (adatom diffusion length) is controlled by the energy of the adatom, the binding energy for the film material and the deposition rate by the plume flux [49]. For the film with relaxation, i.e. the diffusion length is large enough for the atoms to diffuse over some range after initial contact with the film but are constrained to diffusion a single column, the resulting column structure has the column diameters are significantly larger than that of the initial nucleus.

This leads to a columnar film structure where the boundaries or voids between columns cannot receive flux. The shadowing effect becomes more pronounced for larger incident angle. The film becomes less dense as the incident flux angle α is increased. Fig 15 is a graph that presents the geometry of the shadowing effect for the film with relaxation (initial nucleus of diameter δ much smaller than the column diameter d), where α is the flux angle, β is the column angle, and $a \cdot d$ is the column spacing. Tait [50] developed an expression of the column spacing for the film with relaxation,

$$a = (1 + \frac{1}{\cos\alpha})/2$$

where d At small incident angles, $a \approx 1$, and the columns are in contact to form a dense film. When the vapour arrival angle is made very large >80 degree, significant changes result in film structure, and result in larger column spacing.

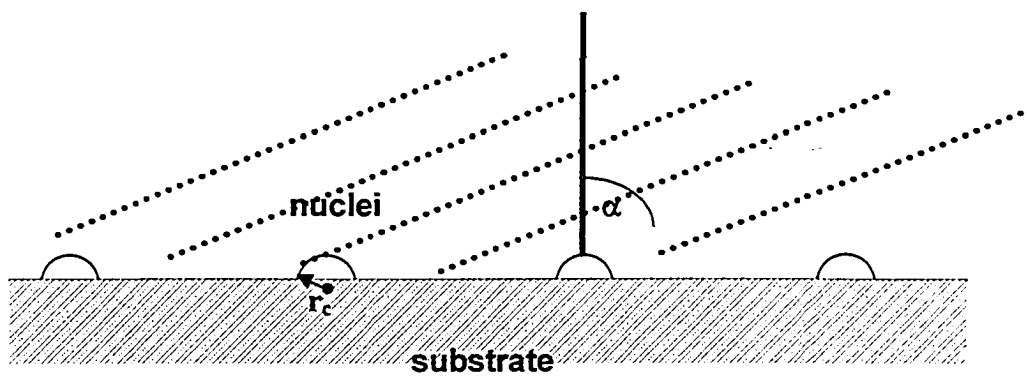

Fig 14 Schematic diagram illustrating the nucleus formation and self-shadowing effect, α is the flux angle, and r_c is the critical radius of the nuclei.

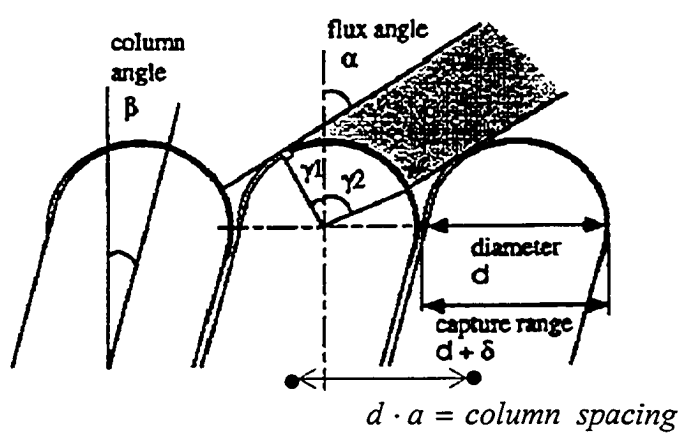

Fig 15 Geometry of the shadowing effect for films with relaxation [50]

2.3 Laser beam and plasma plume characterization

The laser beam and the deposition plume were monitored during the experiments. Schematics for the setup is shown in Fig 16, the label refer to debris shield window (DSW), chamber window (CW), photodiode (PD), calorimeter (C), Langmuir probe (LP), mirror (M), focus lens (FL), and wedge (W).

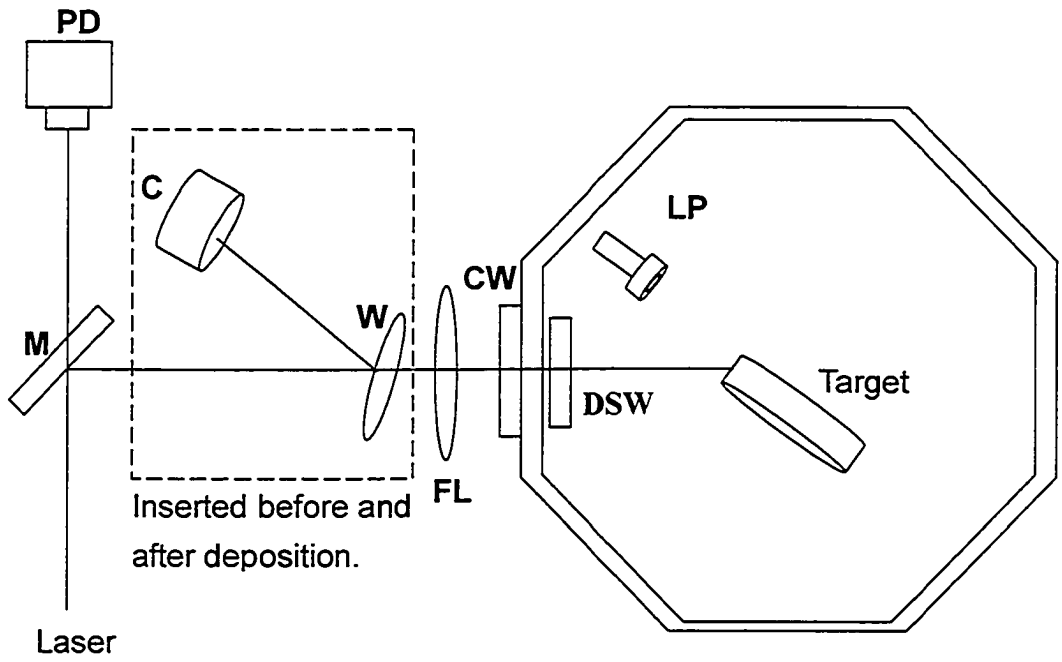

Fig 16 Schematic diagram for set up used to characterize laser beam and plasma plume.

A. Debris shielding window

A debris shield window (DSW) is placed in front of the chamber window in order to protect the more expensive chamber window (CW) not being coated during deposition. By rotating the DSW, the coating will be averaged out over a larger area on the DSW surface instead of forming a very thick coating spot on the DSW when it is not rotating.

The transmission of the DSW was measured after the deposition, typically the transmission of the DSW dropped from ~90% to ~80% after a run (~60,000 laser shots). The DSW was then cleaned with 13% Ammonia Bifluoride to increase the transmission of DSW back to ~90 %

B. Energy monitor-Calibrated Photodiode

The laser beam energy was monitored by a calibrated photodiode using leakage light from mirror (M) as shown in Fig 16. The photodiode was calibrated by placing a wedge in front of the chamber window to reflect 4% of the energy of the laser beam onto the calorimeter. The KrF laser typically gives laser energy of ~100mJ per pulse during the deposition.

C. Plasma characterization-Langmuir probe measurement

Langmuir probes normal to the target surface were placed inside the deposition chamber to study the plasma dynamics. The Langmuir ion probe was bias at around -90V to attract ions. Ion probe signals were recorded for three different pressures (base pressure $1x10^{-4}$ torr, $6.6x10^{-2}$ torr O_2, and 10^{-1} torr O_2) and at different target-to-probe distances. Generally speaking, the higher the chamber pressure and the longer the substrate-to-target distance, the fewer that plasma species that arrived at the substrate. Also the kinetics energy of the plasma varied with the pressure. Fig 17 shows the ion probe signals detected at chamber pressure of (a) 10^{-4} vacuum, (b) $6.6x10^{-2}$ torr O_2, (c) 10^{-1} torr O_2, with a target-to-probe distance of 3cm. Although the species of the plasma can not be distinguished, the results indicating that the total charge decreased with the increase of chamber pressure. As shown in Fig 17, at $6.6x10^{-2}$ torr O_2, the ion kinetic energy distribution is narrower that vacuum or at higher pressure. For pressure higher than 10^{-1} torr, the ion signals become very weak indicating low deposition states and

since good quality ZnO film cannot grow under vacuum condition, the pressure range of few times 10^{-2} torr was chosen for the growth of our ZnO films.

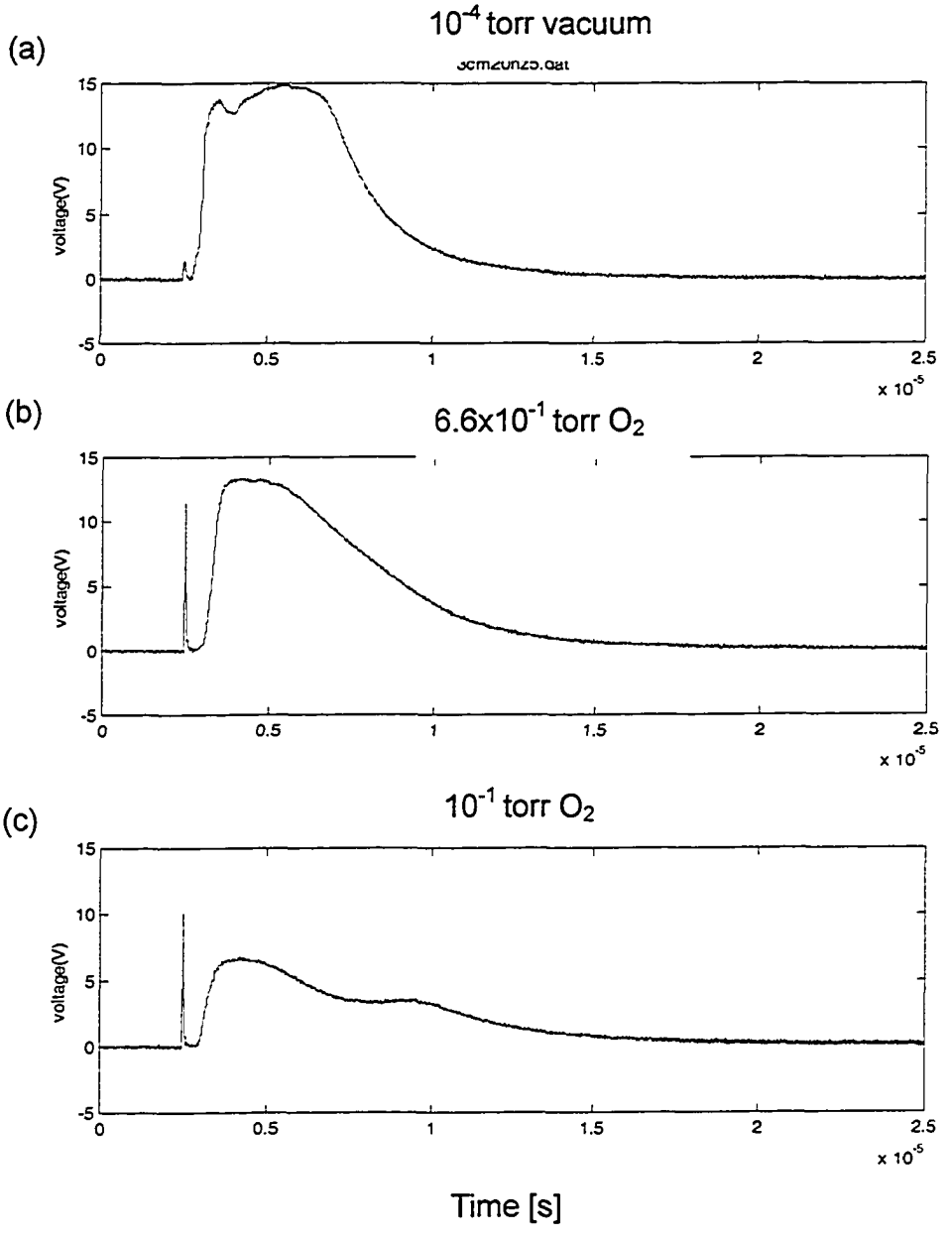

Fig 17 The Langmuir ion probe signals detected at chamber pressure of (a) 10^{-4} vacuum, (b) $6.6x10^{-2}$ torr O_2, (c) 10^{-1} torr O_2, with a target-to-probe distance of 3cm. The total charge decreased with the increasing of chamber pressure.

D. Laser focal spot measurement

The laser fluence was calculated based on laser energy and laser focal spot measurements. Typically the size of laser focal spot was determined by measuring the size of laser burn spot on a piece of paper at the location of the target surface. In order to verify that the laser spot size measured by this technique was accurate, a second experiment was conducted. The set up for this second experiment is shown in Fig 18. Wedges and neutral density filters were used to attenuate the laser beam energy so that it would not damage the CCD camera. The CCD camera (Cohu 6600 Monochrome progressive scan CCD camera) has 659x494 pixels and each pixel has an area of $9.9 \times 9.9 \mu m^2$. The CCD camera was located at the target position. The focal spot images recorded by the CCD camera were analyzed using a commercial software (Spircon).

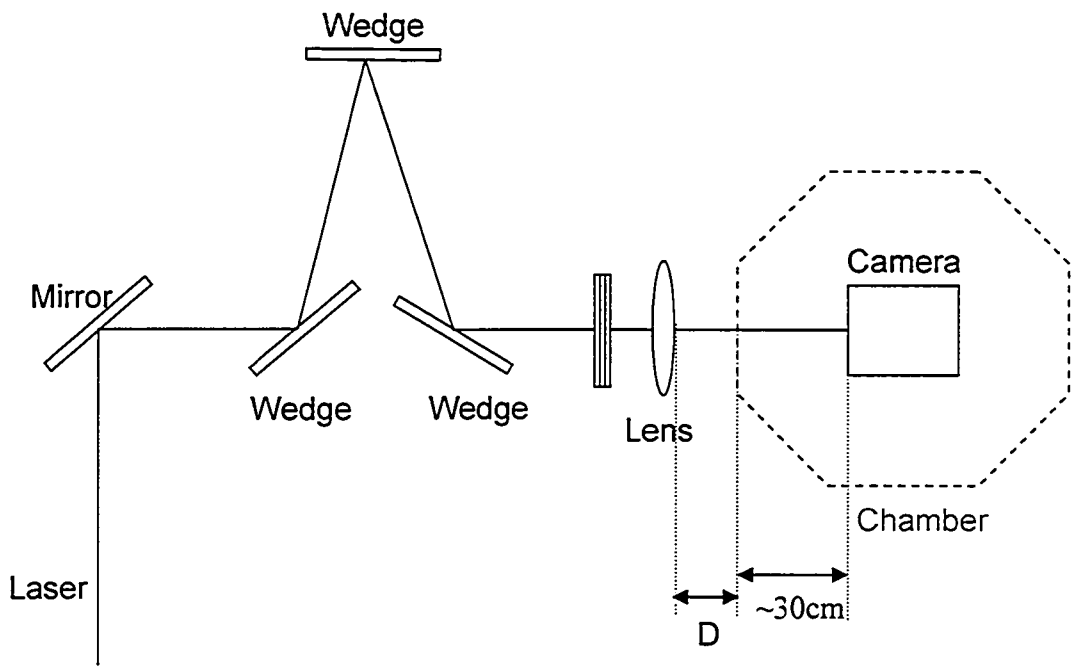

Fig 18 Diagram of setup used to measure the laser focal spot size.

The measured laser focal spot size versus lens position is summarized in Table 2.

Table 2 Laser spot sizes at 90% energy contour for different lens to target distance

D[cm]	Beam size [cm^2]
13.7	0.0546
14.6	0.0436
14.7	0.0440
16.6	0.0193
19.7	0.0018
19.9	0.0013
24.3	0.0270

The focal spot sizes measured by the more sophisticated CCD camera technique and the simple burn paper technique are summarized in Table 3 and Fig 19.

Table 3 The comparison of laser focal spot sizes between CCD and burn paper techniques.

Lens distance [cm]	Beam size [cm^2]		Laser fluence [J/cm^2]		Error %
	CCD 90% energy contours	Burn paper	CCD	Burn paper	Burn paper/ CCD
13.7	0.0546	0.0550	1.83	1.82	0.7
14.6	0.0436	0.0473	2.29	2.12	7.8
14.7	0.0440	0.0462	2.27	2.16	4.8
16.6	0.0193	0.0306	5.18	3.68	29.0
19.7	0.0018	0.0152	55.56	6.58	88.2
19.9	0.0013	0.0140	76.92	7.14	90.7
24.3	0.0270	0.0405	3.70	2.47	33.3

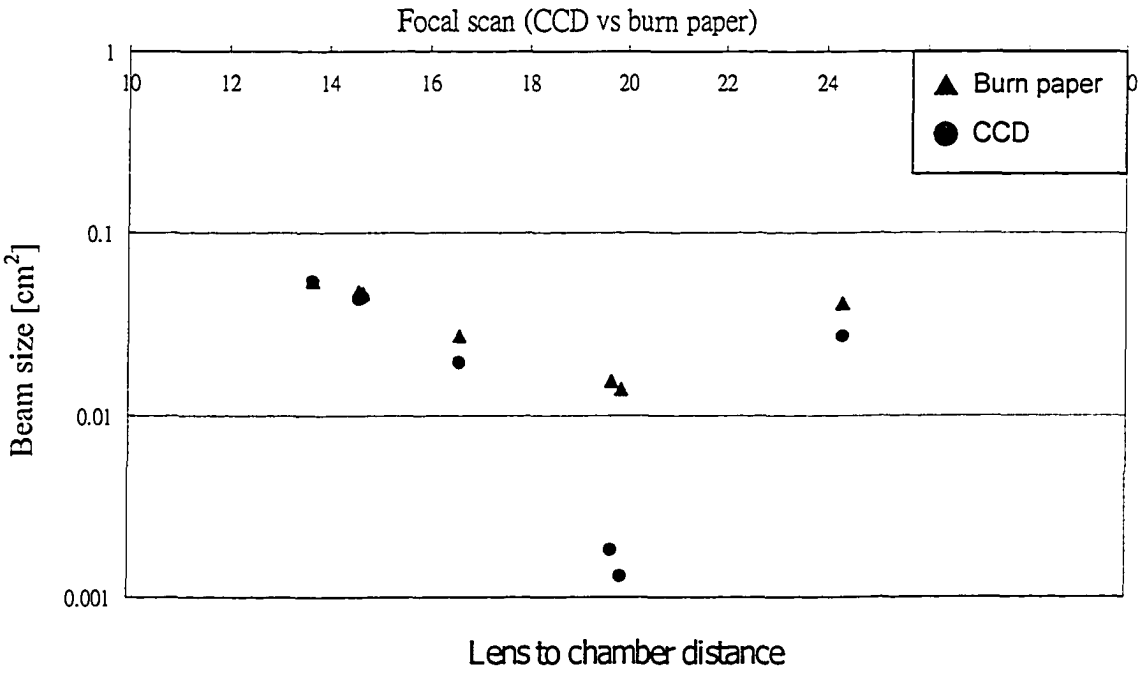

Fig 19 The focal scan plot

The beam size measured by CCD technique is close to the beam size measured by burn paper at lower laser fluence (1-5 J/cm^2). For higher fluence (around the laser focal point), the beam size measured by burn paper could be order of magnitude larger than the beam size measured by the CCD technique. Generally, the laser fluence that was reported by many other groups was based on the burn paper technique

Chapter 3 Film characterization techniques

3.1 Morphology –Scanning electron microscope (SEM)

The morphology of the film was characterized by the scanning electron microscope (SEM) made by JEOL and the model is JSM6301FXV (Field Emission Scanning Electron Microscope). The electron accelerating voltage used for generating the SEM images was 5KV and the magnifications of the images are 1,000x ~ 100,000x. When an electron beam interacts with materials, there's secondary electrons from the material at the depth of ~50 Å. The SEM image is formed by detecting the secondary electron beam generated by the bombardment of the electron beam. The thickness of the ZnO thin film could also be determined from the SEM image of its cross-section of a sample.

3.2 Crystalline structural property-X-ray Diffraction (XRD)

The crystalline structure of the film was characterized by using the X-ray diffraction (XRD) technique (Rigaku, Model Geigerflex 2173, Vertical Gonimeter type). X-ray source used is Cobalt, $k\alpha$ wavelength $\lambda = 1.79021$ Å, which provides longer wavelength X-ray light source than that of a Cu source. The system has an online computer for data processing, and routine search/match procedures of diffraction patterns using the JCPDS database, which is an online international X-ray diffraction database. Table 4 is the ZnO PDF file from the JCPDS database. The database is the X-ray diffraction pattern of the hexagonal ZnO powder. It has main peaks index at (h,k,l)=(100), (002), (101). Each index represents a facet in the ZnO crystal structure. For example, the (002) facet has the c-axis growth direction. Fig 20 gives the XRD pattern of the ZnO target powder, which shows the peaks in the XRD patterns of the ZnO powder pattern

match those in the JCPDS database.

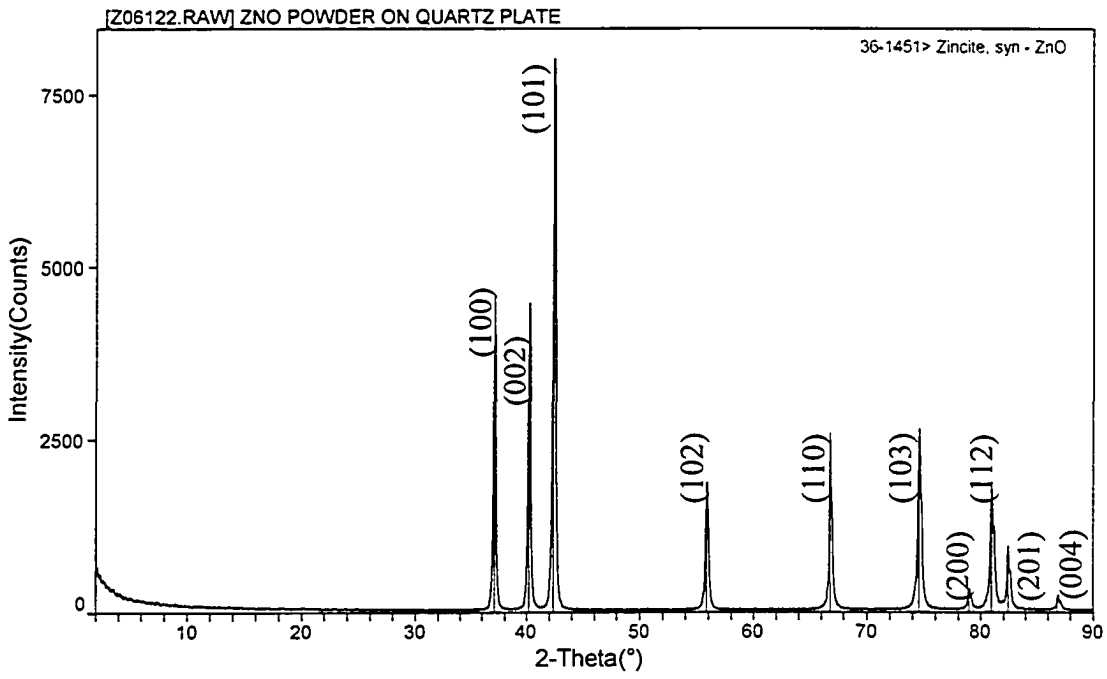

Fig 20 XRD diffraction pattern of ZnO powder (from the ZnO PLD target), this shows that the pattern matches the ZnO data baselines (h, k, l) as listed in Table 4.

Table 4 The ZnO PDF card from the XRD database

PDF#36-1451: QM=Star(S); d=Diffractometer; I=Diffractometer — PDF Card

Zincite, syn — mWTZsWTZ

Zn O

Radiation=CuKa1 — Lambda=1.5405981 — Filter=Graph

Calibration= — d-Cutoff=17.7 — I/Ic(RIR)=

Ref: McMurdie, H., Morris, M., Evans, E., Paretzkin, B., Wong-Ng, W., Ettlinger, L., Hubbard, C.

Powder Diffraction, 1 76 (1986) — CAS#1314-13-2

Hexagonal - Powder Diffraction, P63mc (186) — Z=2 — mp=

CELL: 3.24982 x 3.24982 x 5.20661 <90.0 x 90.0 x 120.0> — P.S=hP4 (S Zn)

Density(c)=5.675 Density(m)=6.43A Mwt=81.38 Vol=47.62 — F(27)=130.7(.0071,29)

Ref: 1. Bragg, W.

Philos. Mag., 39 647 (1920)

NOTE: The sample was obtained from the New Jersey Zinc Co., Bethlehem, Pennsylvania, USA. The structure was determined by Bragg (1) and refined by Abrahams, Bernstein (2). A high pressure cubic NaCl-type of ZnO is reported by Bates et al. (3) and a cubic, sphalerite type is reported by Radczewski, Schicht (4). The approximate temperature of data collection was 26 C. To replace 5-664 (5) References to other early patterns may be found in reference (5).

Color: Colorless

Strong Line: 2.48/X 2.81/6 2.60/4 1.62/3 1.48/3 1.91/2 1.38/2 1.36/1 0.91/1 1.09/1

27 Lines, Wavelength to Compute Theta = 1.78897A(Co), I%-Type = Peak Height

#	d(A)	I(f)	(h k l)	2-Theta	Theta	1/(2d)	#	d(A)	I(f)	(h k l)	2-Theta	Theta	1/(2d)
1	2.8143	57.0	(1 0 0)	37.064	18.532	0.1777	15	1.0423	6.0	(2 1 1)	118.234	59.117	0.4797
2	2.6033	44.0	(0 0 2)	40.192	20.096	0.1921	16	1.0159	4.0	(1 1 4)	123.391	61.696	0.4922
3	2.4759	100.0	(1 0 1)	42.357	21.178	0.2019	17	0.9846	2.0	(2 1 2)	130.581	65.290	0.5078
4	1.9111	23.0	(1 0 2)	55.814	27.907	0.2618	18	0.9766	5.0	(1 0 5)	132.664	66.332	0.5120
5	1.6247	32.0	(1 1 0)	66.809	33.405	0.3077	19	0.9556	1.0	(2 0 4)	138.793	69.397	0.5232
6	1.4771	29.0	(1 0 3)	74.536	37.269	0.3385	20	0.9381	3.0	(3 0 0)	144.912	72.456	0.5330
7	1.4072	4.0	(2 0 0)	78.940	39.470	0.3553	21	0.9069	8.0	(2 1 3)	160.985	80.492	0.5513
8	1.3782	23.0	(1 1 2)	80.936	40.469	0.3628	22	0.8826	4.0	(3 0 2)	—		
9	1.3583	11.0	(2 0 1)	82.380	41.190	0.3681	23	0.8677	1.0	(0 0 6)	—		
10	1.3017	2.0	(0 0 4)	86.809	43.405	0.3841	24	0.8370	3.0	(2 0 5)	—		
11	1.2380	4.0	(2 0 2)	92.526	46.263	0.4039	25	0.8293	1.0	(1 0 6)	—		
12	1.1816	1.0	(1 0 4)	98.401	49.200	0.4231	26	0.8237	2.0	(2 1 4)	—		
13	1.0931	7.0	(2 0 3)	109.827	54.914	0.4574	27	0.8125	3.0	(2 2 0)	—		
14	1.0638	3.0	(2 1 0)	114.451	57.226	0.4700							

Department of Earth & Atmospheric Sciences

[X-RAYLAB] Monday, Nov 24, 2003 02:31p (MDVJADE6)

3.3 Compositional properties-Electron Microprobe Analysis

The composition of the films was characterized by the electron microprobe (JXA 8900 Superprobe). It is a high resolution SEM combined with an electron probe microanalyzer (EPMA) with five wavelength dispersive spectrometers (WDS), an energy dispersive spectrometer (EDS), and cathode luminescence detector. The diagnostics used for characterizing our samples are the wavelength dispersive X-ray analysis (WDX), which provides better detection limits than the energy dispersive X-ray analysis (EDX). The detection limit of the quantitative analysis is typically at the level of a tens to hundred part per million (ppm) by weight. Electron microprobe was used to quantitatively analyze the composition of ZnO and to give the atomic ratio of zinc and oxygen in the films. The analysis is done by characterizing the X-rays emitting from the sample while there is an electron beam (0.2-40KeV) bombarding the sample (Fig 21).

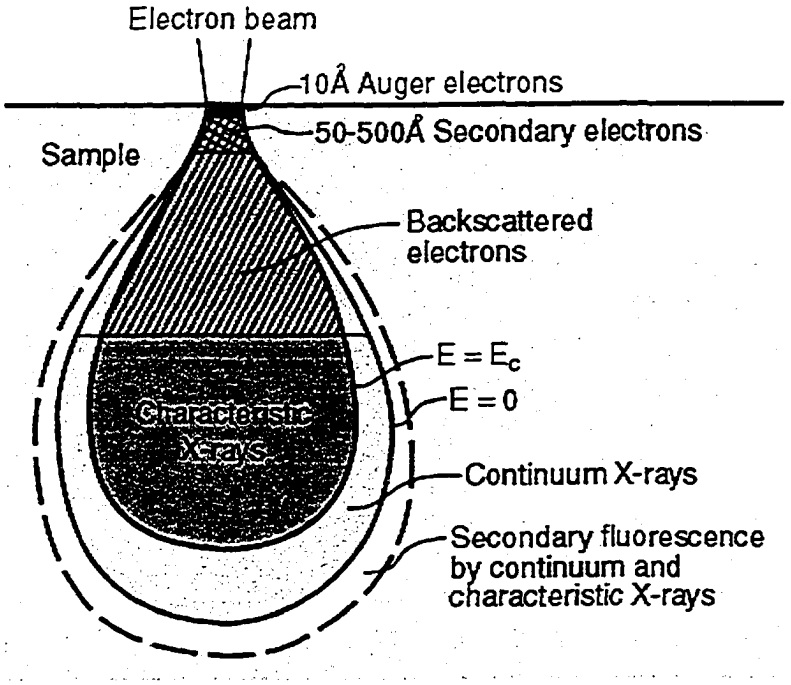

Fig 21 The electron beam and matter interaction. The Auger electron emerges from a very thin region of the sample surface (maximum depth about 50 Å) compared to the secondary electrons (50-500 Å) [51].

For the compositional analysis of our ZnO sample, the qualitative analysis was based on the standard data of quartz (SiO_2) for the calibration of oxygen element, and a Zinc metal sample for the calibration Zn element.

3.4 Optical properties

3.4.1 Room Temperature Photoluminescence

The room temperature (RT) photoluminescence of the ZnO thin films is characterized using a setup as shown in Fig 22. A 4ω Nd:YAG laser (266nm, 20Hz, 20ns, 3.3 mJ/pulse) was used to excite luminescence of the film. Two high reflectivity mirrors (HR 268nm) were placed in front of the laser to direct the laser beam. Collimating spherical mirrors were used to collect the photoluminescence signal emitted from the sample. A filter set was placed in front of the 400μm diameter optical fiber to remove the scattered laser light.

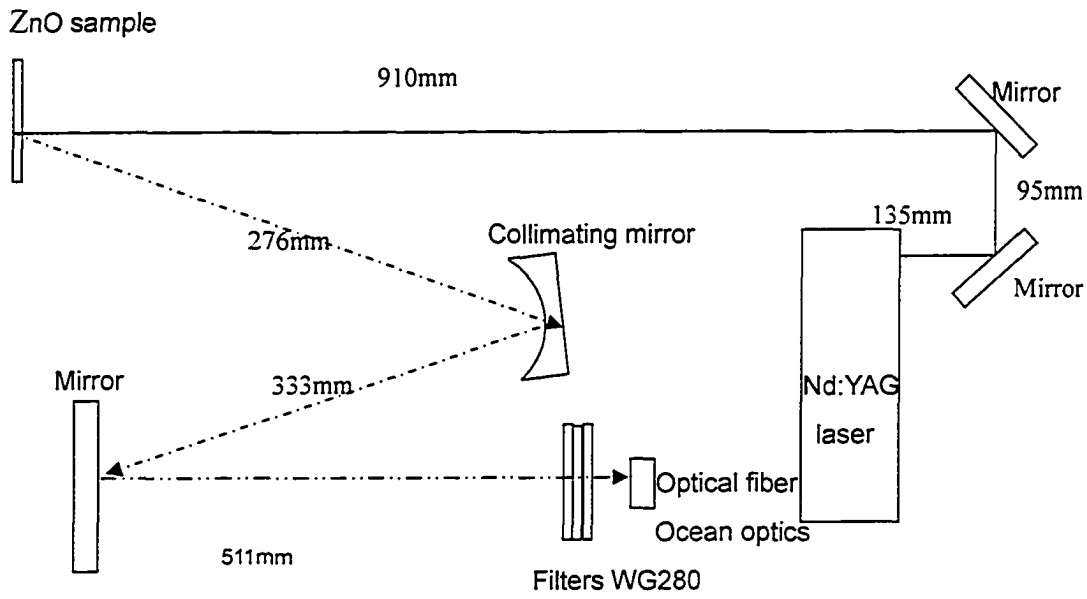

Fig 22 Photoluminescence measurement setup

A spectrometer (Ocean optics, bandwidth 200-850nm, 8nm resolution, 200μm entrance slit, coupled to the optical fiber) was placed after the filter set. A typical photoluminescence spectra of ZnO powder (from ZnO PLD target) was shown in Fig 23.

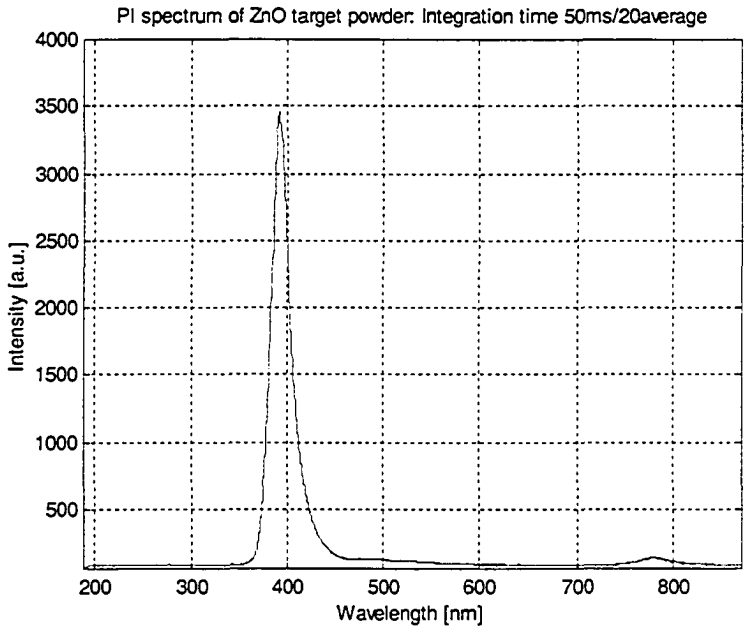

Fig23 Photoluminescence spectra of ZnO powder (grained from the ZnO PLD target) shows a single peak at 388 nm.

3.4.2 Absolute photoluminescence measurement

The absolute photoluminescence of the ZnO thin film was measured using the setup shown in Fig 24 to determine the numbers of photons per steradian. A 4ω Nd:YAG laser, (266nm, 15ns, 1.37 mJ/pulse), was used to excited luminescence emission from the ZnO thin film placed in front of a photomultiplier tube (PMT). The PMT used in the experiment is RCA-7265, a 14-stage, 2"-diameter type PMT. The spectral range of the PMT is 300-800 nm. The RCA 7265 PMT employs a multialkali photocathode providing high quantum efficiency and sensitivity. The PMT has its highest quantum efficiency (~19%) at 400 nm, making it suitable for our measurement at 380nm.

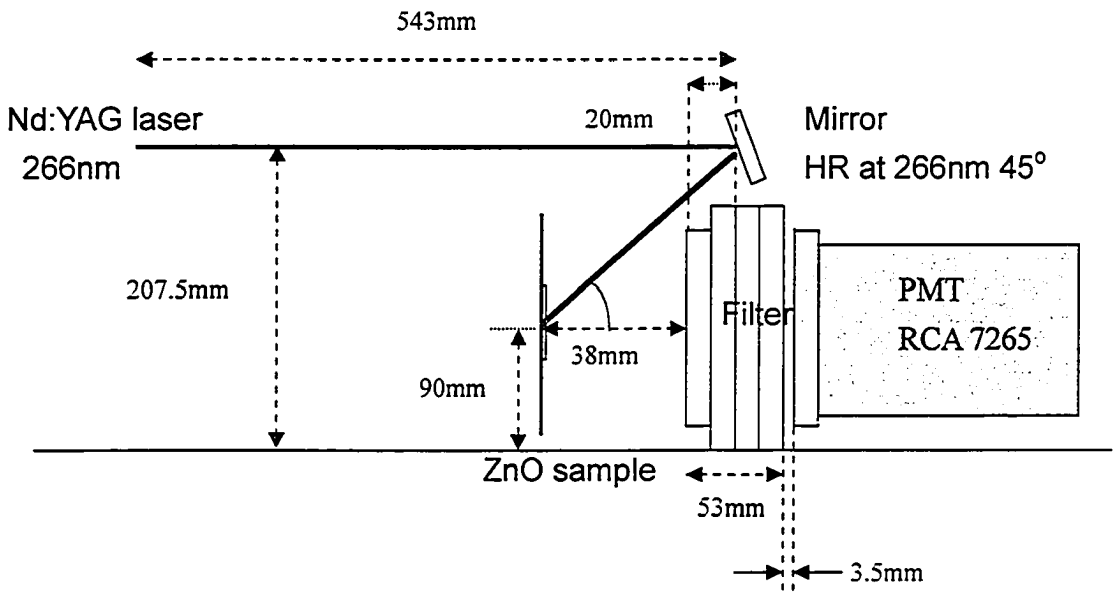

Fig 24 Absolute photoluminescence measurement setup.

A set of filters was placed in between the sample and the PMT. The filter set consists of several high pass and low pass filters to create a band pass filter with a transmission

band from 350-390nm. The transmission of the filters was characterized by a Lambda 900 spectrophotometer.

The PMT is negatively biased from –700 to –900V and the PMT output was connected to an oscilloscope terminated at 50 Ω. Photoluminescence from the ZnO target powder is shown in Fig 25 as an example.

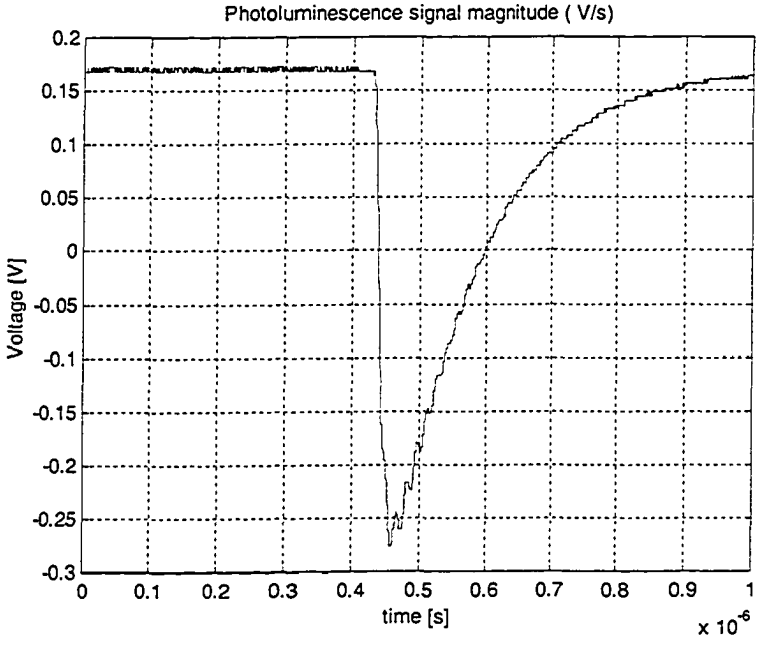

Fig 25 Photoluminescence signal from ZnO target powder detected by the PMT.

The schematic diagram for the setup of the absolute photoluminescence measurement is shown in Fig 26. The light emitted from the ZnO sample (D) were spectrally limited by a band pass filter set (C), and then geometrically limited by the entrance window of the PMT (B). To convert the oscilloscope signal (A) in volts to number of photons emitted from the ZnO sample, we need to accurately measure the distance from the ZnO sample surface to the entrance window of the PMT, the size of the PMT entrance window, the transmission of the filters, and the sensitivities $G(\lambda,V)$ of the PMT.

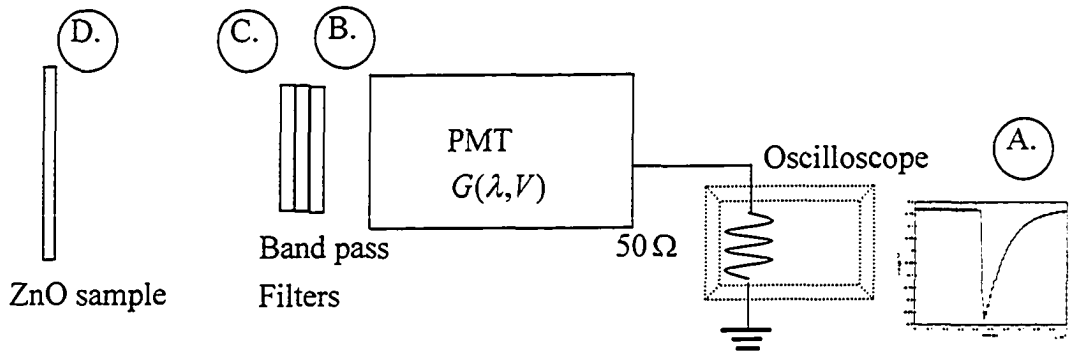

Fig 26 The system diagram of the absolute photoluminescence measurement.

Number of photons recorded by the PMT (A-B):

The total charge detected by the PMT is given by

$$V = IR$$

$$\int V\,dt = R\int I\,dt$$

$$Charge = \int I\,dt = \frac{1}{R}\int V\,dt$$

where V is the output of the PMT in volts, $R = 50\,\Omega$ is the resistance of the oscilloscope, and t is the time.

The PMT was calibrated, and the calibration was carried out by another graduate

student (Mike Taschuk) at 337nm with –1500 V bias. Number of photons detected by the PMT as a function of $\int Vdt$ (Vns) is shown in Fig 27.

The number of photons detected by the PMT at wavelengths different from 337 nm can be determined by using the relative sensitivity curve in Fig 28. The relative sensitivity is 58.5% at 337 nm, and 94% at 388nm. The ratio of sensitivities for wavelength 388nm to 337 nm for the same PMT bias is $G(388nm,V)/G(337n,V)=1.61$ (ie the PMT is more sensitive to 388nm photons) For example, if $\int Vdt$ is 20.8 Vns, according to Fig 27, the number of 377nm photons that entering the PMT will be 11,218 photons and the number of 388 nm photons should be 11,218/1.61=6,986.

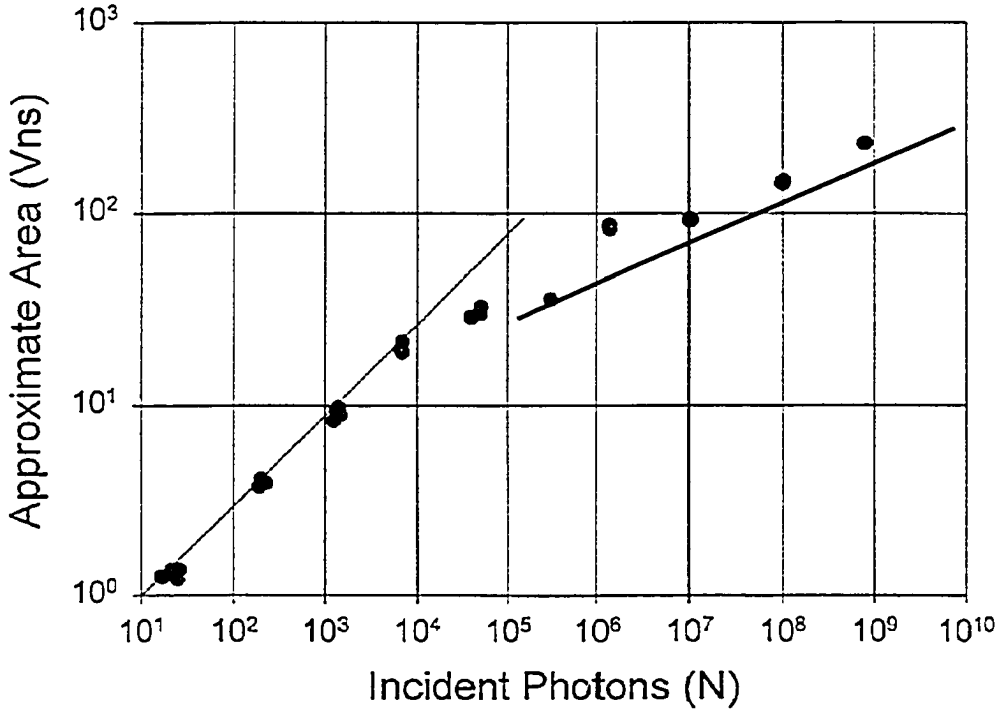

Fig 27 Calibration curve for RCA 7265 PMT. The linear region has a slope of 0.43, and the second linear region has a slope of 0.22.

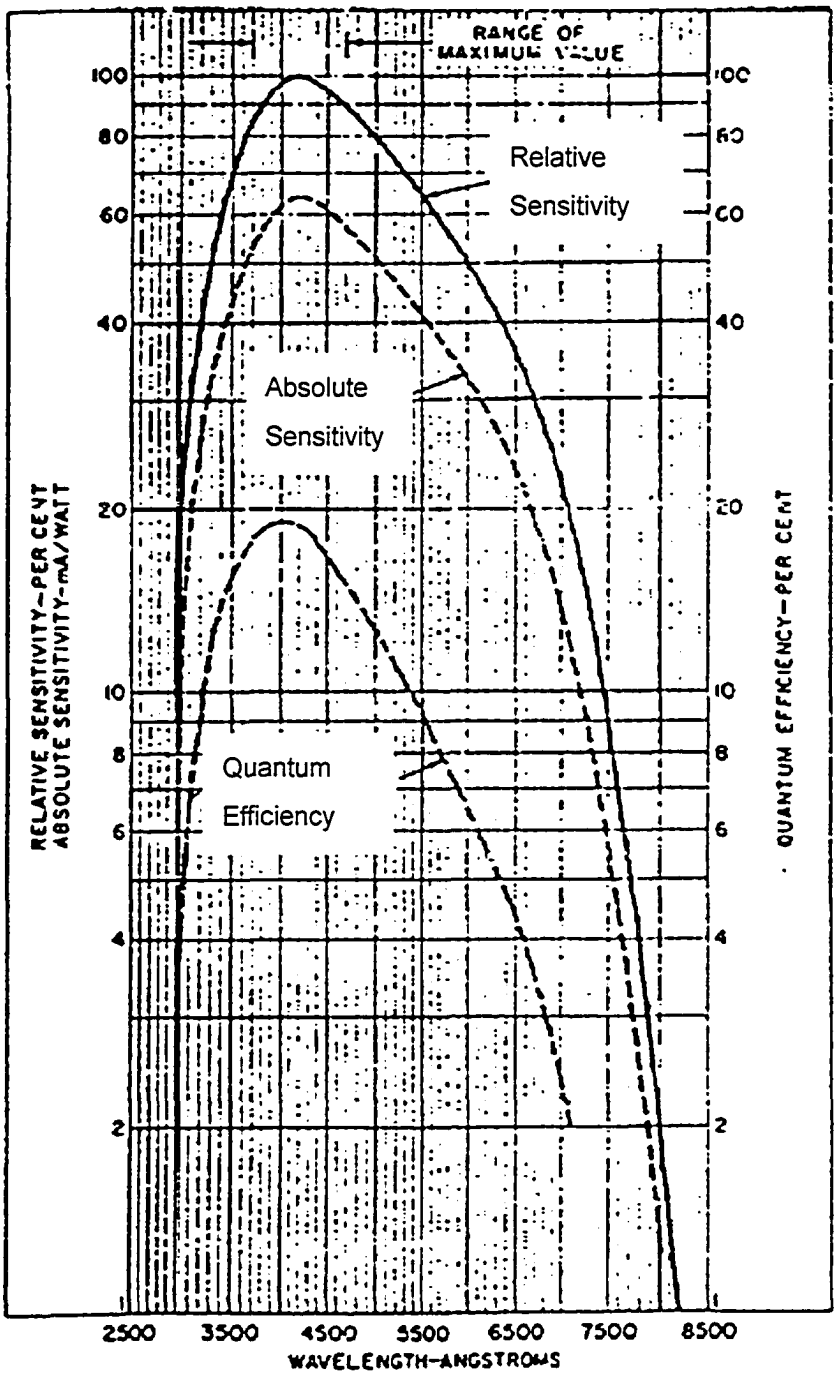

Fig 28 Typical spectral response characteristics of RCA- 7265 PMT

The sensitivity and current amplification characteristics of the PMT as a function of power supply voltage, $G(V)$, is shown in Fig 29. The current amplification to supply voltage is a straight line when plotted in log-log scale, which is $\log G(V) = a \cdot \log V + C$,

where V is the supply voltage, $G(V)$ is the gain, a and c are constants. From the typical sensitivity line B in Fig 29, find the slope a=11.8. Thus the gain equation is

$$\log G(V) = 11.8 \cdot \log V + C$$

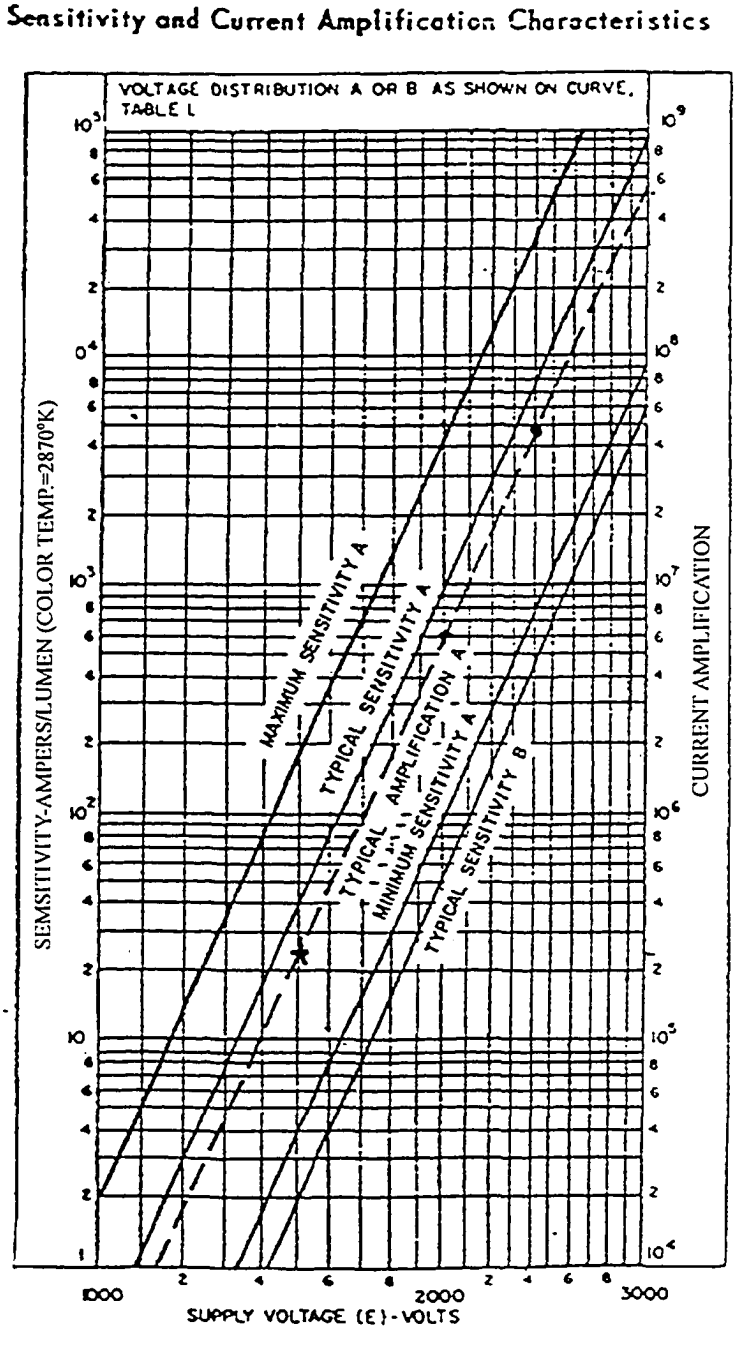

Fig 29 Sensitivity and current amplification characteristics of RCA 7265 PMT

So the gain difference of the PMT between the two different bias voltages is

$$\frac{G(V_2)}{G(V_1)} = \frac{V_2^{11.8}}{V_1^{11.8}}$$

The correction factor for operating at bias voltages different from –1500V is summarized in Table 5.

Table 5 The gain G(1500)/G(V) ratio.

Gain ratio	
G(1500)/G(1100)	39
G(1500)/G(1000)	120
G(1500)/G(900)	414
G(1500)/G(800)	1662
G(1500)/G(700)	8036
G(1500)/G(600)	49533

With the correction factors, the number of incident photons (wavelength 388nm) at any bias voltage can be calculated from the area of PMT signal.

Thus if $\int Vdt$ =20.8 Vns for 388nm photons was actually detected with a -800V bias on the PMT instead of -1500V, the number of photons would be 6,986x1662=1.2 x10^7 instead of 6,986.

Numbers of photons emitted by the ZnO sample (C-D):

The transmission of the band pass filter is shown in Fig 30, and the transmission at 388 nm is 6.15%. Note the photoluminescence spectrum peaked at 388 nm.

If PMT detected $8.6x10^6$ 388 nm photons, the number of photons before entering the band pass filter should be $1.2x10^7/6.15\%=1.9x10^8$.

The solid angle subtended by the PMT is 15^0 as shown in Fig 31. The numbers of photons per steradian that emitted form the ZnO film is $1.9\times10^8 \div \frac{\pi x^2}{d^2} = 3.4\times10^9$ photons. Assume the radiation is isotropic and is emitting only from the front surface of the film (half sphere), the total number of photons that emitted from the film is $3.4\times10^9 \times 2\pi = 2.1\times10^{10}$ 388nm photons, and this corresponds to about 8nJ energy.

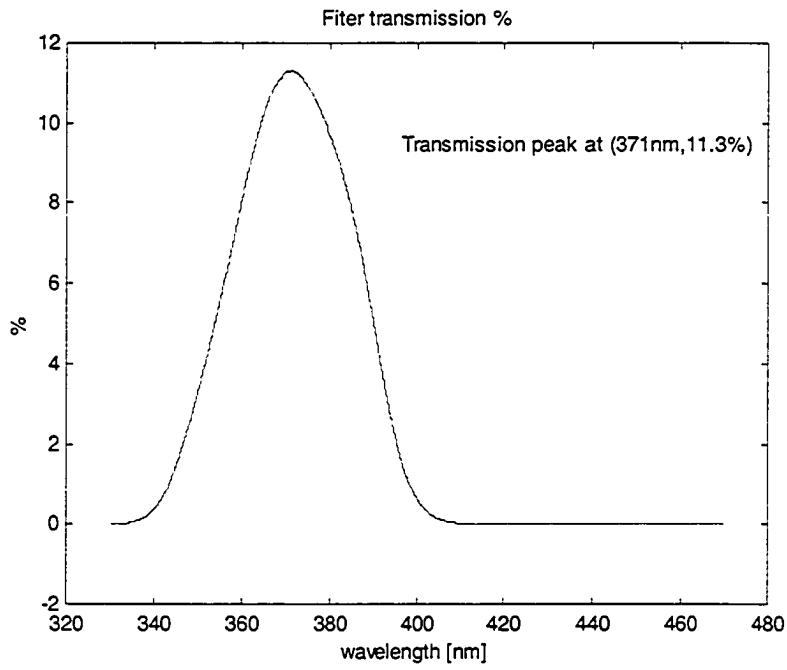

Fig 30 Transmission curve for the filter set

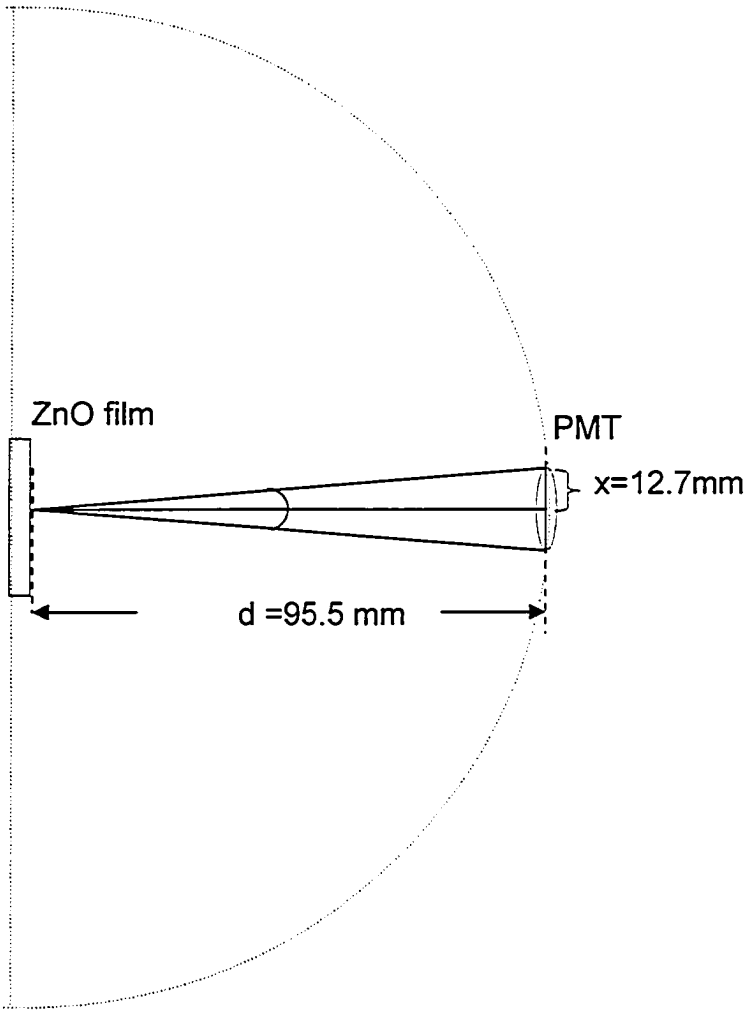

Fig 31 The solid angle subtended by the PMT is $\frac{\pi x^2}{r^2}$. Assume the photoluminescence is isotropic emitting from the front surface of the ZnO thin film

Chapter 4 Results and Discussion

4.1 Dense ZnO thin films

4.1.1 Fabrication Procedures

The substrate materials used in most of our experiments were Si wafers, made by Silicon Valley Microelectronics, Inc. They were p-type, <100> orientation, Si substrates (Appendix A). Before deposition, the Si wafers were clean by Piranha, which is a 3:1 ratio of Sulfuric acid and Hydrogen Peroxide. This solution is for cleaning all organic contamination. After cleaning the wafer was diced to 1cm by 1cm pieces for deposition. The arrangement of the substrates on the substrate mount and the setup of target and substrate are shown in Fig 32, and Fig 33.

All the experiments were done with KrF excimer laser. First, the chamber was pumped down to base pressure ~10^{-5} torr. After the pressure stabilized the deposition process began. For experiment I, the films were deposited under vacuum. For experiment II and III, oxygen was injected into the vacuum chamber continuously while the chamber was concurrently pumped to keep the chamber pressure of 10^{-1} torr and $6.6x10^{-2}$ torr respectively. The target was rotating at 3.37 r.p.m. to ensure a uniform ablation of the target. The substrate was stationary and 2-6 cm away from the target. After the depositions, ZnO thin films were annealed in an oven at 600°C in air for 2 hours. The deposition conditions are listed in Table 6.

The deposition rate varies with the background pressure. The deposition rate of the film deposited in vacuum is higher that that of the film deposited in 10^{-1} torr O_2.

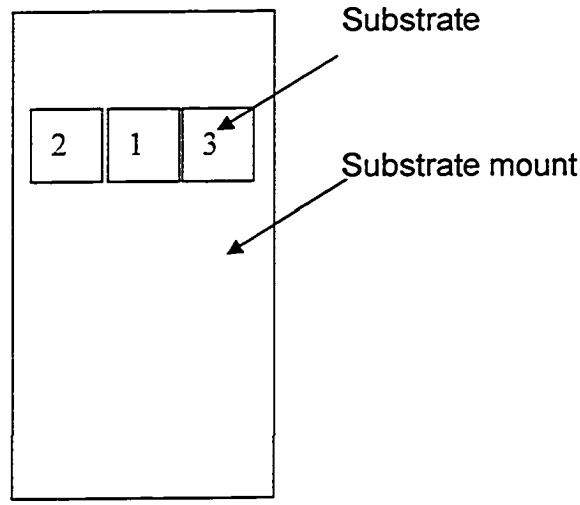

Fig 32 The arrangement of substrates on the substrate mount.

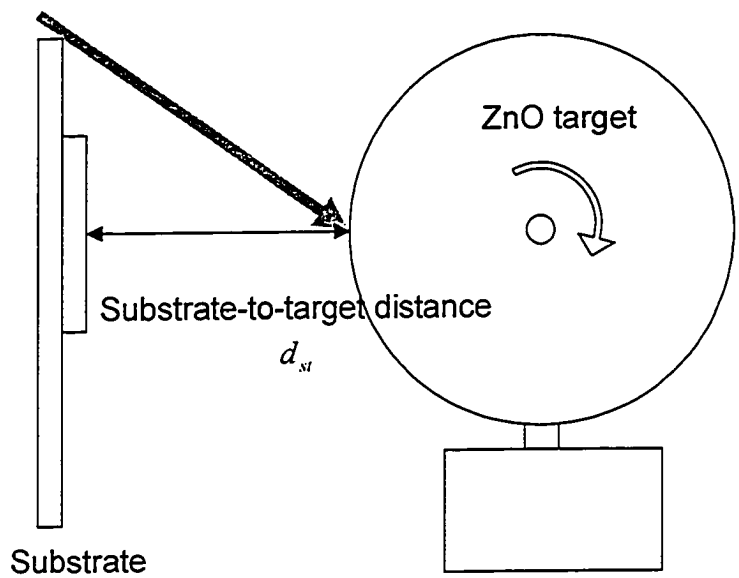

Fig 33 ZnO pulsed laser deposition target and substrate set up

Table 6 ZnO pulsed laser deposition experimental conditions

Exp. #	Sub. #	Sub. Mater.	Pressure [torr]	Laser fluence	d_{st}	Laser repetition rate	Thickness [nm]	Deposition rate [Å/pulse]
I	1	Si	$8.0x10^{-5}$	3.3 J/cm^2	2.0 cm	30Hz	940	0.26
	2	Si	$8.0x10^{-5}$	3.3 J/cm^2	2.0 cm	30Hz	940	0.26
	3	Si	$8.0x10^{-5}$	3.3 J/cm^2	2.0 cm	30Hz	940	0.26
II	1	Si	O_2, $1.0x10^{-1}$	5.7 J/cm^2	2.0 cm	30Hz	1000	0.18
	2	Si	O_2, $1.0x10^{-1}$	5.7 J/cm^2	2.0 cm	30Hz	1000	0.18
	3	Si	O_2, $1.0x10^{-1}$	5.7 J/cm^2	2.0 cm	30Hz	1000	0.18
III	1,2	Si	O_2, $6.6x10^{-2}$	4.0 J/cm^2	6.0 cm	20Hz	NA	NA
	3,4	Al_2O3	O_2, $6.6x10^{-2}$	4.0 J/cm^2	6.0 cm	20Hz	NA	NA

* Exp. =experiment, Sub. =substrate, Mat. =material, d_{st} =substrate to target distance.

4.1.2 Characterization and discussion for dense ZnO films

4.1.2.1 Substrate to target distance

The films grown with a substrate-to-target distance ~2cm do not adhere very well to the substrate surface. By increasing the substrate to target distance, the film adhesion was improved, and this is in agreement with previous results of chalcogenide thin films [18]. In addition, sapphire substrates were introduced in PLD experiment III and this gives butter adhesion for the growth of ZnO.

4.1.2.2 Oxygen background gas

In order to study the effect of oxygen on the film properties, ZnO thin films were deposited in vacuum and in 10^{-1} torr oxygen. These films were examined by SEM, Electron Microprobe, XRD and PL measurements.

i). Film Composition

Table 7 summarizes the electron microprobe compositional analysis results for ZnO films deposited in vacuum (~10^{-4} torr air), and deposited in 10^{-1} torr O_2. Because oxygen is a light element, it is more difficult to detect than metals. Therefore, it is difficult to measure the zinc to oxygen atomic ratio very accurately. However, the result clearly indicates the increase of oxygen content when oxygen background gas was used in deposition.

Table 7 Atomic ratio of solid ZnO thin films deposited in vacuum and in 10^{-1} torr O_2 (Film No. I-1, II-1).

Pressure	Zn	O	Si	Total
Vacuum	48.6	51.4	0.03	100
10^{-1} torr O_2	44.3	55.5	0.2	100

ii) Film Crystallinity

Fig 34 is the XRD pattern of the as-grown ZnO thin film deposited in vacuum, which shows both zinc oxide and zinc peaks. Fig 35 is the XRD pattern of the as-grown ZnO thin film deposited in 10^{-1} torr O_2 which show mainly ZnO peaks. ZnO films deposited in 10^{-1} torr oxygen also have a preferred direction of growth of (002), which is the c-axis. Fujimura et al reported that the (002) orientation has the lowest surface energy while other orientations have higher surface energies [52]. The XRD result is consistent with the electron microprobe analysis indicating that the ZnO PLD film deposited in 10^{-1} torr O_2 contain more ZnO crystallites, less Zn interstitials and less oxygen vacancies. A shift of 2-Theta(0)=0.35° is introduced in the pattern in order to match the ZnO peaks from the database. The shift of the XRD pattern is probably caused by the surface strains of the film [53].

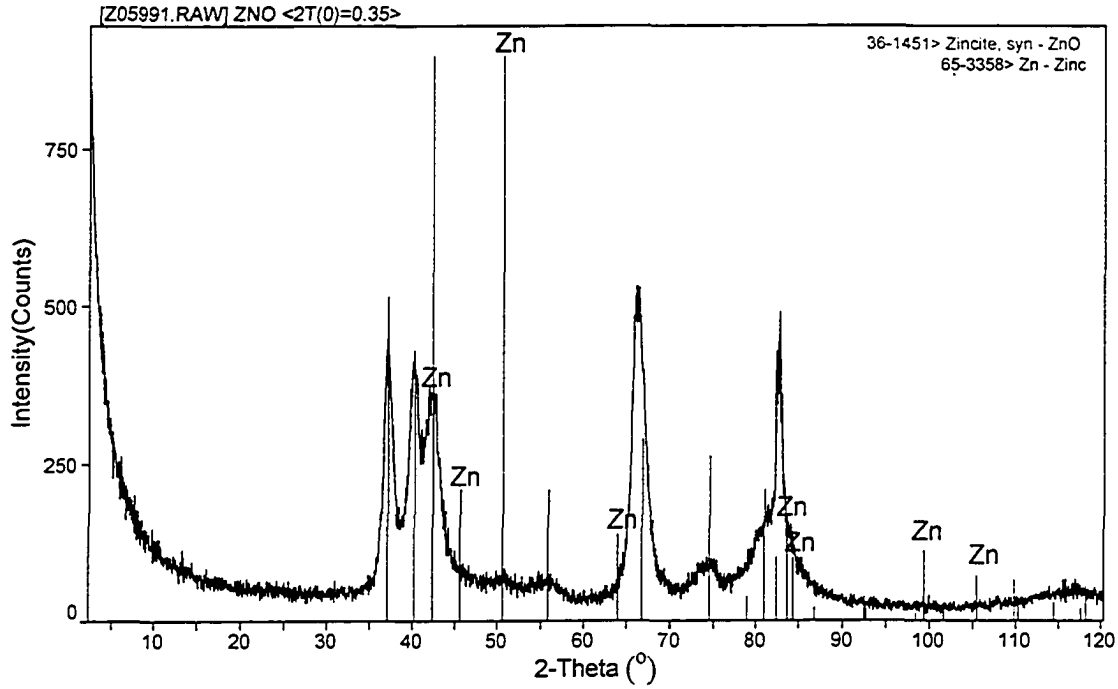

Fig 34 XRD pattern of as-grown dense ZnO deposited in vacuum, 'Zn' marked lines are the zinc peaks from database and the unlabelled lines are ZnO peaks.

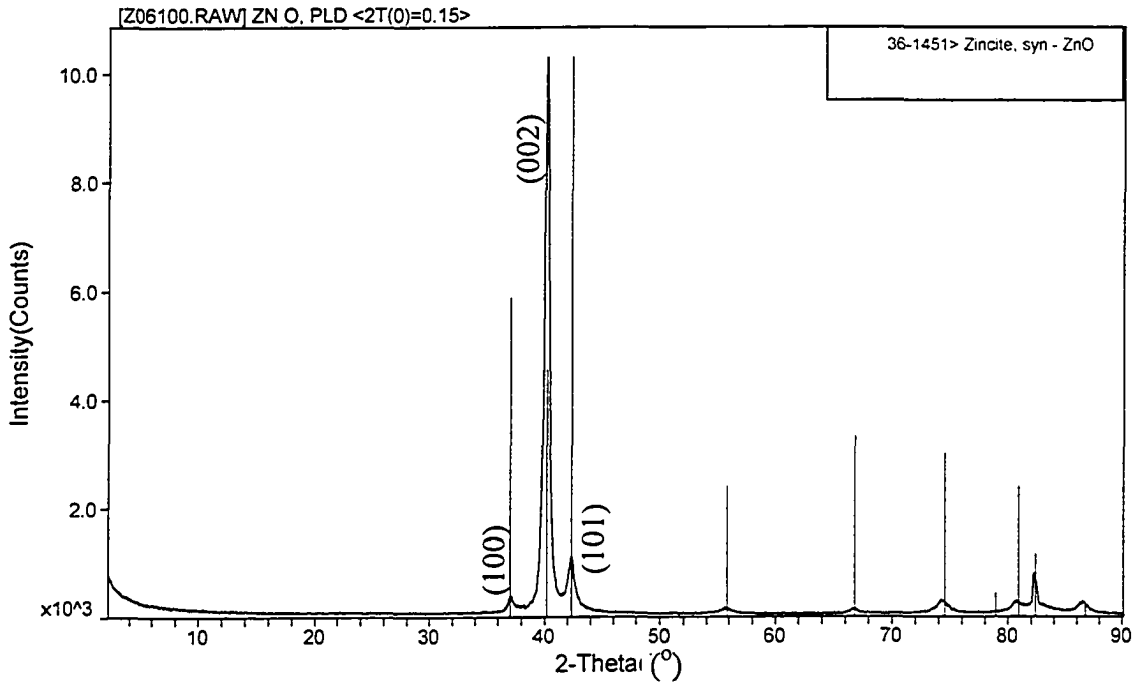

Fig 35 XRD pattern of as-grown dense ZnO film deposited in O_2, unlabeled positions of solid lines are the ZnO peaks from database.

iii) Photoluminescence

Fig 36 illustrates the UV and visible PL mechanism of ZnO. The top and button lines are the conduction band and the valence band, respectively. The band gap for the ZnO is 3.37 eV at room temperature. In our photoluminescence spectra, there is UV emission at 380 nm correspond to 3.26 eV, which is the near band emission. The visible emission peak at 505nm, and 657nm corresponding to 2.45 eV and 1.89 eV, are mainly due to the transition from deep donor level by the Zn interstitials and oxygen vacancies in ZnO to the valence band.

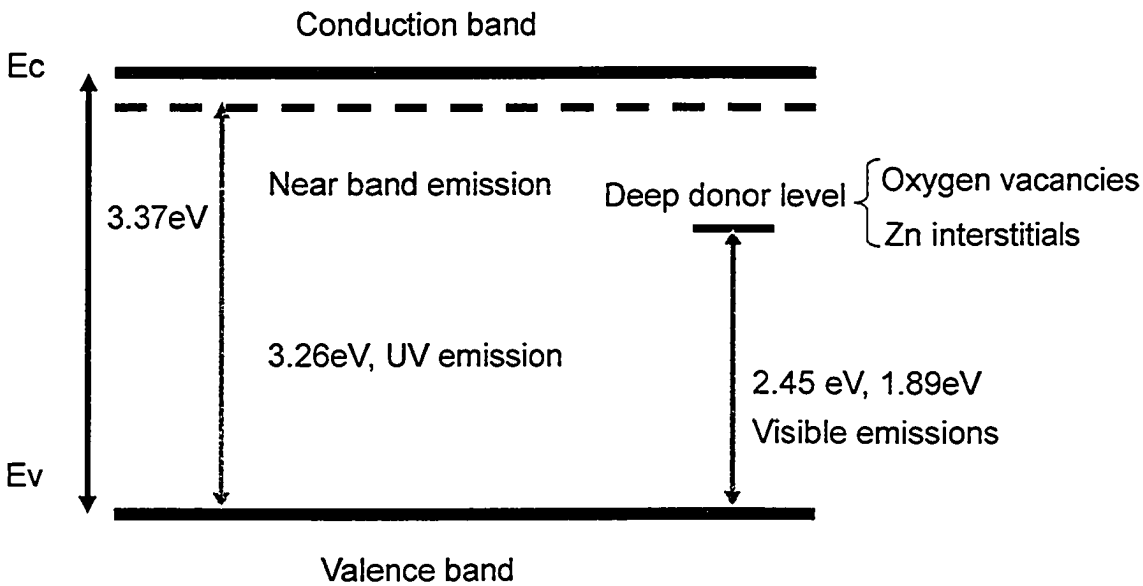

Fig 36 Photoluminescence mechanism of ZnO.

The PL spectrum of the ZnO thin film deposited in vacuum is shown in Fig 37. There are two peaks at 266nm, and 532nm which are leakage laser light from the Nd:YAG laser and higher order diffraction from the grating. Although the leakage laser light can be eliminated by placing more UV cut-off filters, or can be removed by signal

process (Appendix D), they were left on the graph to be used for wavelength calibrations. The PL from the ZnO thin film is broad and with three peaks: peak I is the near band gap UV emission peak at 380 nm (3.26 eV), and peak II is the band edge green emission peak at 505 nm (2.45eV), peak III is the red emission peak at 657nm (1.89eV). It is well known that visible luminescence is mainly due to defects, which are related to deep level emissions, such as Zn interstitials and oxygen vacancies [11].

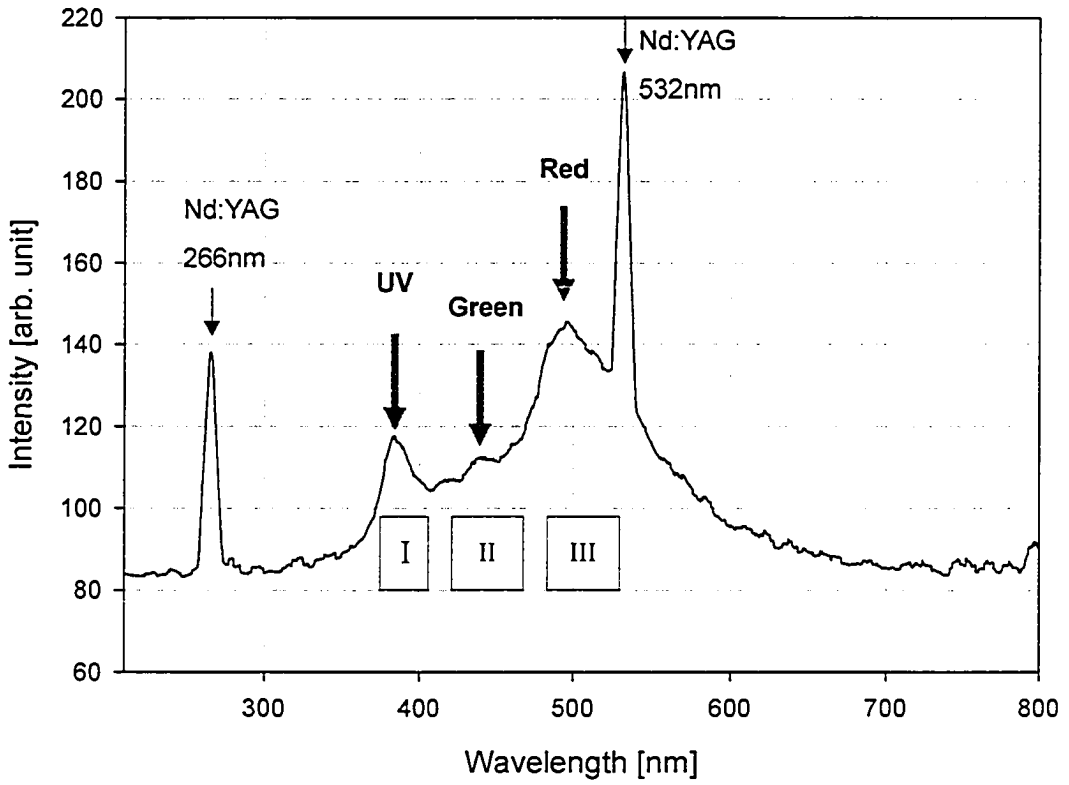

Fig 37 Photoluminescence spectra of as-grown dense ZnO thin film deposited in vacuum. A UV peak at 380 nm, green peak at 505 nm and red peak at 657nm were observed.

4.1.2.3 Annealing

After the deposition, the film was annealed in an oven in air for 2 hours at 600°C in atmosphere.

I. Annealing effect on the properties of ZnO film deposited in vacuum (PLD II)

The SEM pictures of the ZnO film before and after annealing are shown in Fig 38 and Fig 39 at different magnifications. The films changed from a rough surface to a crystalline surface which contains hexagonal crystalline structures.

The as grown and annealed films were also characterized by X-ray diffraction (XRD) and the results are shown in Fig 34 and Fig 40 respectively. The XRD results indicate that the as grown film consists of a mixture of both zinc oxide crystals and zinc crystals, while the annealed film consist mainly of zinc oxide crystals grown in the direction of (002), (100), (101).

Annealing has affected both the full width half maximum (FWHM) and the peak position of XRD peaks. The main peak (002) of ZnO thin film approached to that of the bulk zinc oxide (40.192° from JADES data), and the FWHM of the peak is narrower compared to that of the as-grown film (Table 8). Both patterns were shift by 2 Theta=0.35° to match the database ZnO pattern. The shifting of the pattern indicates there is stress inside the ZnO thin films [54].

In the lattice-mismatched epitaxial growth, usually the film will grow with built-up strain [55] and the strain can be relaxed by providing sufficient thermal energy [41][56].

(a). (b)

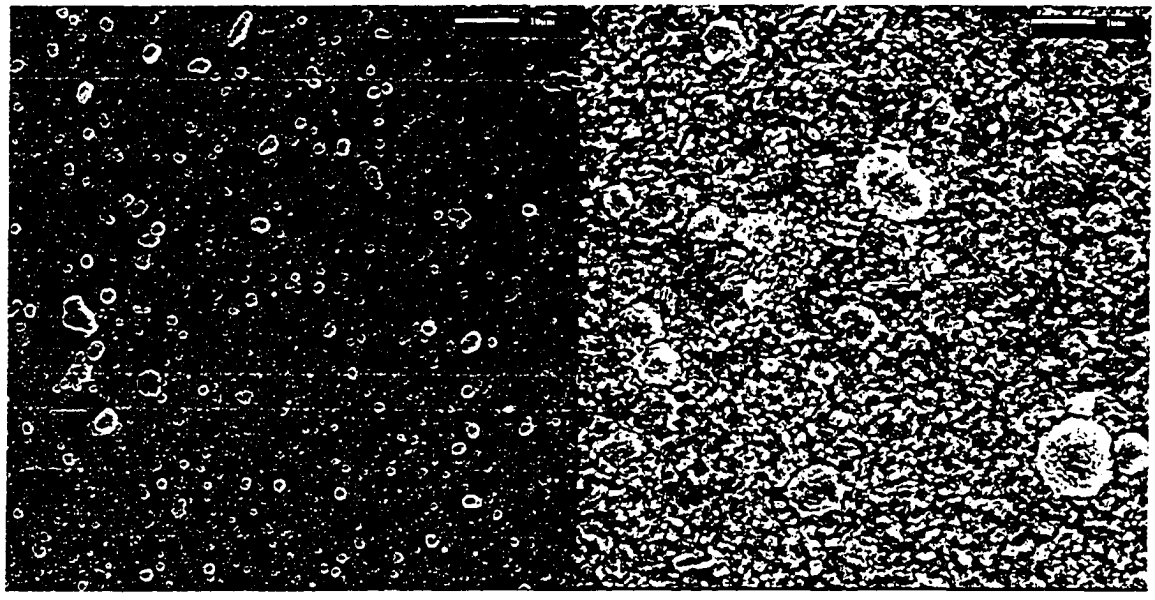

Fig 38 SEM pictures for dense ZnO films deposited in vacuum (ZnO PLD I): (a) as-grown film, (b) annealed film; magnification10000x.

(a). (b)

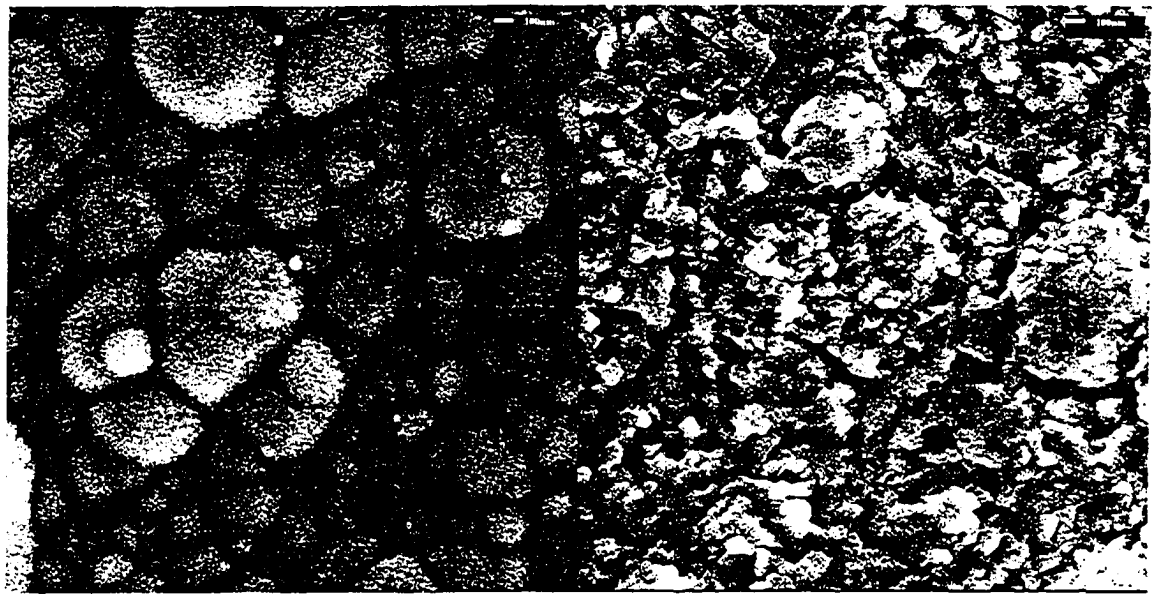

Fig 39 SEM pictures for dense ZnO films deposited in vacuum (ZnO PLD I): (a) as-grown film, (b) annealed film; magnification 30000x.

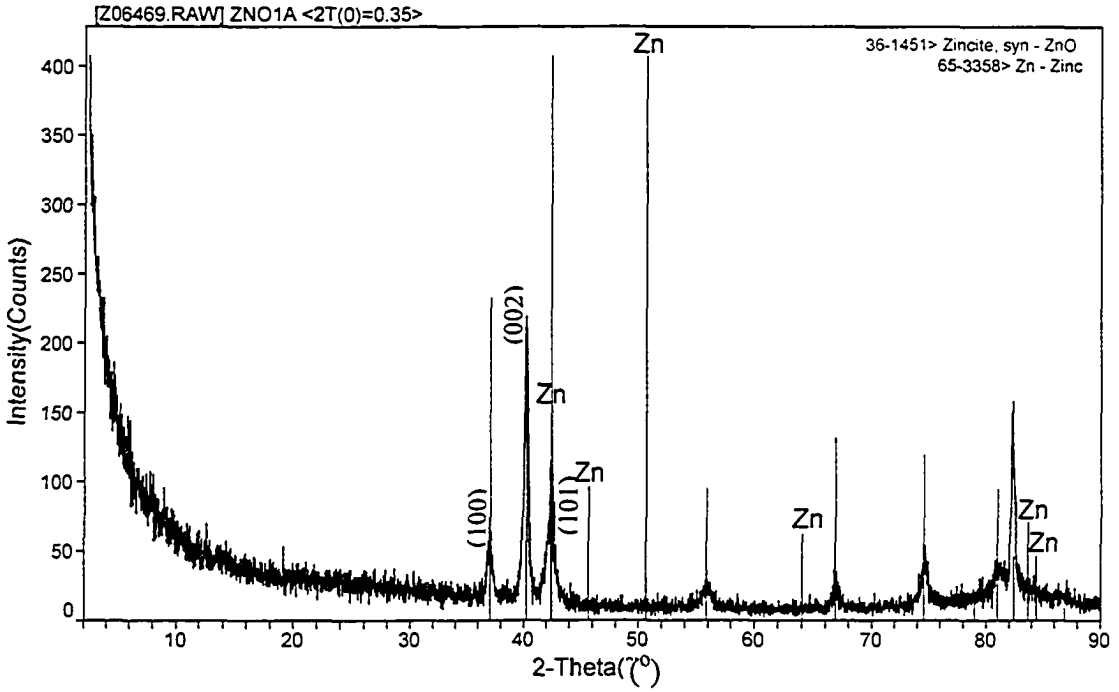

Fig 40 XRD pattern of annealed dense ZnO film deposited in vacuum. (002) (100) (101) are the main zinc oxide peaks. A shift of 2 Theta(0)=0.35° is applied.

Table 8 The (002) peak of ZnO PLD I films (deposited in vacuum)

Thin film (002)	2 Theta	FWHM (ω)	D
As grown	39.795°	0.697°	14.08nm
Annealed	39.800°	0.375°	26.18nm
ZnO (database)	40.192°	NA	NA

The full width half maximum (FWHM) values are related to the average size of crystals in the film. The average crystallite size was calculated based on the FWHM of the XRD spectra by using the relation [57],

$$D = 0.9\frac{\lambda}{\omega \cdot \cos\theta}$$

, where λ is the diffractrometer wavelength, ω is FWHM, and θ is the diffraction angle

of the XRD spectra. The smaller the FWHM the larger the crystallite size and the better crystal quality of the film [54].

Table 9 is the electron microprobe composition analysis in terms of quantitative Zn to O atomic ratio. It is shown that the oxygen percentage increased by 78% after the annealing. There are phosphors exits in the annealed film, which is due to some residue of phosphors in the oven.

Table 9 Atomic ratio of solid ZnO thin film deposited in vacuum (Film No. I-1, I-1A)

Film	Zn	O	Si	P	Total
As-grown	48.6	51.4	0.03	0	100
Annealed	31.2	58.6	0.34	9.9	100

The PL spectrum of the as grown ZnO thin film deposited in vacuum is shown in Fig 37. There are two main peaks show in the spectra: peak 1 at 380 nm is due to the near band gap UV emission, and peak 2 at 495 nm peak is due to the band edge green emission, which is mainly due to defects in the films [11]. Fig 41 gives the photoluminescence spectrum of the annealed ZnO thin film. The decrease of the visible emission and the increase of UV emission are clearly observed. The increase of the UV to Green emission ratio can be used as an indicator for the reducing of the oxygen vacancies and Zn interstitials in the film. Photoluminescence result is consistent with the result of XRD indicating the film crystallinity has improved.

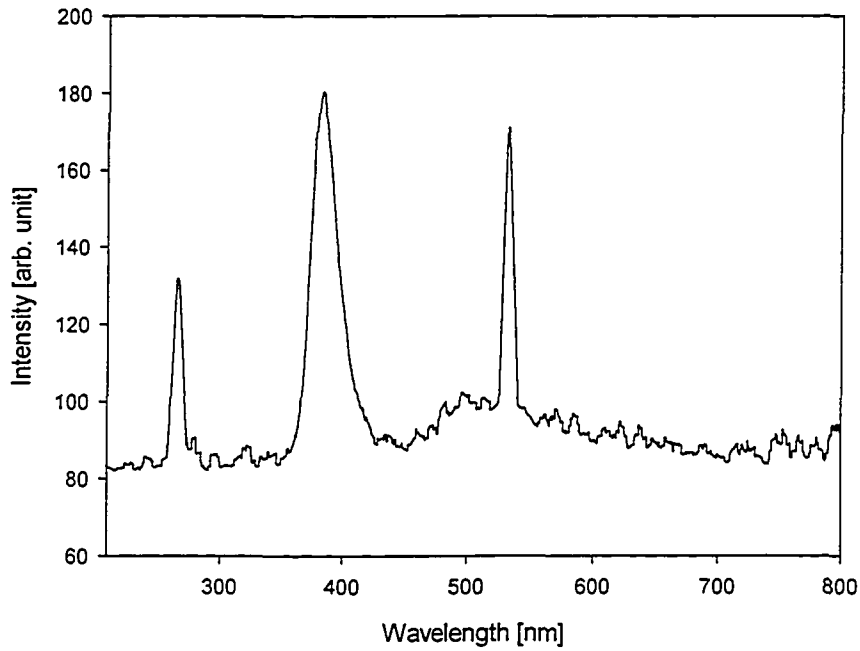

Fig 41 The photoluminescence spectra of the annealed dense ZnO film deposited in vacuum (PLD Exp. I).

II. Annealing effect on the properties of ZnO film deposited in 10^{-1} torr oxygen.

The SEM pictures for ZnO thin film deposited in 10^{-1} torr O_2 before annealing (a) and the after annealing (b) are shown in Fig 42 (1,000x magnification, top view), Fig 43 (3,0000x magnification, top view), and Fig 44 (10,000 magnification, side view). The pictures clearly show that the ZnO films become more crystalline after annealing, with grain sizes are on the order of 0.3μm.

(a) (b)

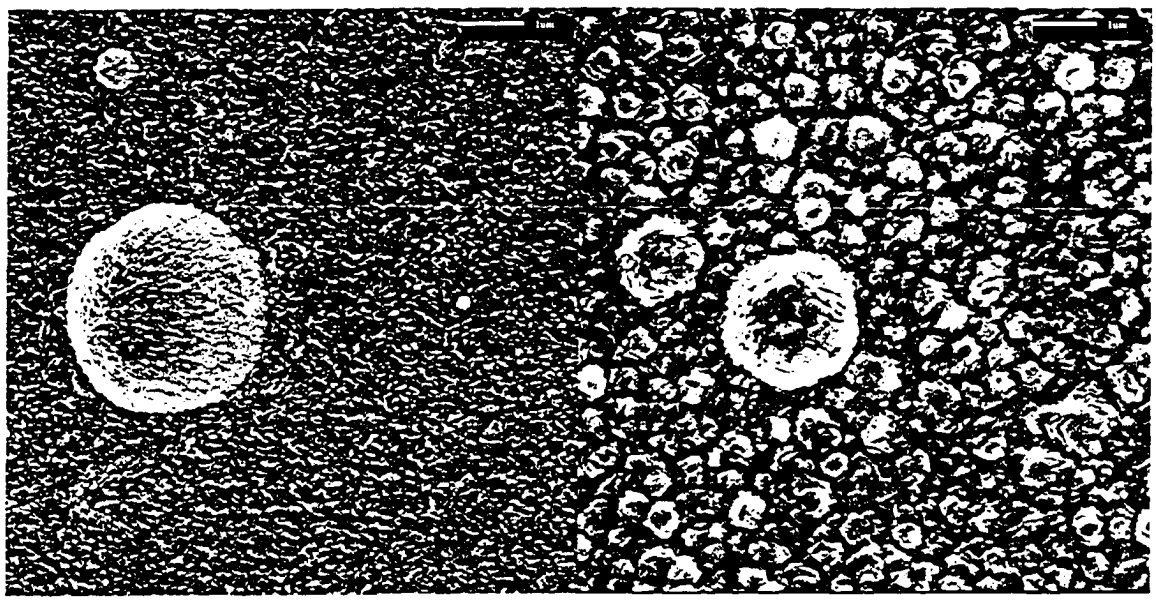

Fig 42 SEM pictures of dense ZnO thin film deposited in 10^{-1} torr O_2 (PLD II films): (a) as-grown film, (b) annealed film; magnification10,000x.

(a) (b)

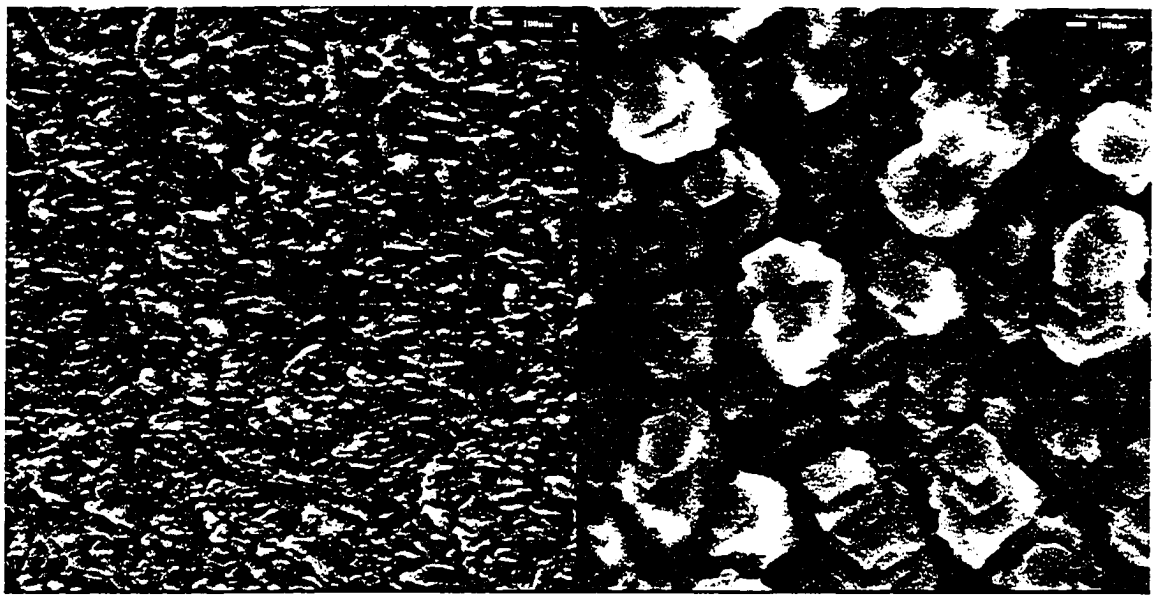

Fig 43 SEM pictures of dense ZnO thin film deposited in 10^{-1} torr O_2 (PLD II films): (a) as-grown film, (b) annealed film; magnification 30,000x.

(a) (b)

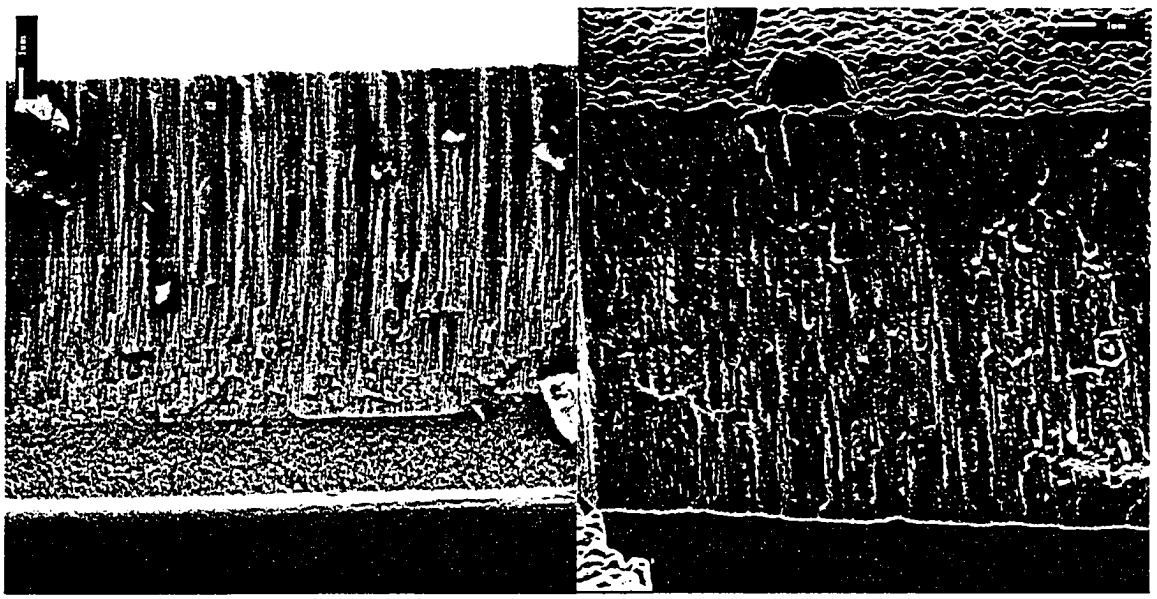

Fig 44 SEM pictures of dense ZnO thin film deposited in 10^{-1} torr O_2 (PLD II films): 70° angel view (a) as-grown film, (b) annealed film; magnification 10000x.

XRD results for the as grown film and for the annealed film deposited in 10^{-1} torr O_2 are shown in Fig 45 and Fig 46 respectively. The XRD patterns from the two films look similar, and both have a (002) main peak, (c-axis of the zinc oxide crystallite). The difference between the two patterns is the position of the main peak (002), and FWHM of the peak. The (002) peak of the annealed film shifted 0.028° away from that of the bulk ZnO (40.192°) (Table 10). The FWHM narrows down to 0.327°, and this means the larger crystallites size was formed after annealing which is in agreement with SEM observations.

Table 10 The (002) peak of ZnO PLD III films (deposited in 10^{-1} torr oxygen)

Thin film	(002) 2 theta	FWHM	D
As-grown dense film (O_2)	40.045°	0.471	20.86 nm
Annealed dense film (O_2)	40.017°	0.327	30.04 nm
Bulk ZnO	40.192	-	-

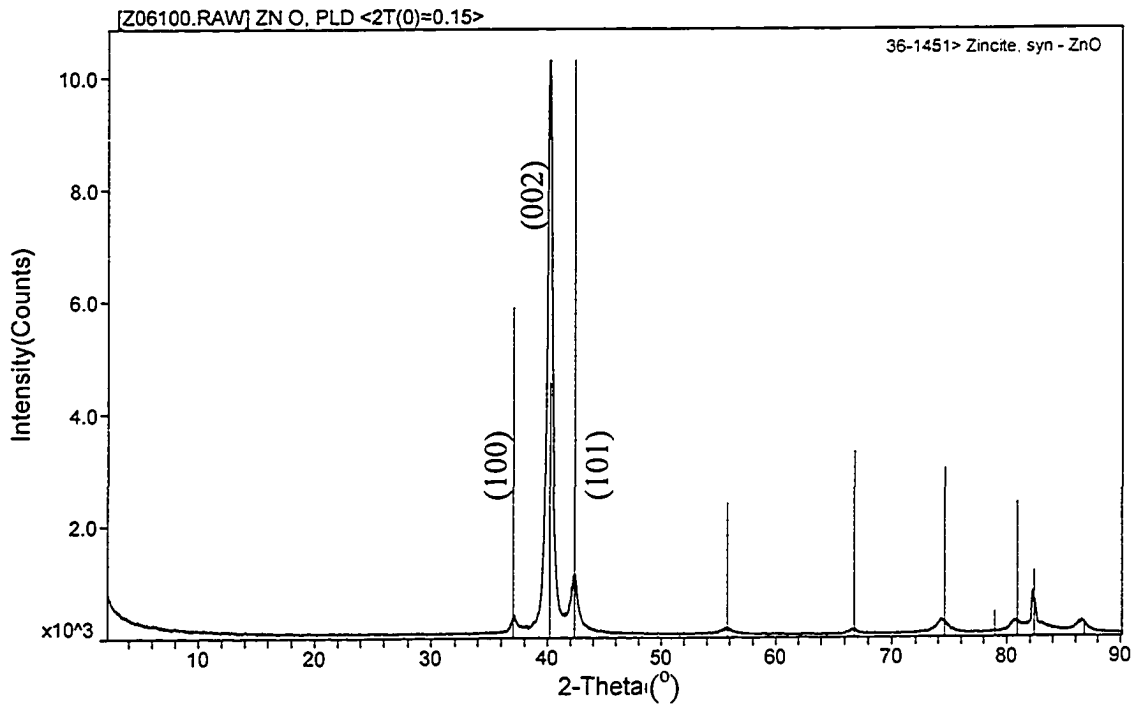

Fig 45 XRD pattern of as-grown dense ZnO thin film deposited in 10^{-1} torr O_2. (002) (101) (100) are zinc oxide peaks.

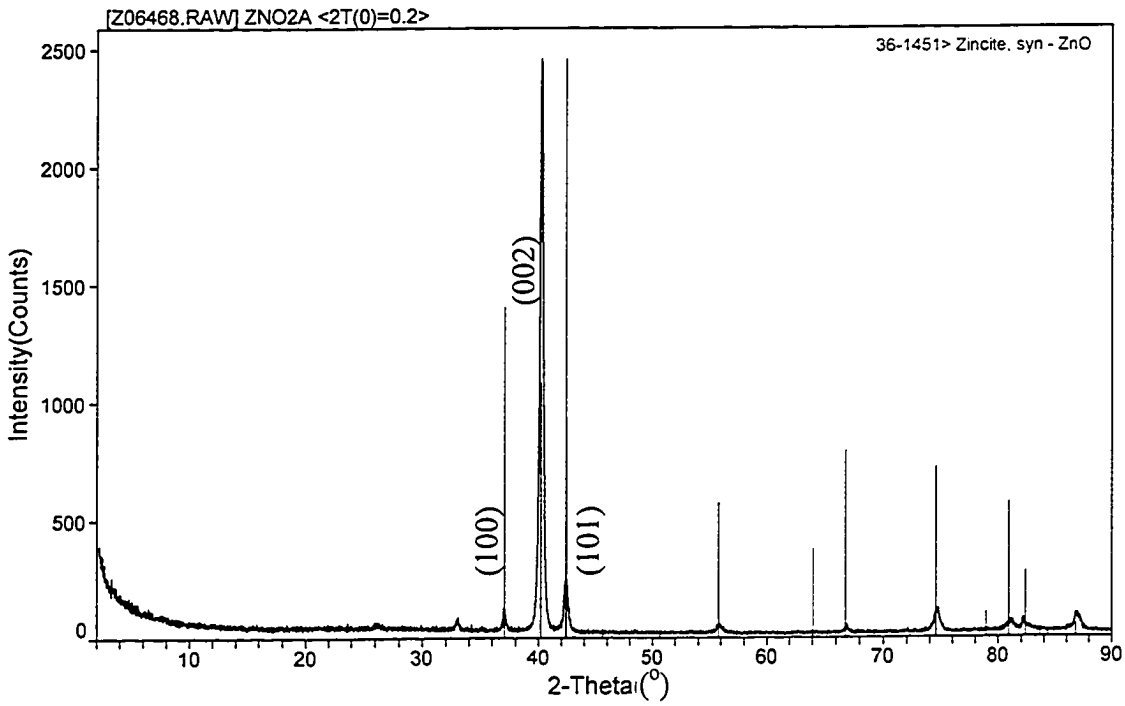

Fig 46 XRD pattern of annealed dense ZnO thin film deposited in 10^{-1} torr O_2.

Table 11 gives the Electron Microprobe results, and shows that the oxygen to zinc ratio in the ZnO film deposited in oxygen has increased by ~30% by annealing at 600°C in air for 2 hours.

Table 11 Atomic ratio of solid ZnO thin film deposited in 10^{-1} torr O_2 (Film No. II-1, II-1A)

Film	Zn	O	Si	P
As-grown	44.3	55.5	0.2	0
Annealed	34.9	57.3	0.2	7.6

The PL signals for the as-grown ZnO thin film deposited in 10^{-1} torr O_2 were not detectable. After the annealing process, the UV emission of the annealed film becomes stronger than that of the as grown film, and it has an emission peak at ~390 nm (see Fig 47). The PL spectrum of the annealed ZnO films is identical to that of the ZnO PLD target (see appendix G for PL of the ZnO PLD target). This result is consistent with the result of XRD and the result of Electron Microprobe analysis, which indicated the increase of oxygen content and the better crystalline of ZnO films.

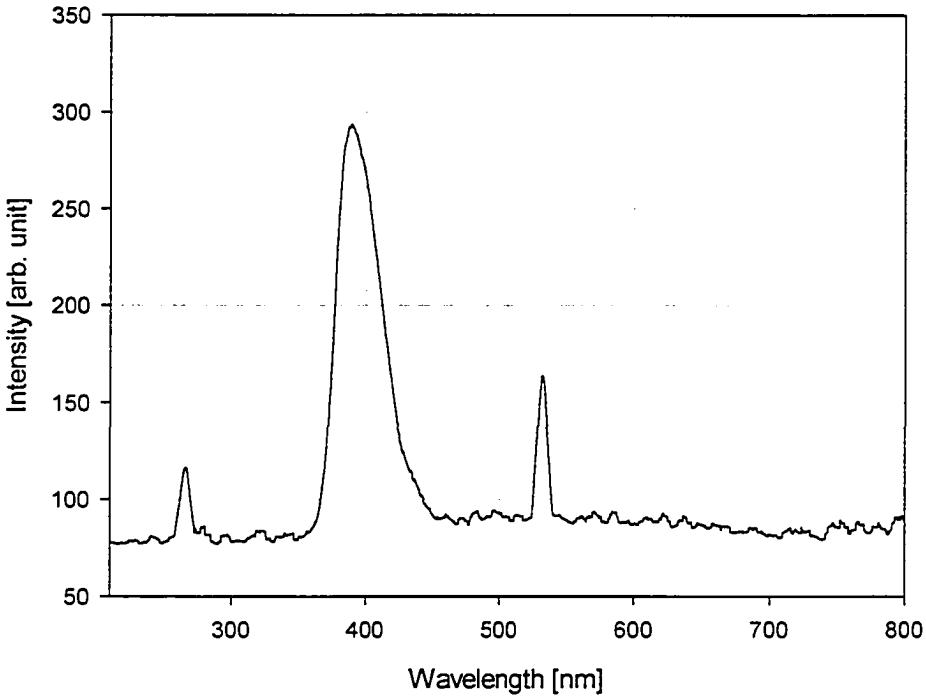

Fig 47 The PL spectra of the annealed dense ZnO thin film deposited in 10^{-1} torr O_2. UV emission at 389nm dominates.

The result from the present study for ZnO films deposited without substrate heating is quite different from that of those results reported previously for ZnO films deposited at high substrate temperature. For ZnO films deposited at high substrate temperature, annealing the films in oxygen degrades the UV emissions and increases the green emissions. This is probably due to the formation of excessively oxidized layer on the film surface or around the gain boundary. The XRD and PL measurements indicate our annealed ZnO films deposited without substrate heating are comparable to those deposited with substrate heating. This is a useful finding since it is easier and less expensive to do depositions in a vacuum chamber without a substrate heating system. Various properties of the dense ZnO films are summarized in Table 12.

Table 12 Summary of properties of dense ZnO films

Environment	Annealing	XRD		E-Microprobe Quantitative O/Zn ratio	PL spectrum
		Pattern	(002) FWHM		
Vacuum	No	ZnO, Zn mix	0.70	1.06	Low UV, high visible
Vacuum	Yes	ZnO	0.38	1.88	High UV, low visible
O_2	No	ZnO(002)	0.47	1.25	NA
O_2	Yes	ZnO(002)	0.33	1.64	High UV

4.2 ZnO Porous films

4.2.1 Fabrication Procedures

a) Setup

The schematic diagram for fabricating porous ZnO thin film is shown in Fig 48. The substrate arrangement as viewed from the top is shown in Fig 49. The centre piece is located at the centre of the mount, middle piece located at 2.3 cm away from the centre, and the edge piece is located at 3.8 cm away from the centre. The substrates used in the experiments were 1cmx1cm Si (100).

b). Deposition condition

The experimental conditions are listed in Table 13. The deposition parameters include the laser fluence, substrate orientation angle, target-to-substrates distance, substrate rotation speed, substrate materials, and oxygen background gas.

The deposition procedure for depositing porous ZnO films is similar to that of dense films. The chamber is pumped down to a vacuum (~10^{-5} torr). Depositions VII-X were done with back filling oxygen ($6.6x10^{-2}$ torr or 10^{-1} torr). Various substrates and coating were used in the experiments: Si, Au coated Si, Al patterned Si, Sapphire, and glass. The Au coated Si substrates was coated with 10nm Au. After deposition the films were annealed at 600°C in air for 2 hours.

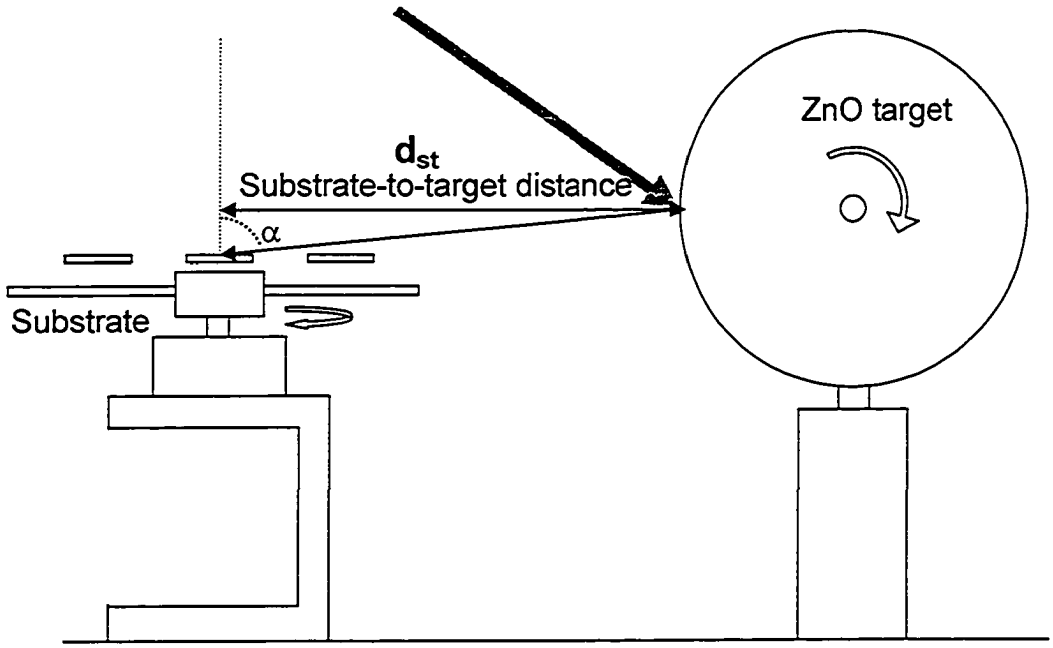

Fig 48 Setup for the fabrication of porous ZnO thin films.

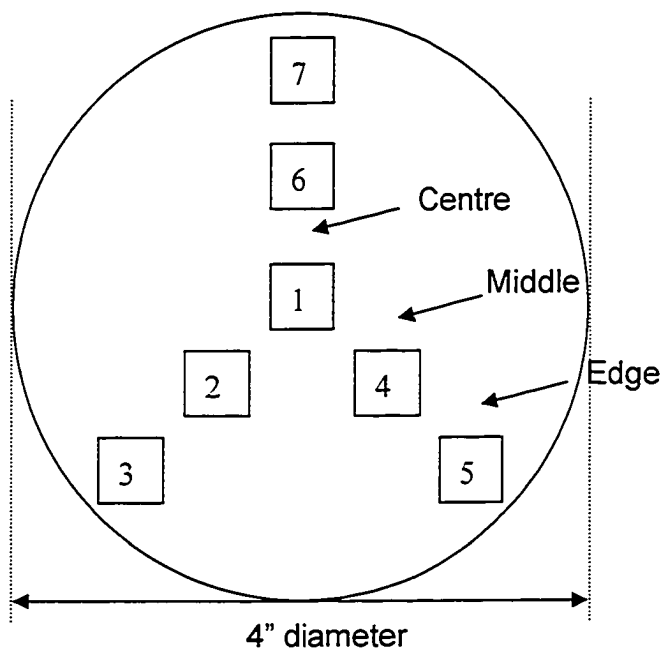

Fig 49 The arrangement of substrates (top view).

Table 13 Conditions of each ZnO glancing angle pulsed laser deposition

Exp.	Sub#	Sub. Mater.	Position	Pressure [torr]	α [°]	Fluence [J/cm^2]	d_{st} [cm]	Sub. Rotation [rpm]	Thickness [nm]	Dep. Rate [Å/p]
I	1	Si	Centre	$7x10^{-5}$	87.5	2.9	7.0	0.5	380	0.044
	2	Si	Middle	$7x10^{-5}$		2.9	7.0		447	0.052
	3	Si	Edge	$7x10^{-5}$		2.9	7.0		670	0.078
II	1	Si	Centre	$4.7x10^{-5}$	89	3.4	7.0	0.5	182	0.051
	2,4,6	Si	Middle	$4.7x10^{-5}$		3.4	7.0		257	0.071
	3	Si	Edge	$4.7x10^{-5}$		3.4	7.0		313	0.087
III	0,	Si	Centre	$6.2x10^{-5}$	89.1	3.6	7.6	0.5	20	0.021
	1,2	Si	Middle	$6.2x10^{-5}$		3.6	7.6		N/A	N/A
III	3,4	Au/Si	Middle	$6.2x10^{-5}$		3.6	7.6		N/A	0.016
IV	0	Si	Centre	$7x10^{-5}$	89.1	3.6	7.6	320	60	0.02
	1,2	Si	Middle	$7x10^{-5}$		3.6	7.6		N/A	N/A
	3,4	Au/Si	Middle	$7x10^{-5}$		3.6	7.6		50	0.017
V	0	Si	Centre	$7x10^{-5}$	89.1	3.0	7.6	320	245	0.028
	1,2	Si	Middle	$7x10^{-5}$		3.0	7.6		80	0.009
	3,4	Au/Si	Middle	$7x10^{-5}$		3.0	7.6		54	0.006
VI	0	Si	Centre	$5.3x10^{-5}$	89.1	3.0	7.6	0	362	0.066
	1,2	Si	Middle	$5.3x10^{-5}$		3.0	7.6		411	0.075
	3,4	Si	Middle	$5.3x10^{-5}$		3.0	7.6		287	0.053
VII	0	Si	Centre	$O_2\ 10^{-1}$	89.1	3.7	7.6	0	157	0.014
	1,2	Si	Middle	$O_2\ 10^{-1}$		3.7	7.6		387	0.035

Exp.	Sub#	Sub. Mater.	Position	Pressure [torr]	α [°]	Fluence [J/cm^2]	d_{st} [cm]	Sub. Rotation [rpm]	Thickness [nm]	Dep. Rate [Å/p]
VII	3,4	Si	Middle	10^{-1} O_2		3.7	7.6		127	0.012
VIII	1	Si	Centre	10^{-1} O_2	88.5	5.9	7.0	0.5	74	0.018
	2,4,6	Si	Middle	10^{-1} O_2		5.9	7.0		53	0.013
	3,5,7	Si	Edge	10^{-1} O_2		5.9	7.0		N/A	N/A
IX	0	Si	Centre	O_2 6.6×10^{-2}	88.5	11.2	3.0	0.5	559	0.075
	1,5	Si	Middle	O_2 6.6×10^{-2}		11.2	3.0		515	0.069
	2,3,7	Au/Si	Middle	O_2 6.6×10^{-2}		11.2	3.0		489	0.066
	4,6	Al/Si	Middle	O_2 6.6×10^{-2}		11.2	3.0		N/A	N/A
X	1	Si	Centre	O_2 6.6×10^{-2}	88.5	4.0	3.0	0.036	670	0.051
	7	Al_2O_3	Centre	6.6×10^{-2}		4.0	3.0		700	0.053
	2-5	Si	Middle	6.6×10^{-2}		4.0	3.0		550	0.042
	8-10	Al_2O_3	Middle	6.6×10^{-2}		4.0	3.0		550	0.042

* Exp. =experiment, Sub. =substrate, Mat. =material, d_{st} =substrate to target distance, α=plume incident angle.

The deposition rate varied with background pressure. The deposition rate of the film deposited in oxygen background gas is much lower than that in vacuum. For example, the

deposition rate for the porous ZnO film deposited in vacuum (experiment I) at a substrate-to-target distance of 7 cm was 0.044 Å/pulse, and the deposition rate for the film deposited in 10^{-1} torr O_2 (experiment XIII) at a substrate-to-target distance of 7.6cm was 0.018Å/pulse. The deposition rate also varied with the location of the substrate on the substrate mount and with the laser fluence. For low fluence (1-4 J/cm^2), the films at edge is thicker than those at the centre. For higher fluence, the films at centre is thicker than those at the edge.

4.2.2 Characterization and discussion for porous ZnO films

4.2.2.1 Oxygen background gas

As discussed in the previous sections, the oxygen background gas plays an important role in the oxidation process, result in the increasing of ZnO crystalline properties. The existence of the oxygen gas may also modify the plume dynamics.

The SEM pictures viewed from the top for annealed porous ZnO films deposited in vacuum and in $6.6x10^{-2}$ torr O_2 background gas are shown in Fig 50 (a) and (b) respectively. The SEM pictures viewed from the side for annealed porous ZnO films in vacuum and in $6.6x10^{-2}$ torr O_2 background are shown in Fig 51 (a) and (b) respectively. The substrate to target distance for the film deposited in vacuum was 7 cm and for the film deposited in O_2 was 3 cm.

The nanostructure of the film deposited in vacuum was significantly different from that deposited in O_2. The film deposited in vacuum displaying random porous structures while those deposited in O_2 shown very ordered ~ 100nm diameter columns.

(a) (b)

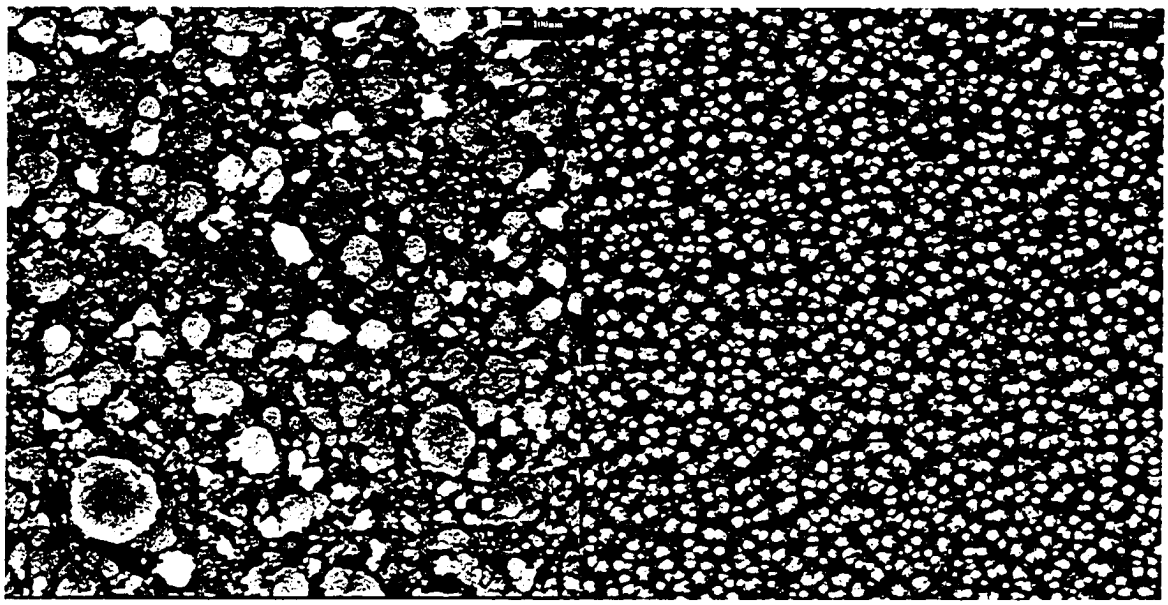

Fig 50 SEM pictures (top view) of the as-grown porous ZnO film deposited (a) in vacuum, substrate-to-target distance 7 cm, α =87.5°, and (b) in 6.6x10^{-2} torr O_2, substrate-to-target distance 3 cm, α = 88.5°. (Film No. (a) I-1, (b) IX-0.)

(a) (b)

Fig 51 SEM pictures (cross-section view) of as-grown porous ZnO film deposited (a) in vacuum, and (b) in 6.6x10^{-2} torr O_2.

Fig 52 gives the XRD result for the as grown porous ZnO film deposited in vacuum. There are three zinc peaks shown in the graph, but no significant zinc oxide peak were observed in the XRD analysis. This suggests that the film contains mostly Zn crystallites. Fig 53 gives the XRD result for the as grown porous ZnO film deposited in O_2. Only the (002) main peak at 2 theta=39.4° and FWHM=0.522° for ZnO crystallites was observed. This suggests that the as grown porous ZnO film deposited in O_2 is mainly consists of c-axis oriented crystalline.

The results of Electron Microprobe analysis of the ZnO porous films deposited in vacuum and O_2 are listed in Table 14. The results are similar to the result of that of dense films. The oxygen content for the films deposited in O_2 background was clearly improved.

Table 14 Atomic ratio of porous ZnO thin films deposited in vacuum and in $6.6x10^{-2}$ torr O_2 (Film No. I-1, IX-1)

Film	Zn	O	Si	P
Vacuum	62.8	32.3	4.9	0
$6.6x10^{-2}$ torr O_2	44.0	55.4	0.5	0

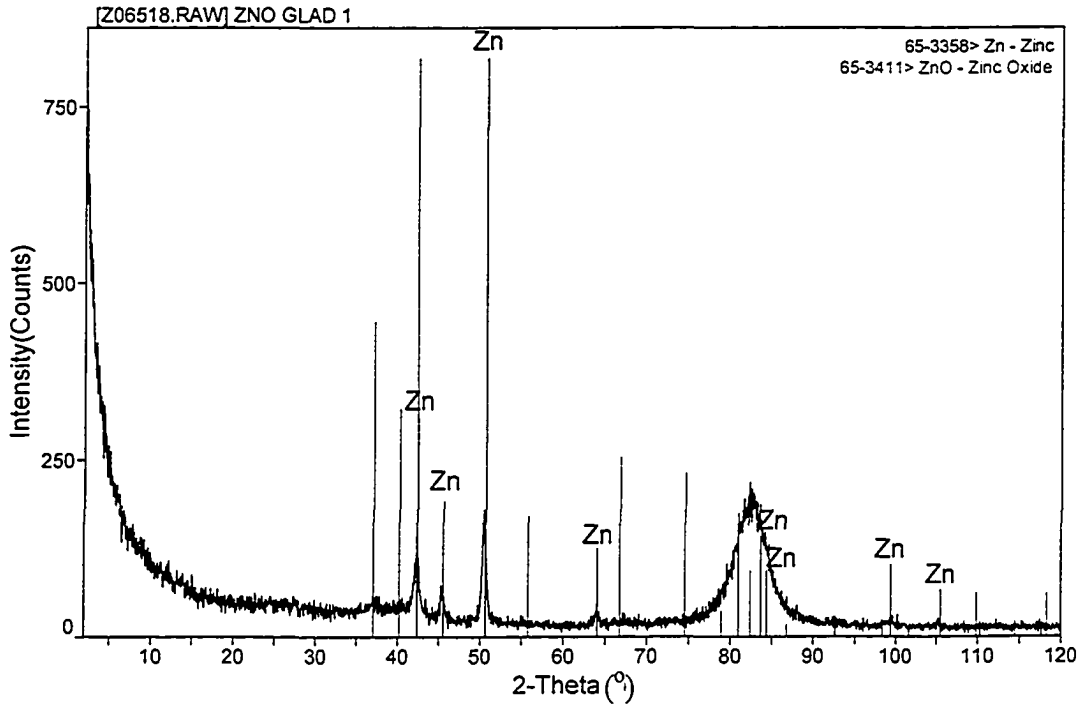

Fig 52 The XRD pattern of as-grown porous ZnO film deposited in vacuum. Zn marked lines are the Zinc peaks, while the rest of lines are the zinc oxide peaks.

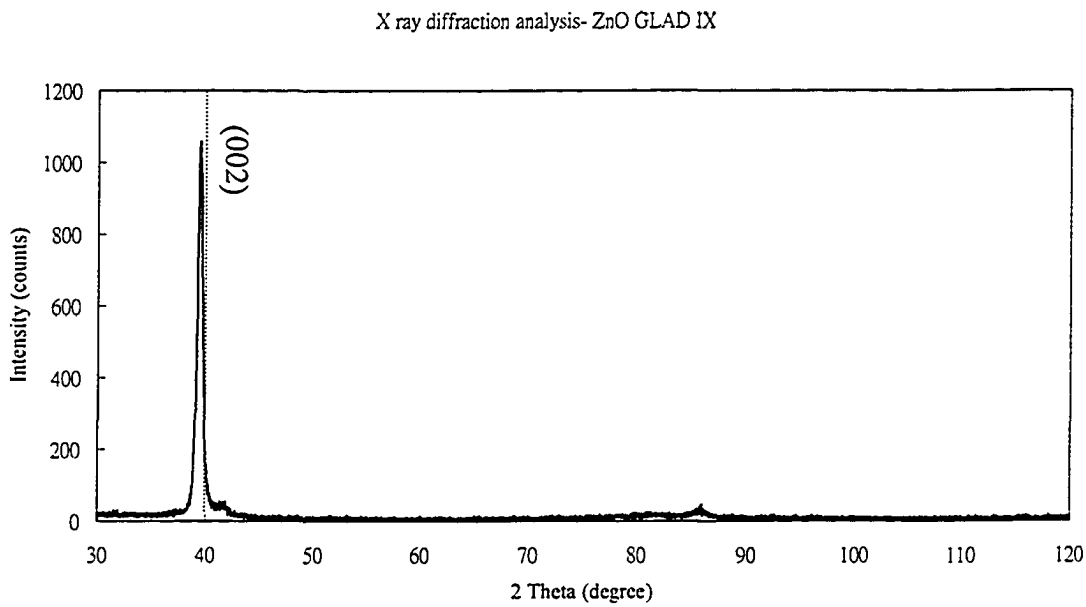

Fig 53 The XRD pattern of as-grown porous ZnO film deposited in 6.6×10^{-2} torr O_2. The film has a zinc oxide (002) preference direction of growth.

4.2.2.2 Annealing

After deposition, the porous ZnO thin film were annealed at 600°C in atmosphere for 2 hours.

a) Porous ZnO film deposited in vacuum

The SEM pictures at two different magnifications viewed from the top for porous ZnO films in vacuum before and after annealing are shown in Fig 54 (10,000x), Fig 55 (30,000x) (a) and (b) respectively. The SEM pictures view from the side for these films before and after annealing are shown in Fig 56 (a) and (b), respectively. The films deposited in vacuum appeared to be melted during anneaing and then resolidified after annealing as would be expected from a metal like Znic.

(a) (b)

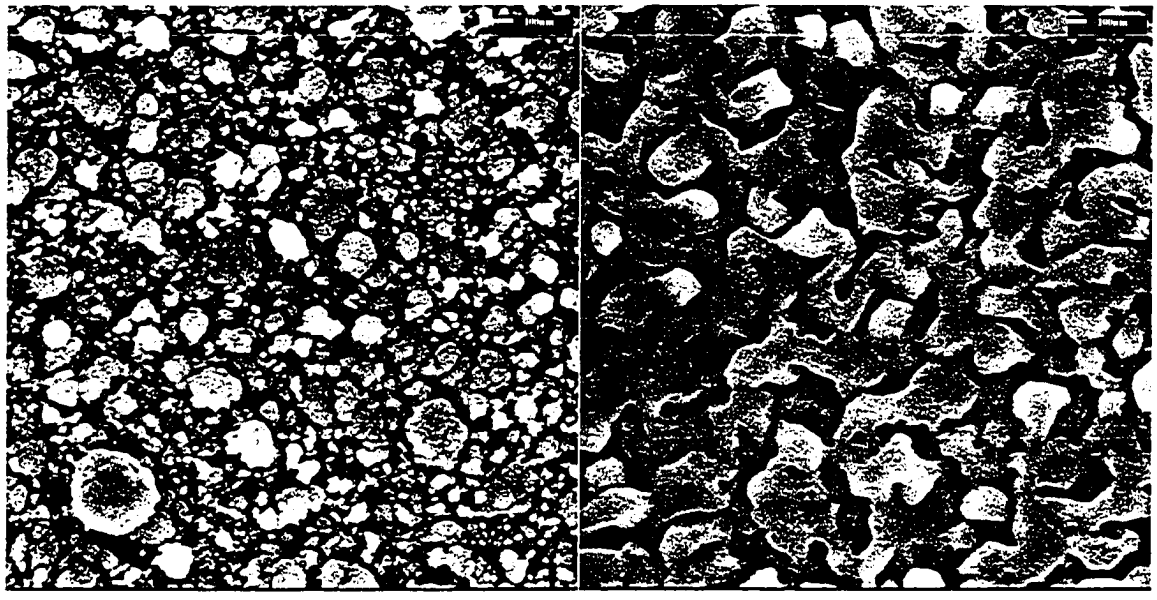

Fig 54 SEM pictures of porous ZnO thin films deposited in vacuum: (a) as-grown film, and (b) annealed film, magnification 10,000x.

(a) (b)

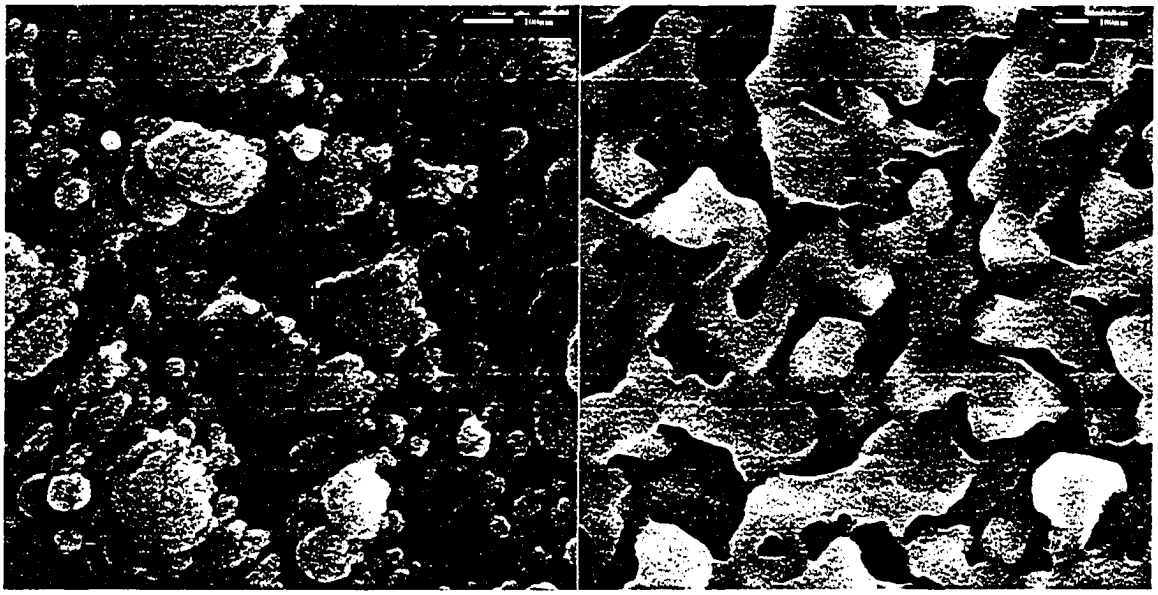

Fig 55 SEM pictures of porous ZnO thin films deposited in vacuum: (a) as-grown film, and (b) annealed film, magnification 30,000x.

(a) (b)

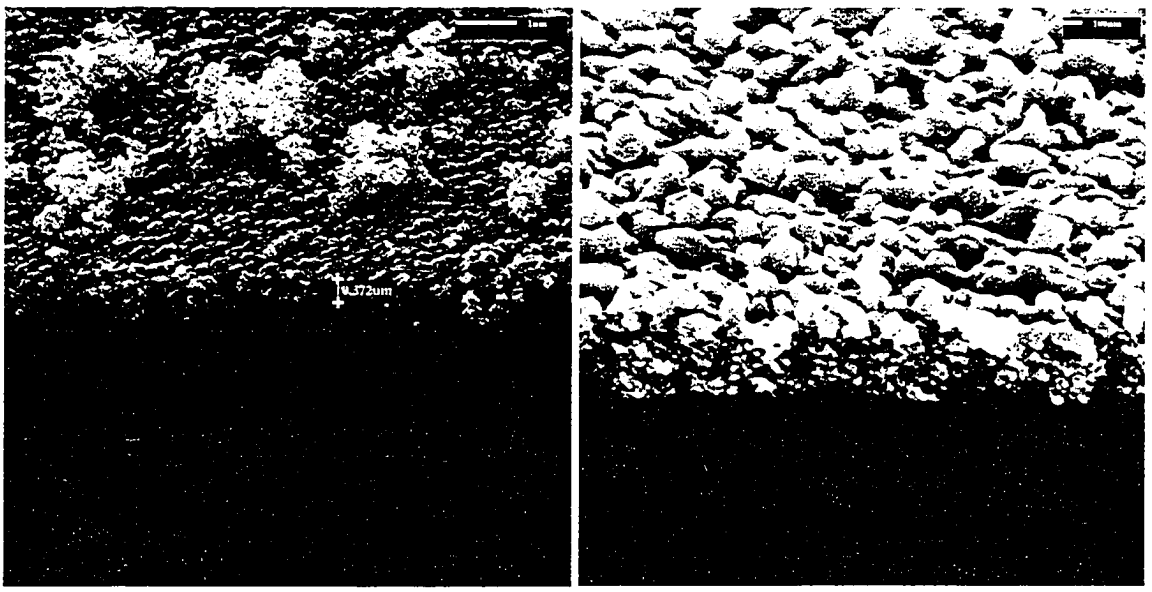

Fig 56 SEM pictures of porous ZnO thin films deposited in vacuum: (a) as-grown film, magnification 50,000x, and (b) annealed film, magnification 30,000x.

The XRD result for the annealed porous ZnO film deposited in vacuum is shown in Fig 57. The FWHM of the (002) peak and the crystallites size D is listed in Table 15.

Table 15 The (002) peak of ZnO PLD II films (deposited in vacuum)

Thin film (002)	2 Theta	FWHM (ω)	D
As-grown	42.4°	0.51°	20.1 nm
Annealed	39.9°	0.41°	24.0 nm
ZnO (database)	40.2°	NA	NA

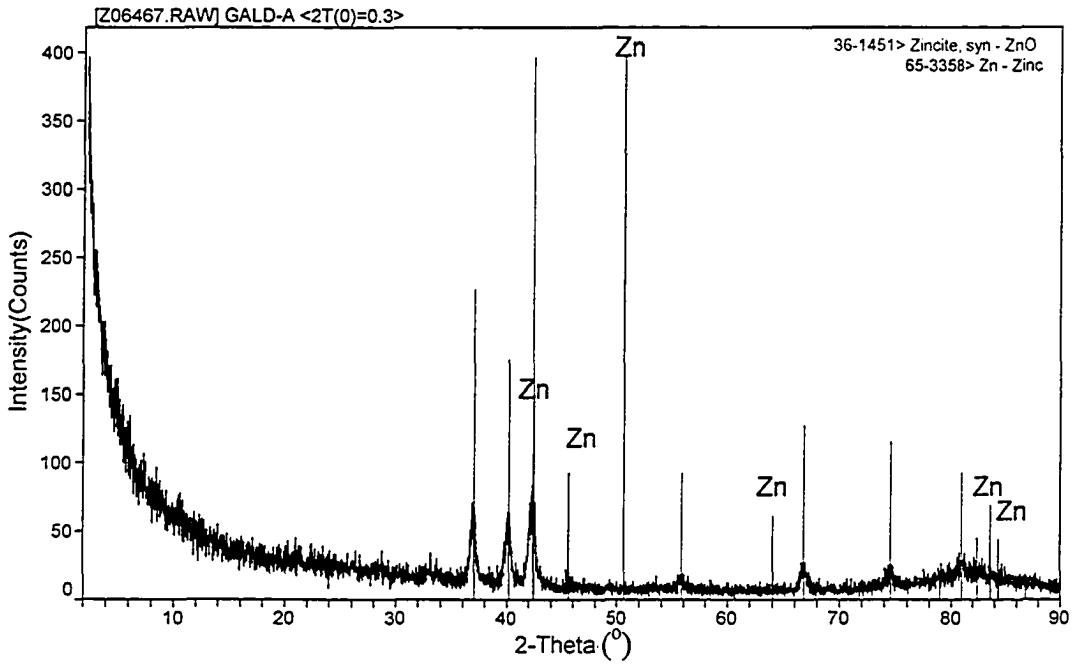

Fig 57 The XRD pattern of annealed porous ZnO film deposited in vacuum. Zn marked lines are the zinc peaks, while the rest lines are ZnO peaks.

Table 16 gives the Electron Microprobe result of the ZnO film deposited in vacuum. The result indicates the as grown films were strongly oxygen deficient, and the number of O_2 defects was decreased by the annealing process, and this is consistent with the XRD results. The electron microprobe results (Table 16) indicate before annealing that porous

films deposited in vacuum were much more deficient of oxygen than dense films deposited in vacuum.

Table 16 Atomic ratio of porous ZnO thin film deposited in vacuum (Film No. I-1, I-1A)

No.	Zn	O	Si	P	Total
As-grown film	62.8	32.3	4.9	0.0	100
Annealed film	37.1	55.8	0.3	6.8	100

No significant luminescence signal was detected for the as grown ZnO porous film deposited in vacuum. This result is consistent with the XRD, and Electron Microprobe results, indicating the films consisted mainly of zinc. The photoluminescence for the annealed porous ZnO film deposited in vacuum is shown in Fig 58. The spectrum consists of both UV and green emissions indicating the annealed film still contained some O_2 vacancies and Zn interstitials.

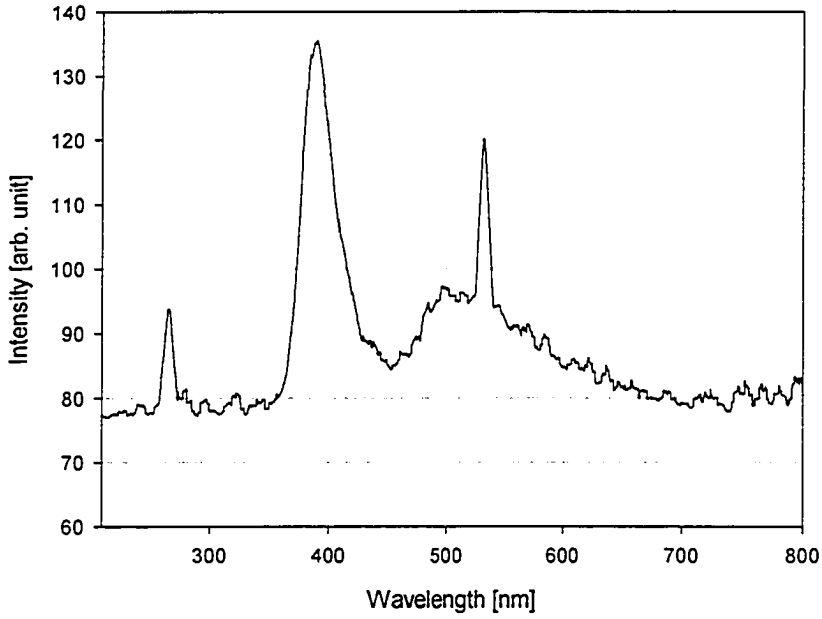

Fig 58 Room temperature photoluminescence spectra of the annealed porous ZnO film deposited in vacuum.

b) Porous ZnO film deposited in $6.6x10^{-2}$ torr O_2

The porous ZnO film deposited in $6.6x10^{-2}$ torr O_2 were annealed at 600°C in air for 2 hours. The SEM pictures for the cross-section view of the film before and after annealing are shown in Fig 59 (a) and (b). The annealed film seems consists of more defined hexagonal crystals.

The XRD results for the films before and after annealing are shown in Fig 60 and Fig 61, respectively. The main (002) peak of the as grown film is located at 39.416° with FWHM=0.522°, while the (002) peak for the annealed film it is located at 40.184° with FWHM=0.364° (see Table 17). As discussed before, the shifting of the (002) peak for the annealed film towards larger angle indicating less stress [54], and the smaller FWHM for the annealed films indicating the films consisted of larger crystals.

Table 17 The (002) peak of ZnO porous thin film deposited in $6.6x10^{-2}$ torr O_2

Thin film	(002) 2 theta	FWHM	D
As-grown film	39.416°	0.522	18.7 nm
Annealed film	40.184°	0.364	27.0 nm
Bulk ZnO (database)	40.192°	NA	NA

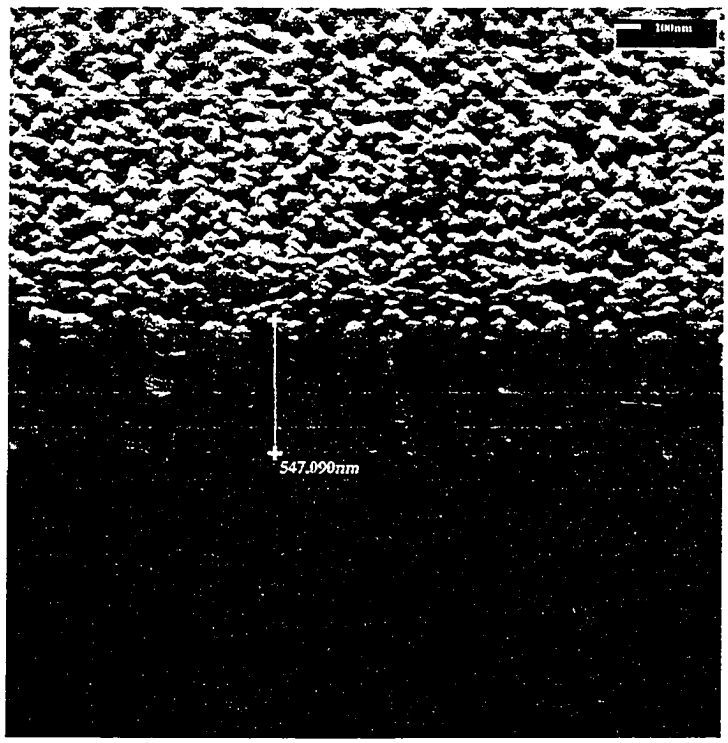

Fig 59 (a)

SEM picture for the as grown porous ZnO film deposited in $6.6x10^{-2}$ torr O_2 (α =88.5°, d_{st}= 3 cm. Film thickness is 547 nm.)
(Film No. IX-0)

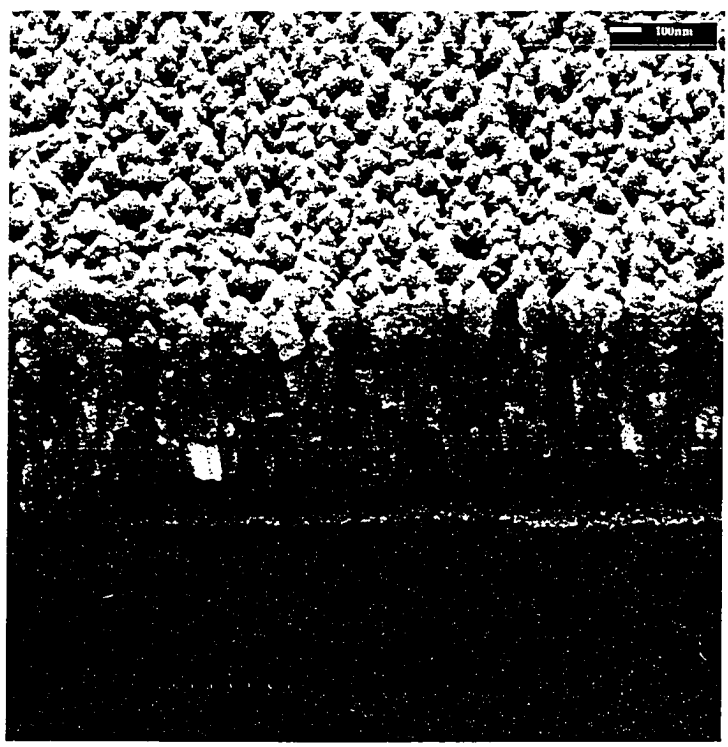

(b)

SEM picture for the annealed porous ZnO film deposited in $6.6x10^{-2}$ torr O_2 (α=88.5°, d_{st}= of 3 cm. Film thickness is 547 nm).
(Film No. IX-0A)

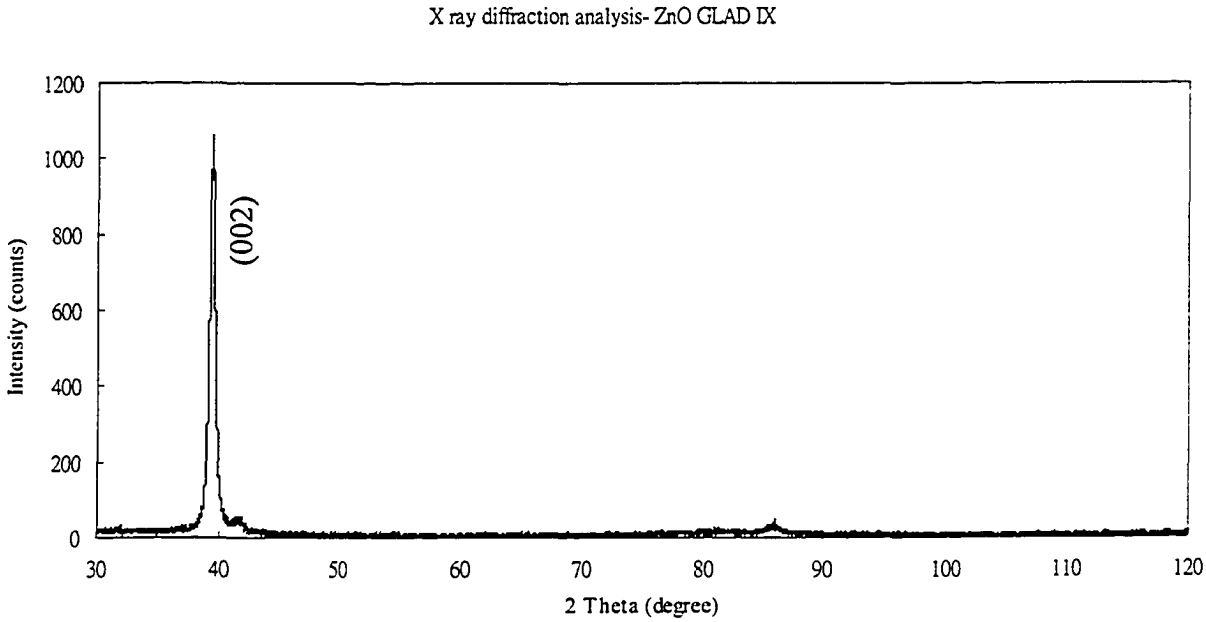

Fig 60 The XRD pattern of as-grown porous ZnO film deposited in $6.6x10^{-2}$ torr O_2. (002) is the main ZnO peak at 39.416°, FWHM=0.522°.

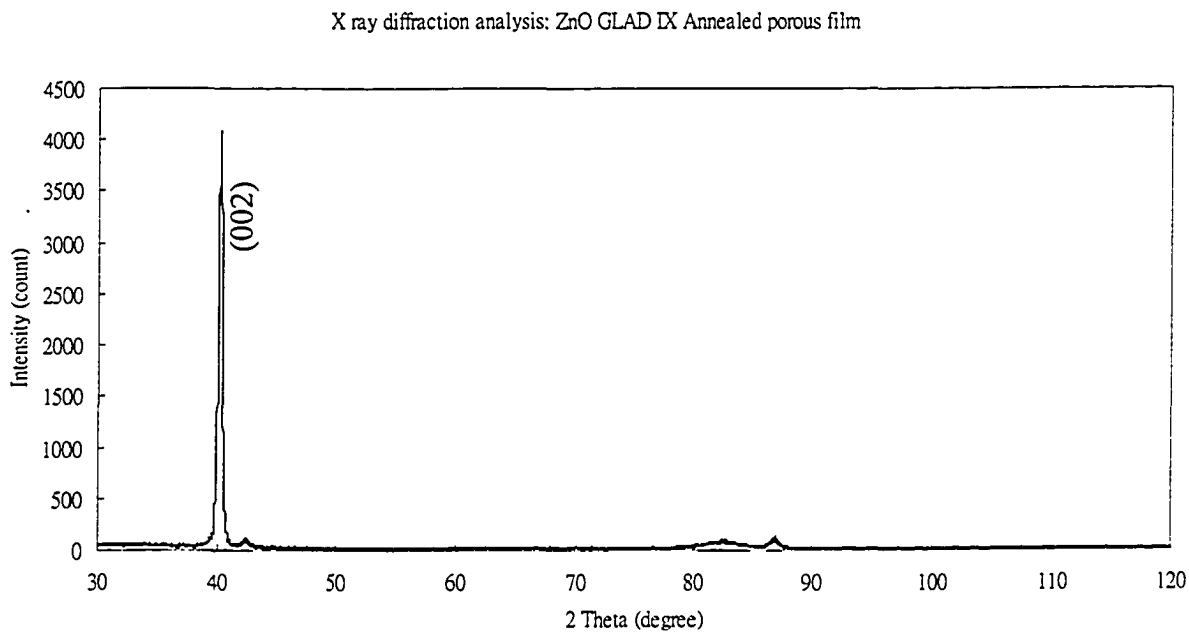

Fig 61 The XRD pattern of annealed porous ZnO film deposited in $6.6x10^{-2}$ torr O_2 (002) is the main ZnO peak at 40.184°, FWHM=0.364°.

Table 18 gives the results from Electron Microprobe compositional analysis for as-grown and annealed ZnO porous films. The results indicate that the oxygen content, in the contrary to the increase of oxygen content in the annealed film deposited vacuum, decreased ~4% after annealing.

Table 18 Atomic ratio of porous ZnO thin film deposited in $6.6x10^{-2}$ torr O_2 (Film No. IX-1, IX-1A)

Film	Zn	O	Si	P	Total
As-grown	44.0	55.4	0.5	0.0	100.0
Annealed film	44.7	54.4	0.6	0.3	100.0

Photoluminescence was very small for the as grown porous ZnO film deposited in $6.6x10^{-2}$ torr O_2 as shown in Fig 62. On the contrary, the annealed film shows a significant UV peak at 388 nm, and also a second peak at 403 nm. The 388 nm peak for the annealed porous ZnO film has a FWHM of 41.6 nm and was narrower than that of the annealed dense ZnO thin film (Fig 63). The origin of the second peak is currently unknown but it may be due to the nanostructure of the film. The properties of porous ZnO thin films are summarized in Table 19.

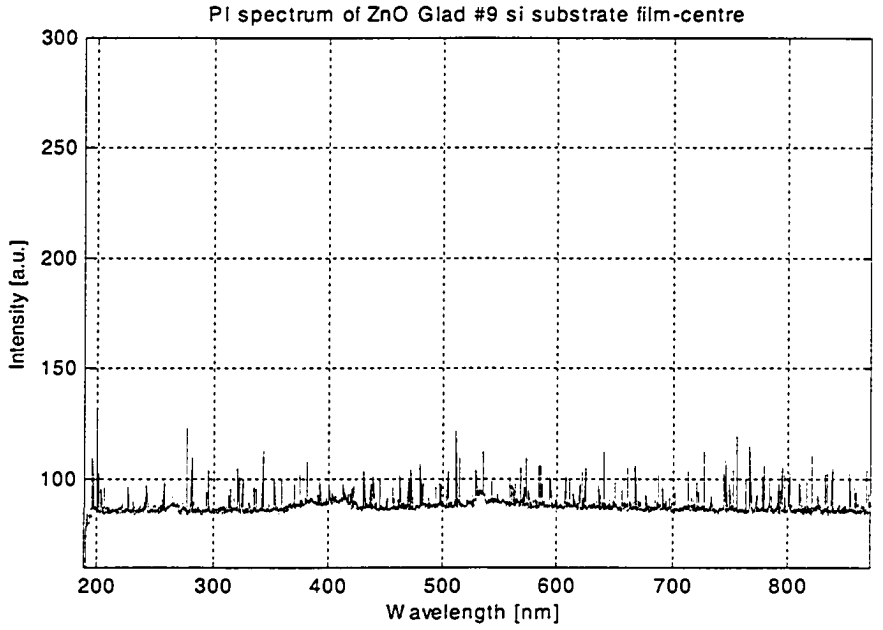

Fig 62 Room temperature photoluminescence spectra of the as-grown porous ZnO thin film. No significant signal was observed.

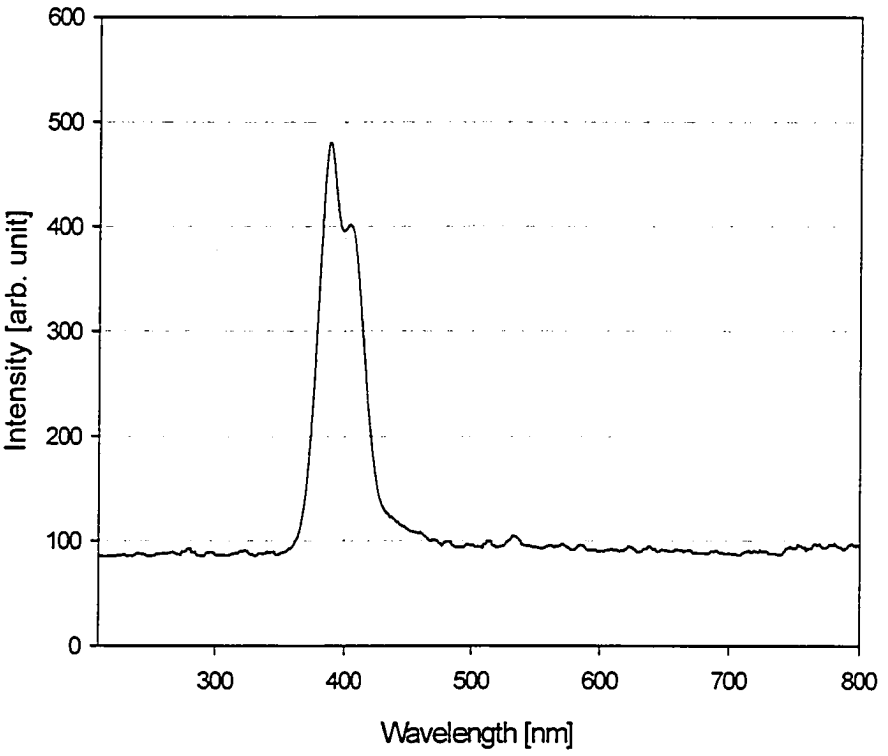

Fig 63 Room temperature photoluminescence of annealed porous ZnO film deposited in 6.6×10^{-2} torr O_2. The UV peak at 380 nm and has a side peak at 403 nm.

Table 19 Summary of properties of porous ZnO films

Environment	Annealing	XRD		E-Microprobe Quantitative O/Zn ratio	PL spectrum
		Pattern	(002) FWHM		
Vacuum	No	ZnO, Zn mix	0.51	0.51	NA
Vacuum	Yes	ZnO	0.41	1.50	High UV, low visible
O_2	No	ZnO(002)	0.52	1.49	NA
O_2	Yes	ZnO(002)	0.36	1.22	High UV

4.2.2.3 Helical film-Substrate rotating speed

Column-like ZnO thin films (nanorod) can be produced with fast substrates rotation speed (0.5 rpm at laser repetition rate of 20 Hz). By changing the rotation speed to 0.036 rpm at laser repetition ratio of 20 Hz, helical ZnO thin film can also be produced. Fig 64 shows the cross-section view of the helical ZnO film with three turns. Fig 65 shows both column-like and helical ZnO thin films and their deposition conditions.

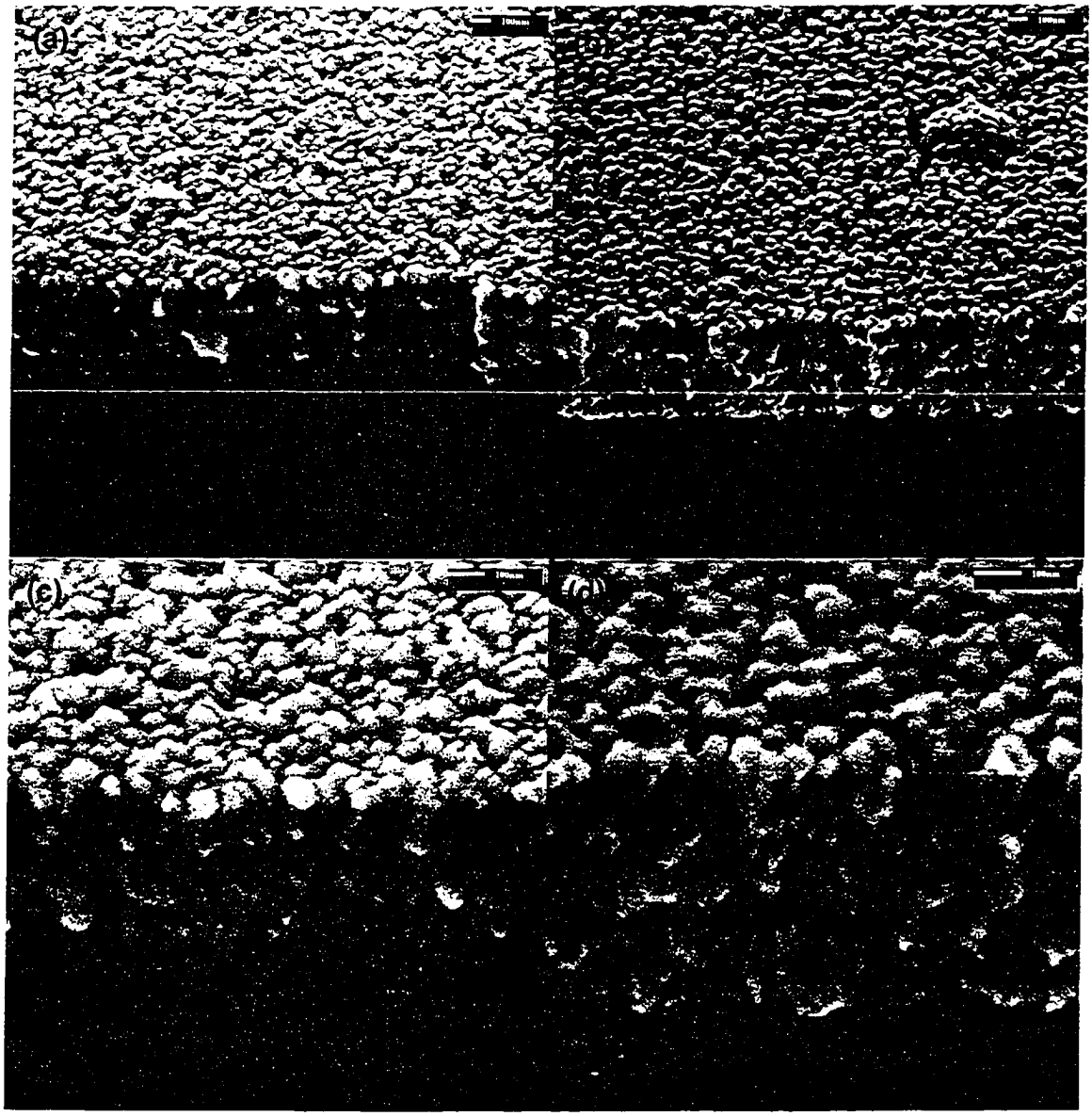

Fig 64 SEM pictures of helical ZnO films: (a) as-grown film 30,000x (b) annealed film 30,000x, (c) as-grown film 60,000x, (d) annealed film 80,000x.

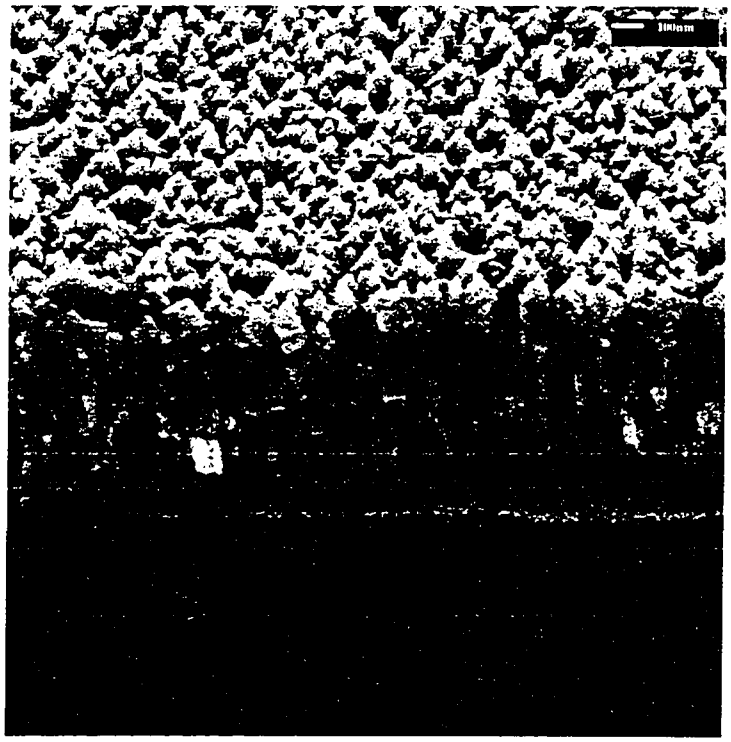

(a)
SEM picture for the annealed column-like ZnO film deposited in $6.6x10^{-2}$ torr O_2 (α=88.5°, d_{st}= of 3 cm. Film thickness is 547 nm, substrate rotation speed at 0.5rpm).
(Film No. IX-0A)

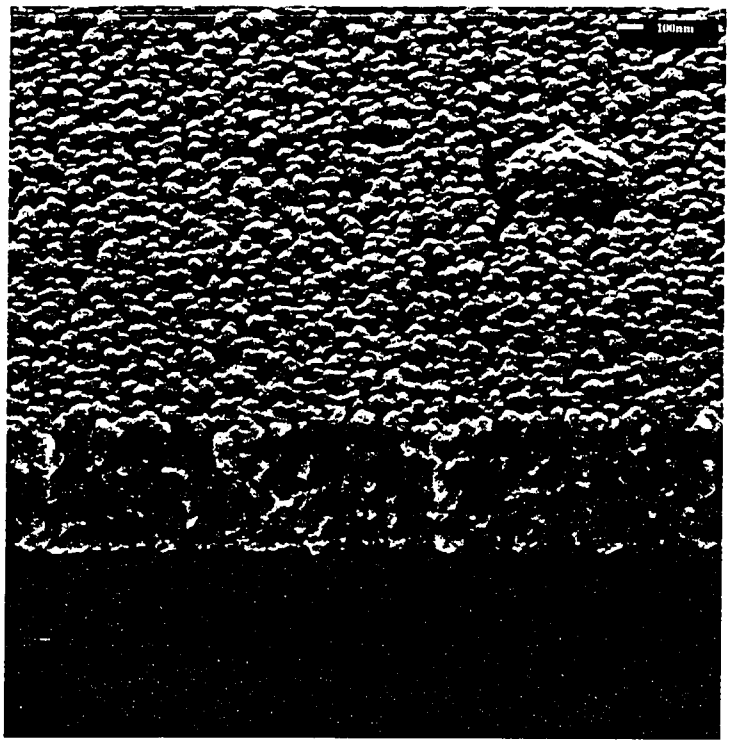

(b)
SEM picture for the annealed helical ZnO film deposited in $6.6x10^{-2}$ torr O_2 (α=88.5°, d_{st}= of 3 cm. Film thickness is 670 nm, substrate rotation speed at 0.036 rpm).
(Film No. IX-0A)

Fig 65 SEM pictures of the porous ZnO thin films, (a) thin film with column-like nanostructure, (b) thin film with helical nanostructure

The conditions used to produce our ZnO films with column-like nanostructure are very different from other groups. Yan et al. produced the ZnO nanorod thin film by doping the 1% Ga into the film and at substrate temperature 500-750°C during the deposition. The author reported Ga doping is essential for the formation of nanorod. Hartanto et al. produced the ZnO nanorod thin film by high background gas (~5 torr) and high substrate heating temperature at 600-700°C. The author reported the high O_2 pressure was essential for the naorods formation. Our films are produced with no target doping and at a much lower O_2 pressure (10^{-1} torr). In addition, the ability to produce helical nanostructures is very unique which distinguishes our technique to those of others. These helical nanostructures in principle can be used to control the polarization of the light emitted from the materials.

4.3 Emission efficiency of ZnO thin films

In order to compare with results from other laboratories or to design optical devices based on these ZnO films, the emission efficiencies in terms of numbers of photons per steradian should be measured. Based on data from the PMT measurements, the emission efficiencies of our films are summarized in Table 20. All films were measured and the number of photons were calculated according to the procedure describe in section 3.4. The excitation laser energy used was 1.37mJ/pulse on average, and a typical laser intensity of ~10^8 W/cm^2. The results show that ZnO porous film deposited in oxygen is the best UV emitting film. The UV emission increased 2 orders of magnitude after annealing indicating the important role of annealing.

The energy conversion efficiency of the photoluminescence is also estimated and is summarized in Table 21. Assuming the emission is isotropic then energy from the best film can be estimated to be ~0.824 μJ when excited with 1.37 mJ of 266nm light and this gives us an efficiency of ~6.0 x 10^{-4} for the photo-induced emission process. The accuracy of the measurement is expected to be connected to the order of magnitude giving the large uncertainty in the calibration of the PMT (see Fig 27, page 36 at incident photons of 10^4-10^5).

Table 20 Estimated number of photons per steradian from ZnO films by PMT measurements

Form	No	Power Supply [V]	(A)area [Vns]	Incident Photons [N]	(B) Gain 388nm	(B) Gain G(V)	(C) Filter [N]	Photons per steradian [photon/SR]	**(D) Total photons**	Rank
Dense Annealed	**PLD2A (Vacuum)**	900	35.5	1.3×10^5	8.7×10^4	3.6×10^7	5.5×10^8	9.9×10^9	**6.2×10^{10}**	5
Dense As grown	**PLD3 (O_2)**	900	20.4	1.1×10^3	6.7×10^3	2.7×10^6	4.3×10^7	7.6×10^8	**4.8×10^9**	7
Dense As grown	**PLD3A (O_2)**	900	54.0	9.6×10^5	6.0×10^5	2.5×10^8	3.8×10^9	6.9×10^{10}	**4.3×10^{11}**	3
Porous annealed	**GLAD1A (Vacuum)**	900	31.7	8.3×10^4	5.2×10^4	2.2×10^7	3.3×10^8	5.9×10^9	**3.7×10^{10}**	6
Porous annealed	**GLAD9A (O_2)**	900	71.8	3.6×10^6	2.2×10^6	9.3×10^8	1.4×10^{10}	2.6×10^{11}	**1.6×10^{12}**	2
Powder	**Nano powder**	900	35.5	1.4×10^5-	8.7×10^4	3.6×10^7	5.5×10^8	9.9×10^9	**6.3×10^{10}**	4
powder	**Target**	700	44.9	4.1×10^5	2.6×10^5	2.0×10^9	3.1×10^{10}	5.7×10^{11}	**3.6×10^{12}**	1

Table 21 Estimated emission efficiency of ZnO films

Film	No	Thickness	Numbers of photons	Equivalent Energy [nJ]	Energy convergent Efficiency (%)
Annealed dense film, deposited in vacuum	PLD2A	478 nm	**$6.2x10^{10}$**	**32**	0.0023
As grown dense film, deposited in O_2	PLD3	940 nm	**$4.8x10^{9}$**	**2**	0.0002
Annealed dense film, deposited in O_2	PLD3A	940 nm	**$4.3x10^{11}$**	**221**	0.0161
Annealed porous film, deposited in Vacuum	GLAD1A	380 nm	**$3.7x10^{10}$**	**19**	0.0014
Annealed porous film, deposited in O_2 on Si	GLAD9A Si	559 nm	**$1.6x10^{12}$**	**824**	0.0601
Powder form of ZnO	nanopowder	~01. mm	**$6.3x10^{10}$**	**32**	0.0023
Powder form of the target	ZnO target	~0.1 mm	**$3.6x10^{12}$**	**1828**	0.1335

Chapter 5 Conclusions

High quality micron thick c-axis oriented ZnO thin films on silicon were fabricated by pulsed laser deposition in O_2 without substrate heating. This is a useful finding since it is easier and less expensive to do deposition in a vacuum chamber without a substrate heating system. The morphological, structural and optical properties of the films were investigated. Strong UV emissions were obtained from the films after annealing at 600 ^{0}C in air for 2 hours. High quality porous ZnO thin films consisting of 100 nm diameter isolated columns were also fabricated by pulsed laser deposition in $6.6x10^{-2}$ torr of O_2.

Deposition rate

Both dense and porous ZnO thin films were deposited using the PLD technique. A 20 Hz KrF laser at 248 nm with pulse duration 15 ns and ~100mJper pulse were used. The average deposition rates for dense and porous ZnO films deposited in $\sim 6.6x10^{-2}$ torr O_2 at substrate to target distances of ~3cm is 0.018Å/pulse and 0.075Å/pulse, respectively.

Effect of oxygen background gas and effect of annealing

Generally speaking, both the dense and porous ZnO thin films deposited in oxygen ambient gas pressure in the range of 10^{-2}~10^{-3} torr show better crystallinity than that deposited in vacuum. The interaction between incoming plume and oxygen gas decreased the number of defects in the films such as oxygen vacancies and zinc interstitials. The annealing of the ZnO thin film at 600°C in atmosphere also improved the film quality. The high thermal energy seems be able to relax the strain of the film and also increased the crystallinity. The photoluminescence spectra of the annealed PLD ZnO thin films deposited in O_2 is similar to that of the original ZnO target. This suggests both thin

film and target materials have similar stoichiometry and crystalline properties. The quality of the ZnO films were greatly improved by depositing in O_2 environment and annealing at 600°C in atmosphere as supported by evidences from SEM, XRD, Electron Microprobe, and photoluminescence measurements.

Emission efficiency

The emission efficiency for the ~0.5μm thick annealed porous ZnO thin films deposited in O_2 was ~$5x10^{-4}$. The measurement of photoluminescence in absolute units is useful since it facilitates comparison with other experiments and theory.

Nanostructures of the porous ZnO films

In addition to porous ZnO thin films with column-like nanostructures (nanorod) films with helical structures were also produced. We believe this is the first time porous ZnO thin film with helical nanostructure is being produced.

Future work

The long terms goals for this ZnO project are to fabricate ZnO based micro UV LEDs or micro UV lasers and piezoelectric sensors/actuators to be used in microfluidic devices. This study represents the first step towards fulfilling such goal. The next step would involve the optimization of the fabrication process and the future study at the properties of those ZnO films such as their optical properties and piezoelectric properties etc. In addition, processing techniques such as laser microprocessing and plasma etching of ZnO film should be studied as well.

Reference

[1] C. Wang, G. Yang, H. Liu, Y. Han, J. Luo, C. Gao, G. Zou, Applied Physics Letter, Vol. 84, No. 13, pp2427-2429 (2004).

[2] R.L. Hoffman, Journal of Applied Physics, Vol. 95, No.10, pp5813-5819 (2004).

[3] Q. Wan, Q.H. Li, Y.J. Chen, T. H. Wang, X.L. He, J.P. Li, C.L. Lin, Applied Physics Letter, Vol.84, No.18, pp3654-3656 (2004).

[4] Y. Shirai, Y. Miyato, M. Taguchi, M. Shiotsu, H. Hatta, S. Muroya, M. Chiba, T. Nitta, IEEE Transactions on Applied Superconductor, Vol. 13, No. 2, pp2064-2067 (2003).

[5] Y. R. Ryu, S. Zhu, J. D. Budai, H. R. Chandrasekhar, P. F. Miceli, H. W. White, Journal of Applied. Physics, Vol. 88, No. 1, pp201-204 (2000).

[6] J. Lee, M. Lee, C. Park, J. Park, Thin Solid Film 447-448, pp296-301 (2004).

[7] E.Guzman, H. Hochmuth, M. Lorenze, H. Von Wenckstern, A. Rahm, E.M. Kaidashev, M. Ziese, A. Setzer, P. Esquinazi, A. Poppl, D. Spemann, R. Pickenhain, H. Schmit, M. Grundmann, Ann. Physics B, No. 1-2, pp57-58 (2004).

[8] S.F. Yu, C. Yuen, S.P. Lau, W.J. Fan, IEEE Journal of Quantum Electronics, Vol. 40, No. 4, pp406-412 (2004).

[9] K. H. J Buschow, R.W. Cahn, M. C. Flemings, B. Ilschner, E. J. Kramer, S. Mahajan, Encyclopedia of Materials: Science and Technology Vol.10 (2001).

[10] S.J Pearton, D.P. Norton, K. Ip, Y.W. Heo, T. Steiner, Superlattices and Microstructures, 0749-6036 (2003).

[11] K. Vanheusden, W.L. Warren, C.H. Seager, D.R. Tallant, J.A. Voigt, B.E.Gnade, Journal of Applied Physics Vol.79, No. 10, pp7983-7990 (1996).

[12] M.H. Huang, S. Mao, H. Feick, H. Yan, Y. Wu, H. Kind, E. Weber, R. Russo, R. Yang, Science, Vol. 292, pp1897-1900 (2001).

[13] K.S. Ramaiah, Y.K. Su, S.J. Chang, B. Kerr, Applied Physics Letter Vol. 84, No. 17, pp3307-3309 (2004).

[14] D.C. Look, Material Science Engineering B 80, pp383-387 (2001).

[15] C.P. Lee, Microelectronics lecture notes, http://140.114.18.41/micro/chap2/chap2-2.htm (2004).

[16] M. Frumar, Z. Cernosek, Z Plak, Non-crystal Solids, 256-257, pp105-110 (1999).

[17] Y.Y. Tsui, D. Vick, R. Fedosejevs, Applied Physics Letter, Vol. 70, No. 15 pp1953-1955 (1997).

[18] PK. Dwivedi et al, to be submitted to Applied Surface Science (2004).

[19] D. Vick, Y.Y. Tsui, M.J. Bress, R. Fedosejevs, Thin Solid Films, 350, pp49-52 (1999).

[20] D.B. Bagnall, Y.F. Chen, Z. Zhu, T. Yao, S. Koyama, M.Y. Shen, T. Goto, Applied Physics Letter, Vol. 70, No. 17, pp2230-2233 (1997).

[21] Y. Segawa, A. Ohtomo, M. Kawasaki, H.Koinuma, Z. Tang, R. Yu, G.K.L. Wong, Riken Review, No 17, pp19-20 (1998).

[22] Y. Segawa, H.D. Sun, T. Makino, M. Kawasaki, H. Koinuma, Phyics Stat. Sol. (a) 192, No. 1, pp14-20 (2002).

[23] Yamamoto, H.K. Yoshida, Japanese Journal of Applied Physics, part 2 38 L166 (1999).

[24] M. Joseph, H. Tabata, T. Kawai, Japanese Journal of Applied Physics, part 2 38 L1205 (1999).

[25] Y.R. Ryu, S. Zhu, D.C. Look, J.M. Wrobel, H.M. Jeong, H.W. White, J. Crystal Growth, 216, pp330-334 (2000).

[26] Y.W. Heo, K. Ip, S.J. Park, S.J. Pearton, D.P. Norton, Applied Physics. A, 78, pp53-57 (2004)

[27] K, Minegish, Y. Koiwai, Y. Kikuchi, Japanese Journal of Applied Physics, part 2 36, L1453 (1997).

[28] A. B. Hartanto X. Ning, Y. Nakata, T. Okada, Applied Physics A, Vol. 78, pp299-301 (2003).

[29] M. Yan, H. T. Zhang, E. J. Widjaja, R. P. H. Chang, Journal of Applied Physics, Vol. 94, No. 8, pp5240-5246 (2003).

[30] K.Ellmer, Phys. D: Applied Physics, 33, R17-R32 (2000).

[31] Y.Chen, H.J. Ko, S.K. Hong, T. Yao, Applied Physics Letter Vol. 79, No. 11, pp1469-1471 (2001).

[32] J. Wu, S. Liu, Advanced Material, Vol. 14, No. 3, pp215-218 (2002).

[33] H.J. Ko, T. Yao, Y Chen, S.K. Hong, Journal of Applied Physics, Vol. 92, No. 8, pp4354-4360 (2002).

[34] S. H. Bae, S. Y. Lee, B. J. Jin, S. Im, Applied Surface Science, 154-155, pp458-461, (2000).

[35] J. Springer, A. Poruba, L. Mullerova, M. Vanecek, O. Kluth, B. Rech, Journal of Applied Physics, Vol. 95, No. 3, pp1427-1429 (2004).

[36] S. Choopun, R. D. Vispute, W. Noch, A. Balsamom R. P. Sharma, T. Venkatesan, A. Iliadis, D.C. Look, Applied Physics Letter, Vol. 74, No. 25, pp3947-3939 (1999).

[37] S.S Kim, B. Lee, Thin Solid Films, 446, pp307-312 (2004).

[38] Y. F. Lu, H. Q. Ni, Z. H. Mai, and Z. M. Ren, Journal of Applied Physics, Vol. 88,

No. 1, pp498-502 (2000).

[39] V. Craciun,J. Elders, J. G. E. Gardeniers, and I. W. Boyd, Applied Physics Letter Vol. 65, No. 23, pp2963-2966 (1994).

[40] S.H. Bae, S.Y. Lee, H.Y. Kim, S. Im, Optical Materials, 17, pp327-330 (2001).

[41] H.S. Kang, J.S. Kang, J.W. Kim, S.Y. Lee, Journal of Applied Physics, Vol. 95, No.3, pp1246-1250 (2004).

[42] Y.X. Liu, Y.C. Liu, D.Z. Shen, G.Z. Zhong, X.W. Fan, X.G. Kong, R. Mu, D.O. Henderson, Journal of Crystal Growth, 240, pp152-156 (2002).

[43] M. Yan, H.T. Zhang, E.J. Widjaja, and R.P.H. Chang, Journal of Applied Physics, Vol. 94, No. 8, pp5240-5246 (2003).

[44] A.B. Hartanto, X. Ning, Y. Nakata, T. Okada, Applied Physics A-Materials Science & Processing, Vol. 78, No. 3, pp299-301 (2004).

[45] R.D. Vispute, V. Talyansky, R.P. Sharma, S. Choopun, M. Downes, T. Venkatesan, Y.X. Li, L.G. Salamanca-Riba, A.A. Iliadis, K.A. Jones, J. McGarrity, Applied Surface Science, 127-129, pp431-439 (1998).

[46] Z.L. Nalwa, Handbook of Thin Film Materials Vol.1, Academic Press (2002).

[47] H. S. Nalwa, Deposition and Processing of Thin Films, Vol. 1, Academic Press (2002).

[48] A.L. Barabasi, H. E. Stanley, Fractal Concepts in Surface Growth, Cambridge University Press (1982).

[49] K. Robbie, Glancing Angle Deposition, University of Alberta (1998).

[50] R. N. Tait, T. Smy, M.J. Brett, Thin Solid Films, 226, pp196-201(1993).

[51] J. H. Wittke, Electron Microprobe Techniques class notes, http://jan.ucc.nau.edu/%7Ewittke/Microprobe/ProbeNotes.html (2003).

[52] N, Fujimura, T. Nishihara, S Goto, J. Xu, T. Ito, Journal Crystal Growth 130, 269 (1993).

[53] J. M. Myung,W. H. Yoon, D. H. Lee, I. Yun, S. H. Bae, S. Y. Lee, Japanese Journal of Applied Physics part 1, No.1 Vol. 41, pp28-31 (2002).

[54] E.S. Shim, H.S. Kang, S.S. Pang, J.S, Kang, I. Yun, S.Y. Lee, Material Science Engineering, B102, pp366-369 (2003).

[55] P. Bhattacharya, Semiconductor Optoelectronics Devices, Prentice-Hall, pp22-30 (1997).

[56] E. S. Shim, H. S. Kang, S. S. Pang, J. S. Kang, H. Yu, S. Y. Lee, Materials Science & Engineering B, B102, pp366-369 (2003).

[57] B.D. Cullity, Elements of X-ray of Diffractions, Addition-Wesley, pp102 (1978).

Appendix

Appendix A Si wafer specification

The substrate that used in the experiment is Si wafer made by Silicon Valley Microelectronics, Inc. The specification is as following,

Table 22 Specification of 4" Si wafer

Diameter	100+/-0.5mm
Dopant	P/ Boron
Orientation	<100>
Resistivity	1-30 ohm-cm
Thickness	500-550um
Grade virgin test	
Flats Two SEMI standard	

Appendix B ZnO microprobe files

Table 23 Atomic ratio of annealed solid ZnO thin film deposited in vacuum (Film No. PLD I-1A)

No.	Zn	Si	O	P	Total	Comment
1	31.112	0.357	58.196	10.335	100	ZnO2A
2	31.219	0.32	59.086	9.375	100	ZnO2A
Average	31.1655	0.3385	58.641	9.855	100	

Table 24 Atomic ratio of annealed solid ZnO thin film deposited in 10^{-1} torr O_2 (Film No. PLD II-1A)

No.	Zn	Si	O	P	Total
1	35.861	0.2495	56.582	7.307	99.9996
2	33.889	0.1994	58.046	7.865	99.9995
Average	34.875	0.22445	57.314	7.586	99.99955

Table 25 Atomic ratio of annealed porous ZnO thin film deposited in vacuum (Film No. GLAD I-1A)

No.	Zn	Si	O	P	Total
1	37.95	0.3457	55.196	6.508	99.9998
2	36.323	0.3392	56.8	6.538	100.0002
3	37.702	0.2802	55.507	6.511	100.0001
4	36.282	0.2526	55.857	7.609	100.0005
5	37.055	0.2982	55.849	6.798	100.0001
Average	37.0624	0.30318	55.8418	6.7928	100.0001

Table 26 Atomic ratio of as-grown solid ZnO thin film deposited in $6.6x10^{-2}$ torr O_2 (Film No. GLAD IX-1)

No.	Zn	O	Si	P	Total
1	43.893	55.641	0.4669	0	100.0008
2	43.552	55.739	0.6905	0.0178	99.9994
3	43.883	55.61	0.4485	0.0581	99.9997
4	44.023	55.205	0.7719	0	100
5	44.043	55.415	0.5418	0	99.9999
6	44.079	55.326	0.5321	0.0634	100.0005
7	44.696	54.995	0.2308	0.0782	100
Average	44.02414	55.41871	0.526071	0.031071	100

Table 27 Atomic ratio of annealed porous ZnO thin film deposited in $6.6x10^{-2}$ torr O_2 (Film No. GLAD IX-1A).

No.	Zn	O	Si	P	Total
1	44.5120	54.5780	0.5601	0.3495	99.9997
2	44.6670	54.5050	0.6399	0.1885	100.0003
3	44.9400	54.2510	0.6291	0.2813	99.9995
4	44.5620	54.2510	0.9155	0.2710	99.9995
5	44.8160	54.5640	0.3799	0.2397	99.9997
Average	44.6994	54.4094	0.6249	0.266	99.99974

Appendix C ZnO nanopowder

The ZnO powder is manufactured by NanoScale Materials Inc., it is a white powder with average pore diameter of 170 Å, and density of 5.6 g/cc. Mean aggregate Size is 4um. The ZnO powder sample was used to be the comparison group with our ZnO samples.

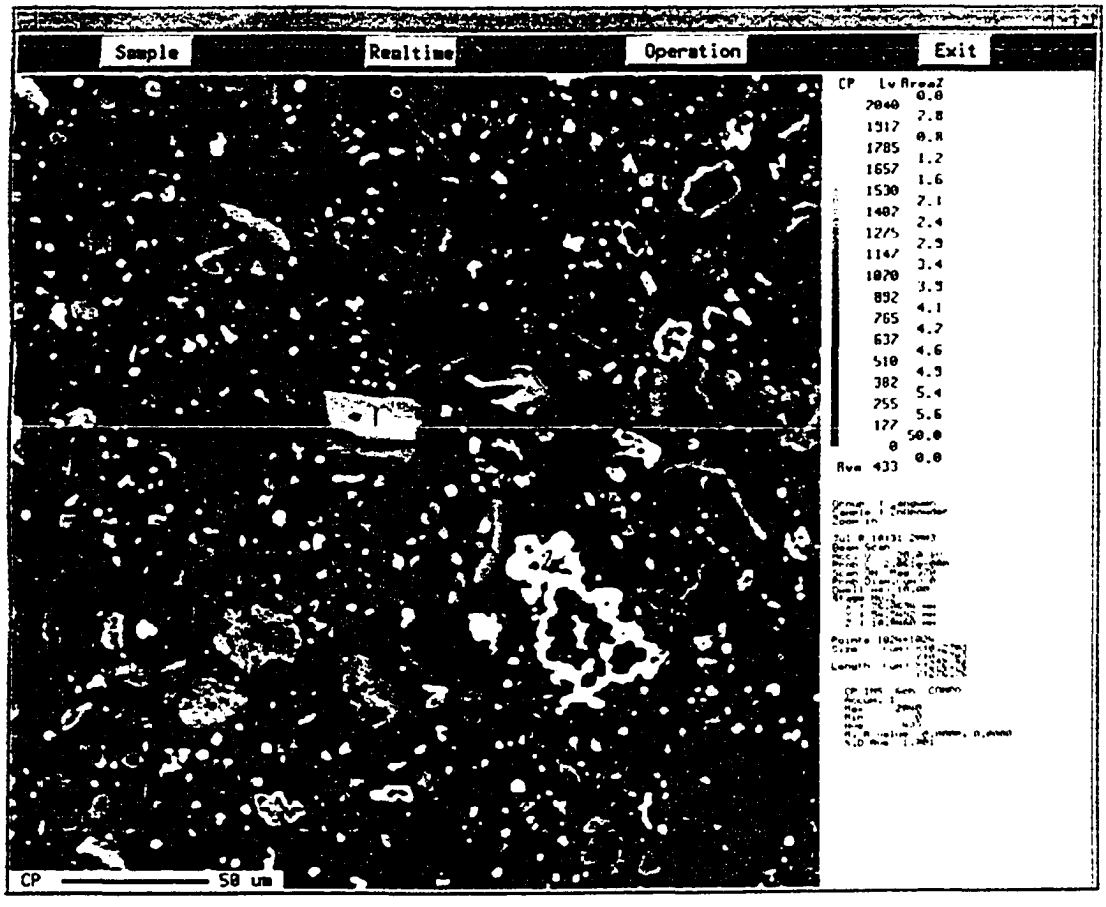

Fig 66 The Microprobe pictures of the nanopowder manufactured by NanoScale Materials Inc. There is a distribution of powder size is in the range of 100nm-50um.

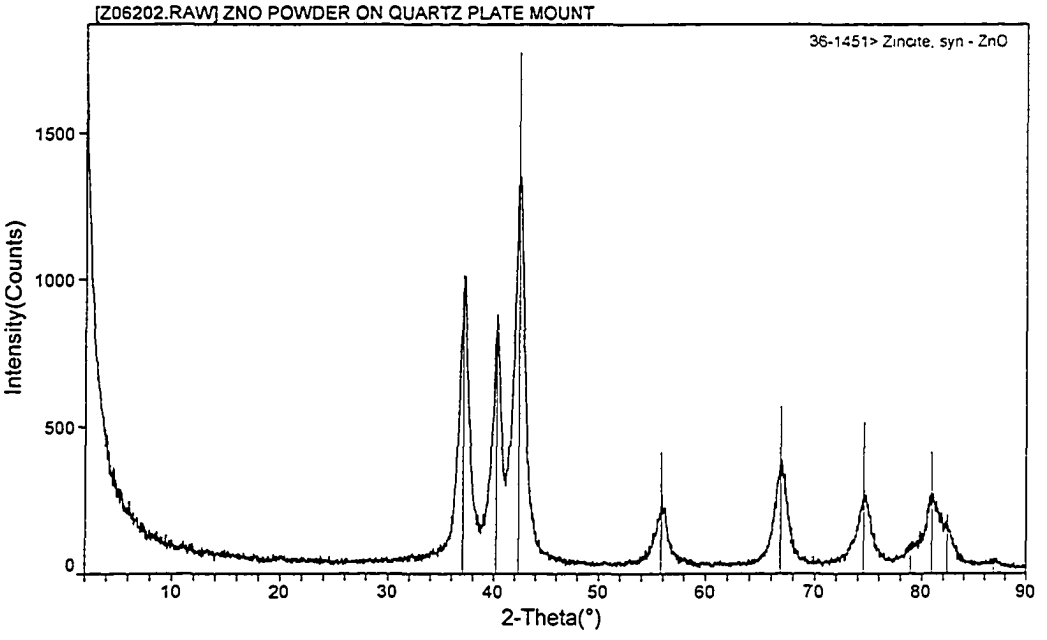

Fig 67 The XRD pattern of the ZnO nanopowder.

Table 28 Atomic ratio of the ZnO nanopowder

ZnO nanopowder by Nanomaterials					
No.	Si	O	Zn	Total	Comment
1	0.087	15.827	84.086	100.000	1
2	0.064	17.005	82.931	100.000	2
3	0.000	18.439	81.561	100.000	2
4	0.095	16.914	82.991	100.000	3
5	0.005	16.275	83.721	100.000	4 small part.
6	0.017	14.479	85.504	100.000	5 small part. grey
7	0.000	14.541	85.459	100.000	6 grey
8	0.000	15.535	84.465	100.000	6 bright
9	0.101	22.406	77.494	100.000	Powder sample
10	0.000	17.489	82.511	100.000	Powder sample
11	0.251	12.897	86.852	100.000	Powder sample
Average	0.056	16.528	83.416	100.000	

Appendix D Filter transmission

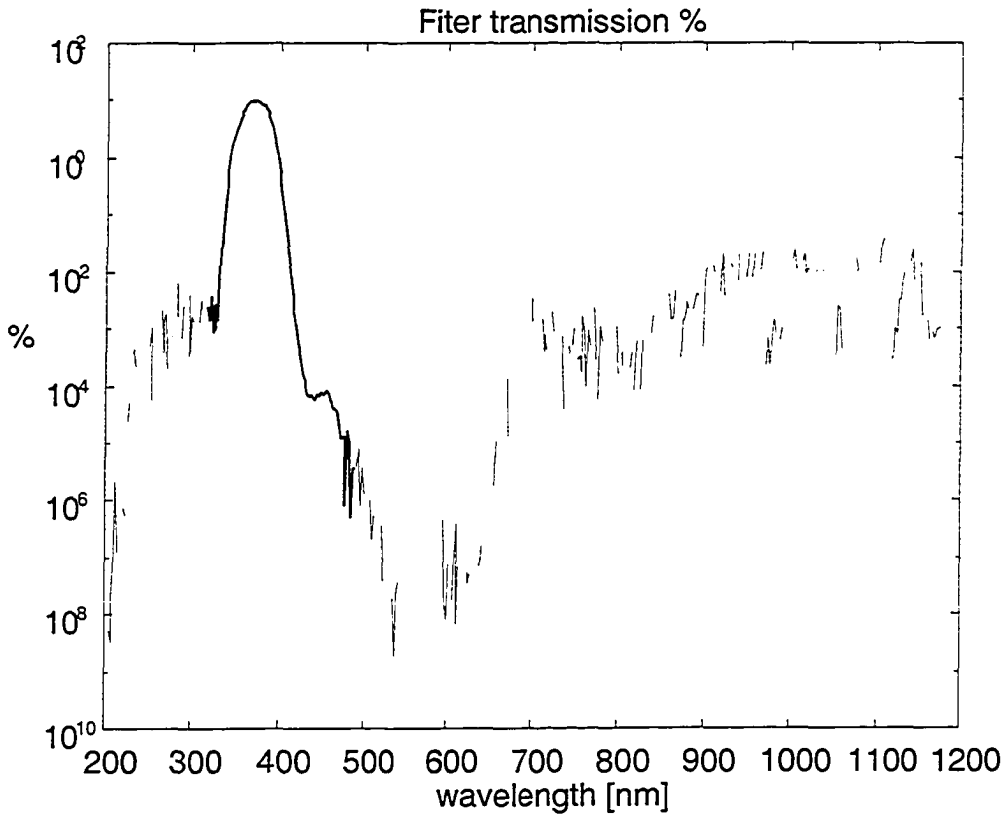

Fig 68 Transmission curve of the filter set which is shown in the absolute emission setup.

Appendix E Photoluminescence data processing

E.1 Remove the noise

The original photoluminescence signal contains high frequency noise. In order to filter out the high frequency noise, a software, SigmaPlot version 8.02, was used to filter out the noise. The procedures and functions that used is the transforms 2D smoother-> running average, and set the sampling proportion to 0.01, and the interval to 10000. In Fig 69 shows a signal process example, the dashed line is the original PL signal, and the solid line is the processed data which has a clear signal without high frequency noise. Fig 70 and Fig 71 are the process PL data and the background noise.

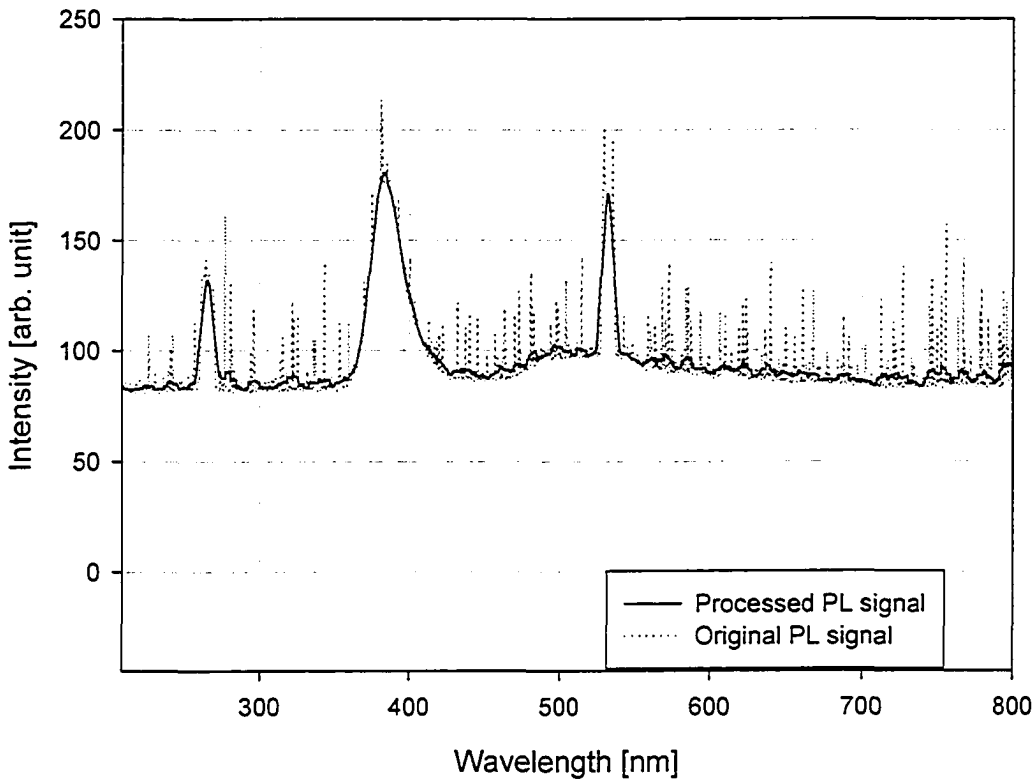

Fig 69 The original PL signal (dashed line) and the processed signal (solid line).

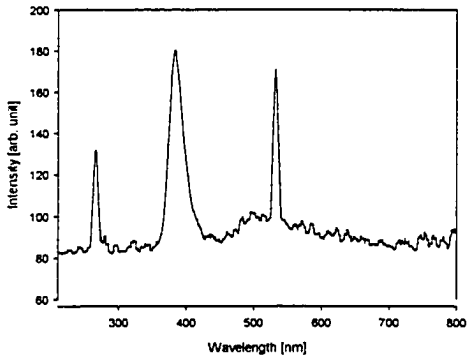

Fig 70 Processed signal shows the smoother variation.

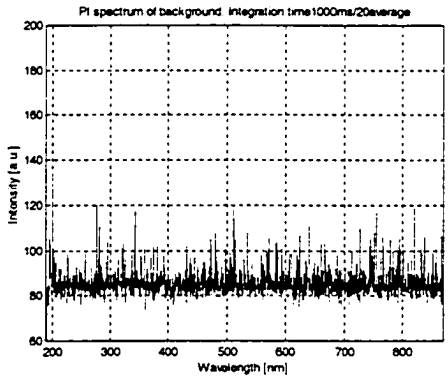

Fig 71 Background noise

Fig 72(a) is the smoothed PL spectrum of the dense ZnO thin film. Besides the PL, we still can see the peak of pumping laser light of Nd:YAG laser wavelength at 4ω of 266nm and some portion of 2ω of 532nm. Following paragraph shows the procedures to remove the pumping laser peak at 532nm. In Fig 2(b) Choose the working region 500nm-590nm. (c) Find the slope of that region. (d) Detrended the data by reverse of the slope to zero. (e) Fit the laser peak by Gaussian function. (f) Original peak-Gaussion peak= the remain signal. (g) Retrended the data. (h). processed PL data.

Laser light removed.

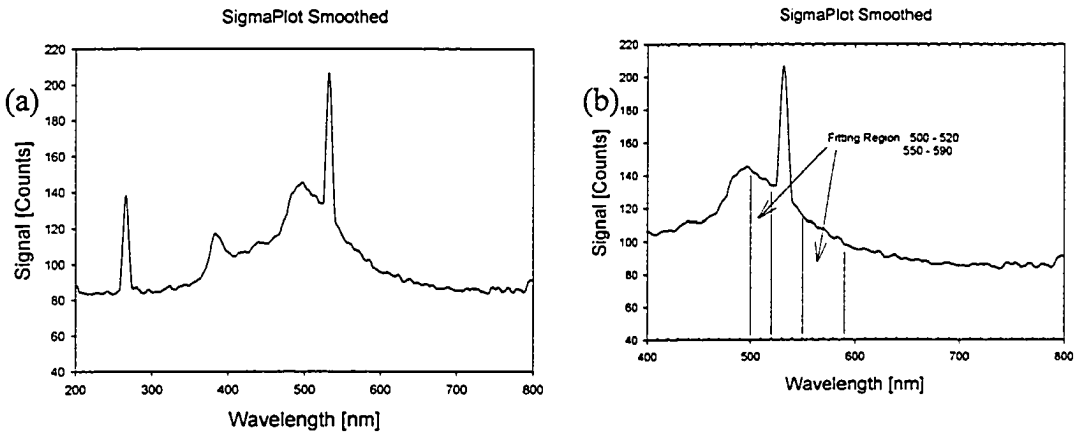

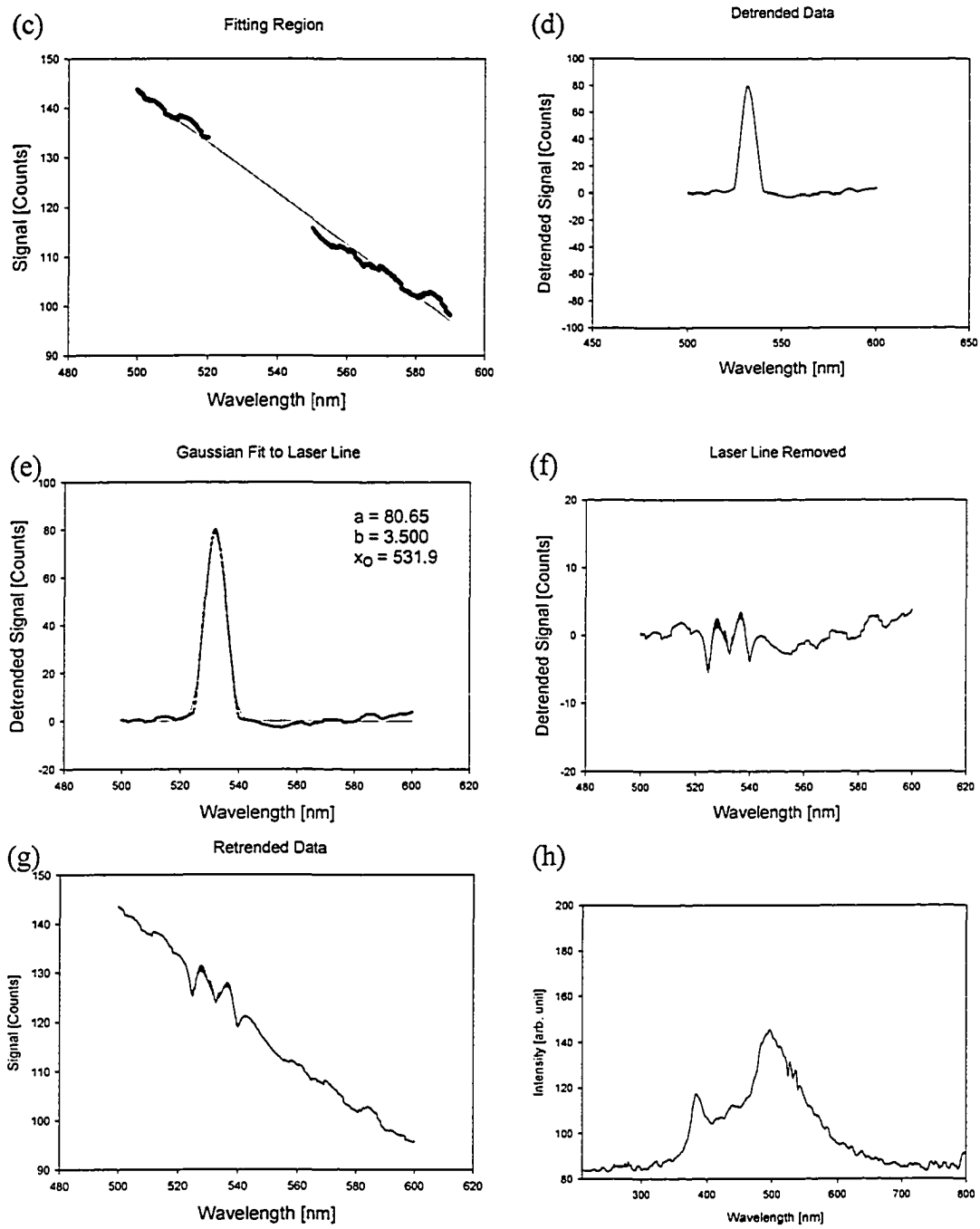

Fig 72 Procedures to remove the laser light at 532nm.(a) Smooth PL signal (b) Choose the working region 500nm-590nm. (c) Find the slope of that region. (d) Detrend the data by reverse of the slope to zero. (e) Fit the laser peak by Gaussian function. (f) Original peak-Gaussion peak= remain signal. (g) Retrend the data. (h) Processed PL data. Laser light removed.

Appendix F Summary of room temperature photoluminescence measurement

Following graphs are the photoluminescence (PL) spectra of ZnO in different form: bulk ZnO, ZnO powder, ZnO nanopowder, dense and porous ZnO thin films to demonstrate difference of the optical properties between different form.

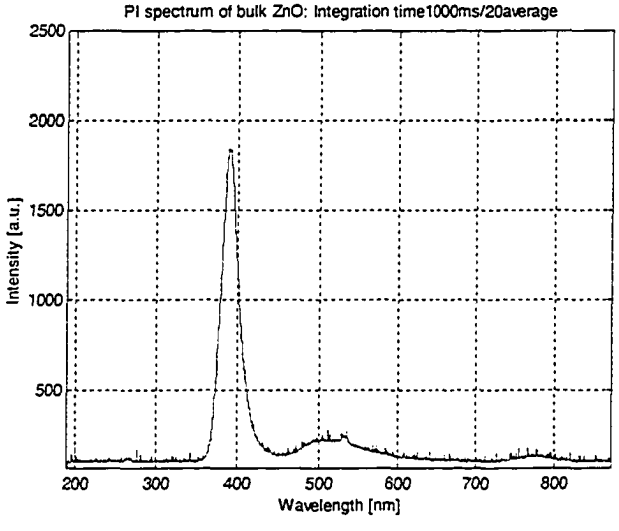

Fig 73

RT PL spectra of the Bulk ZnO (the ZnO PLD target) shows a UV emission peak at 380 nm, and a blue emission tail at around 500nm.

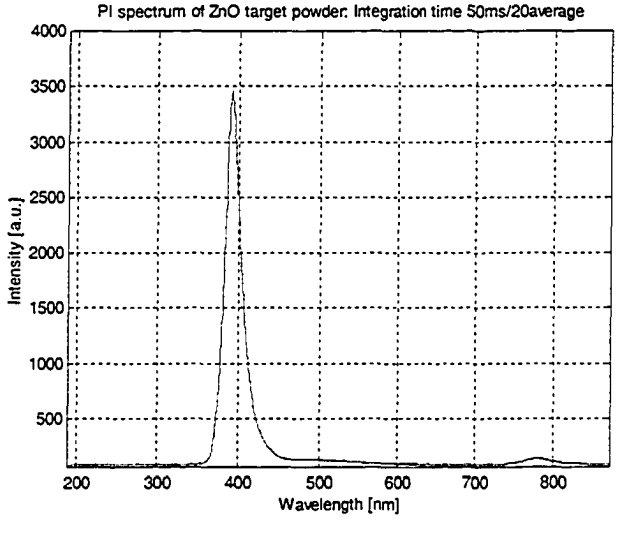

Fig 74

RT PL spectra of the ZnO powder (obtained from the ZnO PLD target) shows a clear UV emission peak at 380nm, the UV emission tail disappeared.

Fig 73 is the PL spectra measured from the Bulk ZnO target. There is a UV emission peak at 380nm, and a blue emission tail at around 500nm. This shows that the surface of the ZnO target is oxygen deficient after the laser fired on the target. During the deposition, the ZnO target is rotating, so that the laser would fire on the oxygen deficient target again and again, and this would be one of possibilities why the as grown film typically were oxygen deficient.

The PL spectra of the ZnO powder (Nanoactive Inc.) is shown in Fig 75 for comparison. Since most of the luminescence from the ZnO powder is situated in the visible region, it is suggested that the powder contains oxygen vacancies.

The PL spectra of the annealed ZnO thin film deposited in vacuum and oxygen are shown in Fig 76 and Fig 77 on the next page. The PL spectra of the annealed ZnO porous film deposited vacuum and oxygen are showing in Fig 78 and Fig 79.

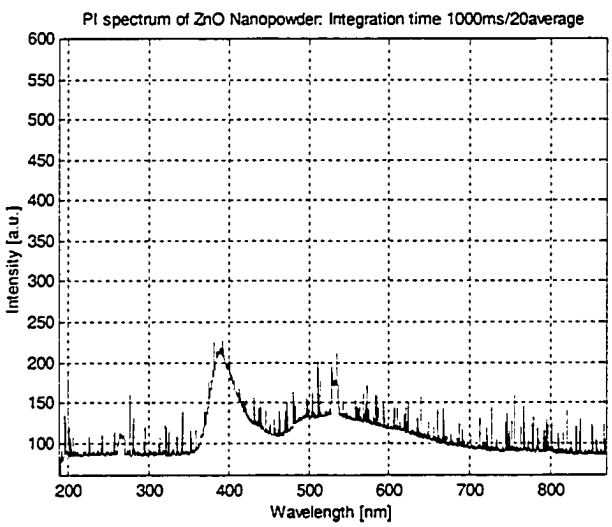

Fig 75

RT PL spectra of commercial nano- ZnO powder (appendix g), UV peak at 380nm and the visible emission show that the powder contains oxygen vacancies.

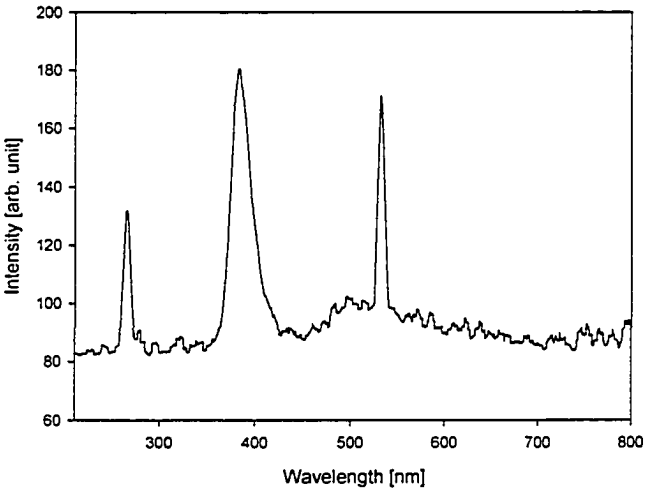

Fig 76

RT PL spectra of the annealed ZnO film deposited in Vacuum, this film emitted a large portion of visible emission.

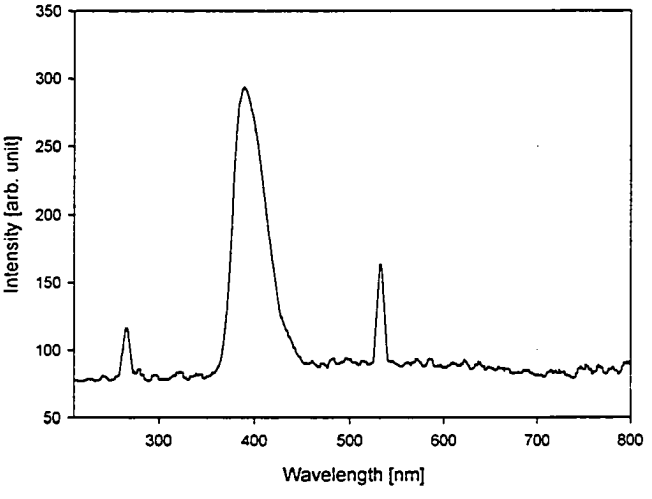

Fig 77

RT PL spectra of the annealed ZnO film deposited in 100m torr oxygen, this film shows a clear UV emission. The pattern is closed to ZnO target powder which means the film crystalline is close to the ZnO target.

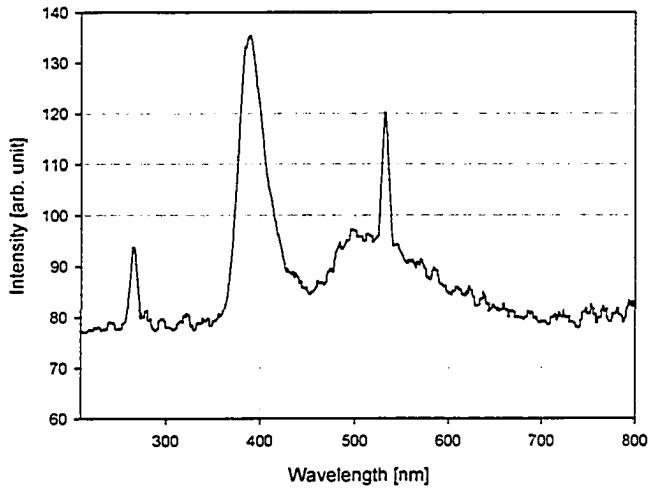

Fig 78

RT PL spectra of the porous ZnO film deposited in vacuum annealed film. P1 is the UV emission peak at 380nm, and P2 is the visible emission peak at 495nm

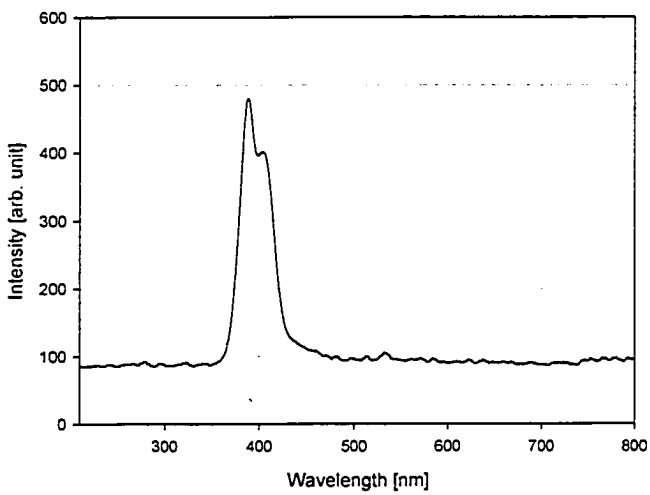

Fig 79

RT PL spectra of the porous ZnO film deposited in 66m Torr O_2, the film show UV emission peak at 380 nm and a side peak at 403nm.

Appendix G Absolute photoluminescence measurement

The ZnO thin films were name in the following: PLD2A is the post-annealed film deposited in Vacuum, PLD3, is the as grown film deposited in oxygen, PLD3A is the post-annealed film deposited in oxygen. GLAD1A is the post-annealed porous film deposited in vacuum, GLAD9Asi is the post-annealed porous film deposited in oxygen, GLAD9A Au is the annealed film deposited on Au coated Si substrate in oxygen. Nanopowder is a powder form of ZnO from Nanoscale material Inc. for comparison. Target powder is the grained powder from the target. The photoluminescence background signal data is summarized in Table 29.

Table 29 PMT background Signals

Film	**No**	Power Supply [V]	(A) a rea [Vns]	Incident Photons [N]	Gain 388nm	(B) Gain Supply V [N]	(C) Filter [N]	**(D) Total photons**
Background	**Si**	900	3.7	$2.1x10^{2}$	$1.3x10^{2}$	$4.2x10^{4}$	$6.5x10^{5}$	**$7.7x10^{6}$**
	Carbon tape	900	12.8	$3.6x10^{3}$	2.3x10-3	$7.3x10^{5}$	$1.1x10^{7}$	**$1.3x10^{8}$**
	Carbon tape	700	0.7	4	2	$1.2x10^{3}$	$2.0x10^{5}$	**$2.3x10^{6}$**